Approval of the Institute of Graduate Studies and Research

_____

Prof. Dr. Elvan Yılmaz
Director (a)

I certify that this thesis satisfies the requirements as a thesis for the degree of Master of Science in Mechanical Engineering.

_____

Assoc. Prof. Dr. Fuat Egelioğlu
Chair, Department of Mechanical Engineering

We certify that we have read this thesis and that in our opinion it is fully adequate in scope and quality as a thesis for the degree of Master of Science in Mechanical Engineering.

_____

Prof. Dr. Hikmet Ş. Aybar
Supervisor

Examining Committee

_____

1. Prof. Dr. Hikmet Ş. Aybar _____
2. Prof. Dr. Murad Annaorazov _____
3. Assoc. Prof. Dr. Fuat Egelioğlu _____
4. Asst. Prof. Dr. Saad Yasin _____
5. Asst. Prof. Dr. Hasan Hacışevki _____

Mathematical Modeling of Magnetic Regenerator Refrigeration Systems

Navid Salarvand

Submitted to the
Institute of Graduate Studies and Research
in partial fulfillment of the requirements for the Degree of

Master of Science
in
Mechanical Engineering

Eastern Mediterranean University
June 2009
Gazimağusa, North Cyprus

ABSTRACT

Active magnetic regenerative refrigeration (AMRR) systems are designed based on magnetocaloric effect of some special solid materials, such as Gadolinium-Silicon-Germanium, Ferrum-Rhodium, etc. During the last three decades, a variety of cooling systems have been proposed using magnetic materials at room temperature. In this thesis, an AMRR system using FeRh as refrigerant is studied. For the simulation, a one-dimensional, time-varying mathematical model is developed. This model consists of two energy equations for the heat transfer fluid and the regenerator which are descritized by finite difference method. The simulation begins at an initial temperature distribution in the regenerator and fluid and takes time steps forward in time and space until the steady state is attained. On the other hand, in order to simulate the system, it was necessary to obtain and code the properties of the FeRh alloy, especially the entropy. The entropy of the alloy was calculated by using the specific heat experimental data. The coding procedure of properties was done by surface fitting and additional interpolation. To verify the developed model, the temperature distribution in the regenerator was obtained for all stages using Gadolinium as the refrigerant validated with some published results. At last, the performance of the refrigerator was optimized in terms of refrigerant porosity, mass flow rate, and type of the heat transfer fluid. The capability to give acceptable results of the performance of the system proves that the model is a powerful tool to predict the performance of AMRR systems. Besides, the high performance of the AMRR gained in this study, shows that this upcoming technology will be a suitable alternative for space cooling in the near future.

ÖZET

Aktif manyetik rejeneratif soğutma (AMRR) sistemlerinin tasarımı Gadoliium-Silicon-Germanium, Ferrum-Rhodium… gibi özel katı maddelerin magnetocaloric etkilerine göre yapılır. Son 30 yıl içerisinde birçok soğutma sistemi oda sıcaklığında manyetik materyaller kullanılarak denenmiştir. Bu tezde, FeRh soğutucu akışkan kullanılan AMRR sistem incelenecektir. Simülasyon için bir boyutlu, değişken zamanlı matematiksel model geliştirildi. Simülasyon rejeneratörde ilk sıcaklık değerinde başlar ve kararlı hale ulaşıncaya kadar devam eder. Sistemin simülasyonunu yapabilmek için, FeRh alaşımının özelliklerinin gözlenmesi ve kodlanması gerekir, entropi bu özelliklerin başında gelmektedir. Alaşımın entropisi özgül ısı deney dataları kullanılarak hesaplandı. Özelliklerin kodlanması ise surface fitting ve additional interpolation yöntemleri kullanılarak yapıldı. Geliştirilen modelin doğrulanmasında, rejeneratöründeki sıcaklık dağılımı bütün aşamalarda soğutucu akışkan olarak Gadolinium kullanılarak gözlendi ve önceden yayınlanmış sonuçlar ile doğrulandı. Son olarak, soğutucunun performansı soğutucu akışkan porozitesi, debisi ve ısı transfer akışkanı yönünden optimize edildi. Sistemin performansı hakkında kabul edilebilir ve geçerli sonuçlar vermesi bu modelin AMRR sistemlerinin performansını ölçmede iyi bir araç olduğunun göstergesideir. Bu çalışma AMRR nin yüksek performansını göstermenin yanında gelecekteki teknolojilerin soğutmada geçerli bir alternatif olacağını göstermektedir.

ACKNOWLEDGEMENT

First and foremost I would like to show my honest gratefulness to my mother and my father for dedicating their love to me all through my life; my beloved friend, Nazanin, who stood by me unconditionally during the fulfillment of this work; my brothers and sister-in-law, for their endless sensational support. Words fail me in expressing my love to them.

I owe my deepest gratitude to my supervisor, Prof. Dr. Hikmet Ş. Aybar, for his critic concern, supervision, and intelligent criticism in the improvement of this study and equipping me with essential tools.

I am heartily thankful to my co-supervisor, Prof. Dr. Murad P. Annaorazov, whose encouragement, guidance, invaluable suggestions, and support from the early to the concluding level enabled me to develop an understanding of the subject.

My sincere and heartfelt thanks to my uncle, Mr. Nosratollah Sanie, who has always encouraged me to continue my education and provided me the necessities for my progress in personal and social life.

It is an honor for me to thank the Turkish Government for endowing me with full scholarship.

Special thanks to Mr. Altuğ Caner Hekimoğlu for translating the abstract into Turkish.

At last but not least, I offer my regards and blessings to the staff and academics of Eastern Mediterranean University, particularly those of Mechanical engineering department, and all of those who supported me in any respect during the completion of the project.

To My Family

TABLE OF CONTENTS

LIST OF TABLES

LIST OF FIGURES

LIST OF SYMBOLS

List of Variables

a_s	specific area (1/m)
A_c	cross-sectional area (m^2)
B	magnetic field induction (Tesla)
c	specific heat (J/kgK)
d	dispersion factor (-)
d_h	particle diameter (m)
f_f	friction factor (-)
k	conductivity (W/mK)
k_1	regenerator effective conductivity (W/mK)
k_2	fluid effective conductivity (W/mK)
h	heat transfer coefficient (W/m^2K)
h_{eq}	equivalent heat transfer coefficient (W/m^2K)
H	magnetic field strength (A/m)
$\dot{m}$	mass flow rate (kg/s)
M	number of time interval
M	mass magnetization (Am^2/kg)
N	number of space interval
p_1	magnetization period (s)
p_2	cold blow period (s)
p_3	demagnetization period (s)
p_4	hot blow period (s)
$\dot{Q}$	energy generation (W)
s	specific entropy (J/kgK)

t	time (s)
T	absolute temperature (K)
T_c	cold end temperature (K)
T_h	hot end temperature (K)
u	velocity (m/s)
$\dot{V}$	volume flow rate (m^3/s)
V	volume (m^3)
$\dot{W}$	input work (W)
x	space (m)

Subscript

el	electric
f	fluid
lat	lattice
mag	magnetic
r	regenerator
s	surface
tot	total
w	wall

List of Greek Symbols

δ	steady state temperature criterion (K)
Δ	change
ε	porosity (-)
Φ	utilization (-)

Φ	viscous dissipation (W/m^3)
μ	viscosity (kg/ms)
ρ	density (kg/m^3)
ρ_{el}	electrical resistivity (Ω m)

Physical Constants

e	elementary charge (1.60217646×10^{-19} C)
k_B	Boltzmann constant (1.38×10^{-23} J/K)
μ_0	permeability ($4\pi.10^{-7}$ N/A)

LIST OF ABBREVIATIONS

AF	Antiferromagnetic
AMR	Active Magnetic Regenerator
AMRR	Active Magnetic Regenerative Refrigeration
Bi	Biot Number
CFC	Chlorofluorocarbon
COP	Coefficient of Performance
CHX	Cold Heat Exchanger
F	Ferromagnetic
Fe	Ferrum (iron)
Gd	Gadolinium
Ge	Germanium
HC	Hydrocarbon
HCFC	Hydrochlorofluorocarbons
HFC	Hydrofluorocarbons
HHX	Hot Heat Exchanger
MCE	Magneto Caloric Effect
MR	Magnetic Refrigeration
NTU	Number of Transferred Units
ODS	Ozone Depleting Substances
RBMR	Rotating Bed Magnetic Refrigerator
Rh	Rhodium
RMMR	Rotating Magnet Magnetic Refrigerator

CHAPTER 1

INTRODUCTION

From the viewpoint of economy and health, refrigeration is one of the most important issues around the world. It is used for a vast range of applications such as, food preservation, air dehumidification, ice making, and specially for air conditioning [1].

This dissertation offers a one-dimensional mathematical model of an Active Magnetic Regeneration Refrigerator (AMRR). Magnetic Refrigeration at room temperature is an arising, energy-efficient technology which is predicted to be an environment-safe substitute for traditional cooling systems [2].

Nowadays, vapor-compression systems are widely used for industrial and household purposes; for instance, more than 25% of residential electric demand and 15% of commercial demand is consumed by such systems in the United States [1]. The efficiency of these systems is 5-10% of Carnot cycle [3]. On the other hand, in spite of the fact that the Montreal Protocol has been confining the deleteriousness of Ozone Depleting Substances (ODS), the greenhouse effect has not been eliminated entirely[1] [3]; thus, as the solicitude for global warming increases, the need for environmentally benign and energy-efficient technologies like magnetic refrigeration rises.

[1] Although chlorofluorocarbons (CFC) and Hydrochlorofluorocarbons (HCFC) are replaced with more environmentally friendly Hydrofluorocarbons (HFC) and Hydrocarbons (HC), these refrigerants are still harmful because of their potential for global warming and lack of safety in some applications [1].

According to the experiments, MR systems have gained Coefficient of Performance (COP) of 3 to 10 [2] and their efficiency is 30-60% of Carnot cycle [3]. In addition, a solid material is applied as the refrigerant, which is not harmful to the environment, and the use of HFCs is omitted; consequently, it is believed that MR will have a terrific feasible future.

MR is firmly related to Magnetocaloric Effect (MCE). When the magnetic field is applied to a material, MCE causes changes in its temperature. Theoretically, MCE is assumed to be an internally-reversible process; so, the material will return to its initial condition once the magnetic field is removed.

1.1 Objectives of the Study

Magnetic refrigeration is an emerging technology which has the potential to substitute the conventional vapor-compression technology. A simulation method will facilitate the procedure of development of AMRRs.

The primary purpose of this thesis is to introduce a model which has the capacity to predict the performance of different AMR systems with various configurations.

The second aim of the project is to predict and optimize the performance of an AMR system consisted of FeRh particles as the refrigerant. In this special AMRR, the porosity of the regenerator and mass flow rate of the heat transfer fluid are to be optimized. Water and water/ethylene glycol mixture will be utilized as the heat transfer fluid.

In order to apply FeRh as the refrigerant it is necessary to find entropy diagram of the alloy as a function of temperature and magnetic field. This is considered as the third aim of this study.

1.2 Thesis Organization

Chapter 2 explains the basics of the MR technology by describing magnetocaloric effect, magnetic refrigeration, active magnetic refrigeration, and the thermodynamic principle of magnetic cooling. A brief history of magnetic refrigeration and various devices is also included in this chapter.

As expressed earlier, FeRh is chosen as the refrigerant in this thesis. Chapter 3 introduces this alloy concisely. Besides, previous mathematical models are presented and reviewed.

Chapter 4 shows what properties of FeRh alloy are applied and how they are coded in the model. This chapter, particularly, focuses on entropy.

Chapter 5 is main chapter of this dissertation. The complete procedure of deriving the mathematical model is expressed in this chapter. It also contains the suitable correlations and fluid properties. A verification of the model is mentioned at the end of the chapter.

Chapter 6 illustrates the results of the optimization process. Te results of porosity and mass flow rate optimization processes are also discussed. In addition, the effect of water and water/ethylene glycol mixture is compared.

Chapter 7, as the conclusion, summarizes the importance of magnetic cooling in practice and modeling. The outcomes of this work are discussed and some recommendations are made for the future work.

It should be noted that the modeling code is shown in the appendix.

CHAPTER 2

MAGNETOCALORIC EFFECT AND MAGNETIC REFRIGERATION

2.1 Brief History of Magnetic Refrigeration and Devices

The basis of MR goes back to 1881 when Warburg discovered MCE in iron. About 24 years later, in 1905, Langevine described that the variations in paramagnetic magnetization results in reversible temperature changes [4]. MCE was demonstrated theoretically by Weiss and Piccard in 1918 [2]. In 1926-1927, Giauque and Debye recommended using adiabatic demagnetization process in order to decrease the temperature of paramagnetic salts. It was experimentally performed by Giauque and McDougall in 1933 on a sample of gadolinium sulfate, $Gd_2(SO_4)_2.8H_2O$. They obtained the minimum temperature of 0.25K from 1.5K under the magnetic field of 8 kOe [4][2]. First MR system at room temperature was invented by Brown in 1976. He could achieve a temperature span of 47K between hot end (T_h = 319K) and cold end (T_c = 272K) after 50 cycles. His reciprocating constantly-performing system proved that it is possible to attain much higher temperature ranges than the largest discovered MCE. Two years later, Steyert presented the idea of active magnetic regenerator (AMR), on which most of the current MR systems are based, to be used in refrigeration systems in order to ease the heat transfer [5].

Brown and Steyert developed an AMR in 1982 based on Brayton cycle [6]. They showed that it is possible to reach much higher temperature raises than just the adiabatic temperature lift of the MR by using the magnetic material at the same time as a regenerator and as the active magnetic component [5].

A recuperative rotary system was designed by Kirol and Dacus in 1988 based on Ericsson cycle where the fluid was in contact with refrigerant except in magnetization and demagnetization [7]. The refrigerators constructed since then are based on a regenerative design [5].

A proof-of-principle magnetic refrigerator was built by Astronautic Corporation of America under the supervision of Zimm in a three-year period from 1994 to 1997. This refrigerator showed that AMR is a feasible and competitive technology [5].

In 2001, Astronautics Corporation utilized a permanent magnetic in an AMR in order to produce magnetic field. This system revealed that it is possible to eliminate the use superconductors and electromagnets and AMRs could also be designed for domestic and automotive applications [8].

Second generation of magnetic refrigerators was devised by Zimm in 2003 [9]. In the second generation refrigerators, a reciprocating machine was replaced with a rotary one and permanent magnetic was applied as the source of magnetic field. These AMRs are called Rotating Bed Magnetic Refrigerator (RBMR) these days [5].

The RBMR operated easily and unfailingly for more than 1500 hours. About 1500 tests were performed on the RBMR. One of the most important problems was instrumenting the stirring magnetocaloric beds. In addition, building the refrigerator in large scales had some difficulties with the central valves and piping. Because of

these restrictions, ACA started studying a new arrangement of the magnet and magnetocaloric beds; which led to third generation of magnetic refrigerators [5].

In the third generation of magnetic refrigerators, the magnet rotates instead of bed and the bed is fixed completely. These refrigerators which were introduced in 2007 by Zimm are called Rotating Magnet Magnetic Refrigerator (RMMR) [10]. The major benefit of the fixed beds is that the valving and timing of the fluid flows through the beds and heat exchangers are easier than that of RMBR [5].

Fig.2.1 shows the growing number of machines invented since 1970. It is predicted that this technology will be commercialized in 2015 [5].

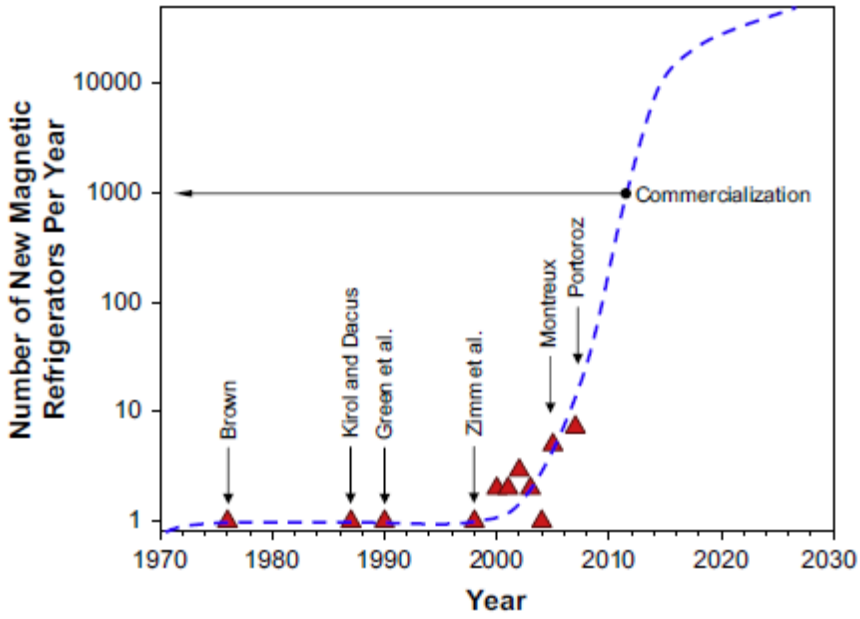

Figure 2.1: Number of magnetic refrigerators vs. year [5].

2.2 Magnetocaloric Effect (MCE)

Magnetocaloric effect is a thermomagnetic effect which is defined as adiabatic temperature changes (ΔT_{ad}) in a reversible process, under the influence of magnetic field.

The total entropy of a magnetic material, at constant pressure, is a function of magnetic field strength and the absolute temperature. It is a combination of three

different entropies: lattice entropy, S_{lat}, electronic entropy, S_{el}, and magnetic entropy, S_{mag} [11].

$$s_{tot}(T,H) = s_{mag}(T,H) + s_{lat}(T) + s_{el}(T) \tag{2.1}$$

As it is shown in Eq.2.1, lattice and electronic entropies are dependent on absolute temperature only, whereas the magnetic entropy is reliant upon absolute temperature as well as magnetic field strength.

Lattice entropy is derived from lattice vibrations of the material, electronic entropy is based on free electrons and the magnetic entropy is related to degrees of freedom of the electronic spin system [2].

When the material is subjected to an external magnetic field, the spins of the electrons are lined up along the direction of the magnetic field. If the magnetic field is removed, in the absence of hysteresis, they will return to their initial conditions which means this process is reversible [2] (see Fig.2.2).

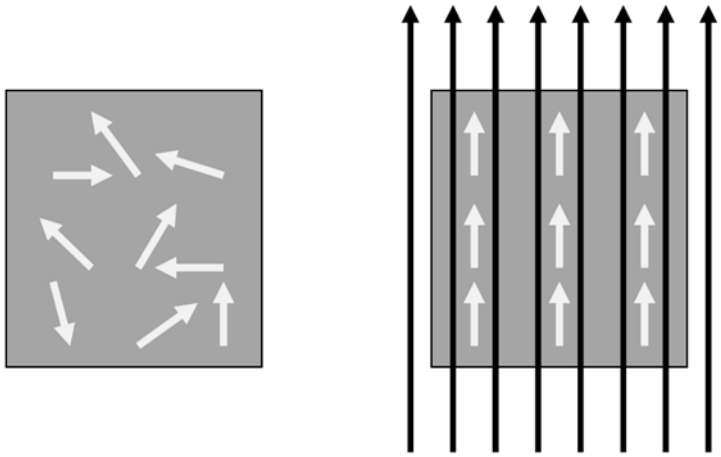

No Field Applied Field

Figure 2.2: The effect of magnetic field on the spins.

The arrangement of the spins causes the magnetic entropy to decrease. If the hysteresis is neglected, in an adiabatic process, the total entropy remains constant;

thus, in order to compensate the reduction of magnetic entropy, electric and lattice entropies will increase which leads to the raise in temperature. In a reversible process, once the magnetic field is removed, the material returns to its initial temperature.

On the other hand, if the magnetic field is applied, in an isothermal process, the magnetic entropy and therefore the total entropy reduces, but electric and lattice entropies remain unchanged.

Fig.2.3 shows the relationship between isothermal and isentropic processes under magnetic field. In this figure Δs_{mag} accounts for magnetic entropy change.

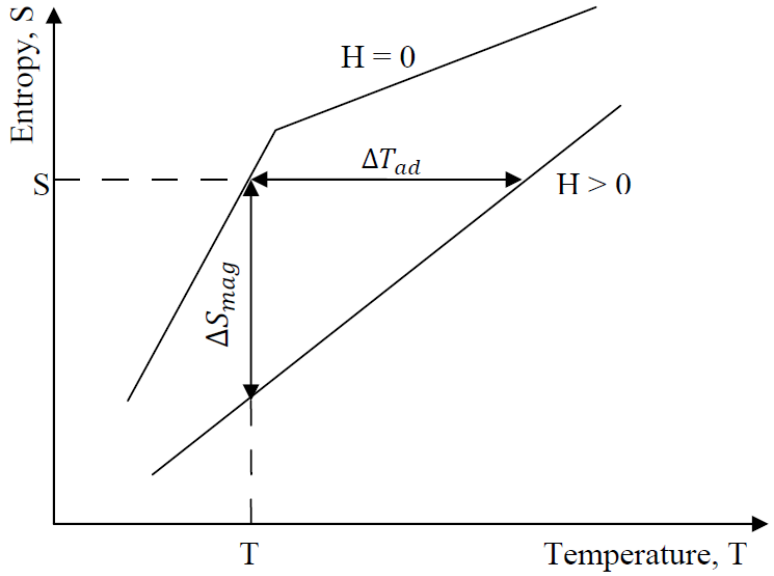

Figure 2.3: Relationship between adiabatic temperature change and isothermal magnetic entropy change.

Fig.2.4 shows how the amount of magnetocaloric effect depends on the initial temperature of the material and the strength of magnetic field for a sample of Gadolinium (Gd) [1].

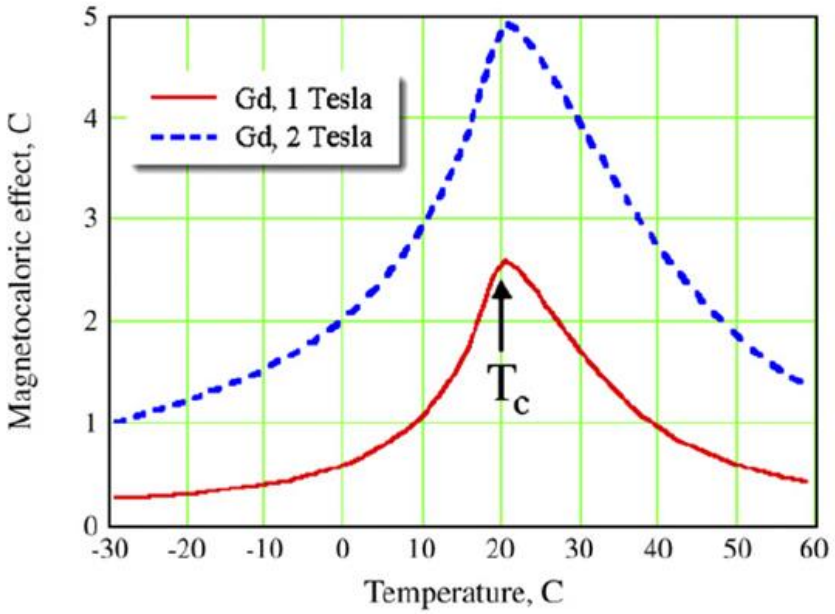

Figure 2.4: Relationship between magnetocaloric effect and initial temperature and strength of magnetic field, T_C accounts for Curie temperature [1].

According to Fig.2.4 the peak for ΔT_{ad} happens at Curie temperature[1], so it is seen that the magnetocaloric effect is confined to a limited temperature span.

2.3 Magnetic Refrigeration (MR)

The purpose of refrigeration is to deliver heat from a cold reservoir to a hot reservoir. In accordance with the second law of thermodynamics, some kind of work must be done on the system to achieve this. In traditional vapor-compression systems, mechanical work is used, but in magnetic refrigeration, magnetic work is applied.

For magnetic refrigeration a magnetocaloric material is used as the refrigerant. Magnetic work is attained through magnetization and demagnetization of this solid refrigerant. In order to ease the heat delivery, a fluid such as water or a combination of water-glycol (as an antifreeze) is utilized. Magnetic field is produced in three ways; superconducting solenoids, electromagnets, and permanent magnets

[1]Curie temperature for a ferromagnetic material is the temperature above which it loses its ferromagnetic ability.

among which the permanent magnet is the most useful one, since it is applicable to automotive and household applications.

A simple MR cycle and the associated T-S diagram are shown in Fig.2.5a [2] and b [12], respectively.

The cycle includes four steps:

1. Adiabatic magnetization warms the refrigerant above the ambient temperature.
2. The heat is rejected to the hot reservoir in an isothermal process.
3. Adiabatic demagnetization cools the refrigerant under the ambient temperature.
4. Under an isothermal process, the heat is absorbed from cold reservoir by the cold refrigerant.

The general principle of MR is analogous to conventional vapor-compression refrigeration. This analogy is depicted in Fig.2.6 [1].

In a vapor-compression cycle, compressing (applying magnetic filed in MR) the refrigerant increases its temperature, then, the compressed (magnetized) refrigerant rejects energy to the hot reservoir, afterwards, the refrigerant is expanded (demagnetized) which leads to reduction in its temperature, the expanded (demagnetized) refrigerant then absorbs heat from the cold -reservoir.

Throughout the last ten years several AMRRs have been devised and different materials such as FeRh have been discovered to have high MCE.

There are three basic thermomagnetic cycles: Carnot cycle, Ericsson cycle, Brayton cycle.

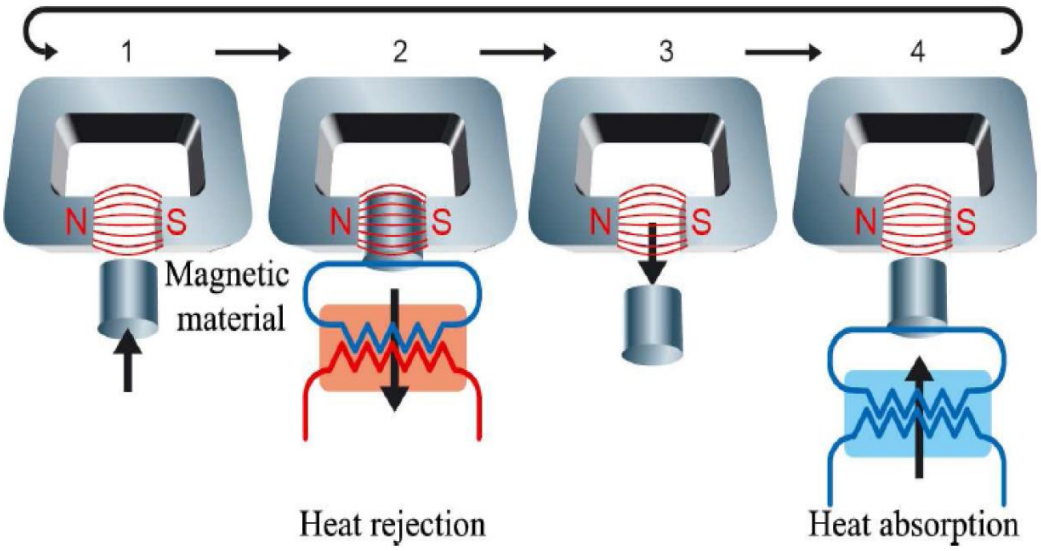

a

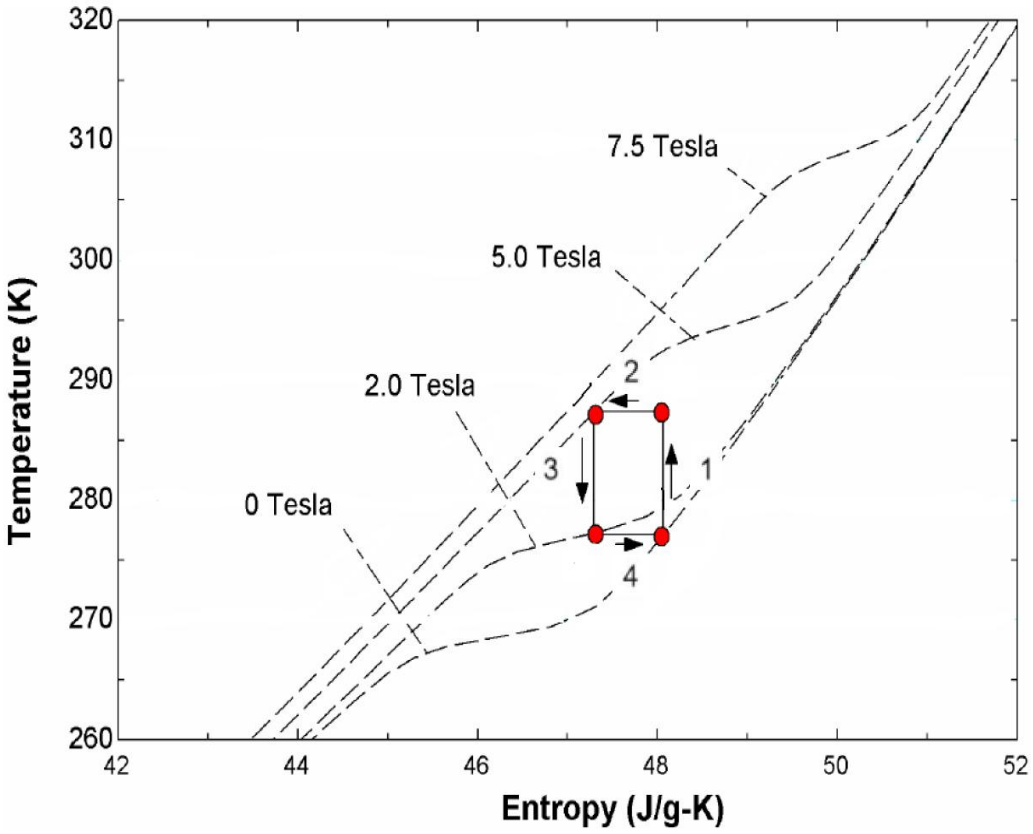

b

Figure 2.5: (a) Schema of a simple MR cycle [2], (b) Associated T-S diagram [12].

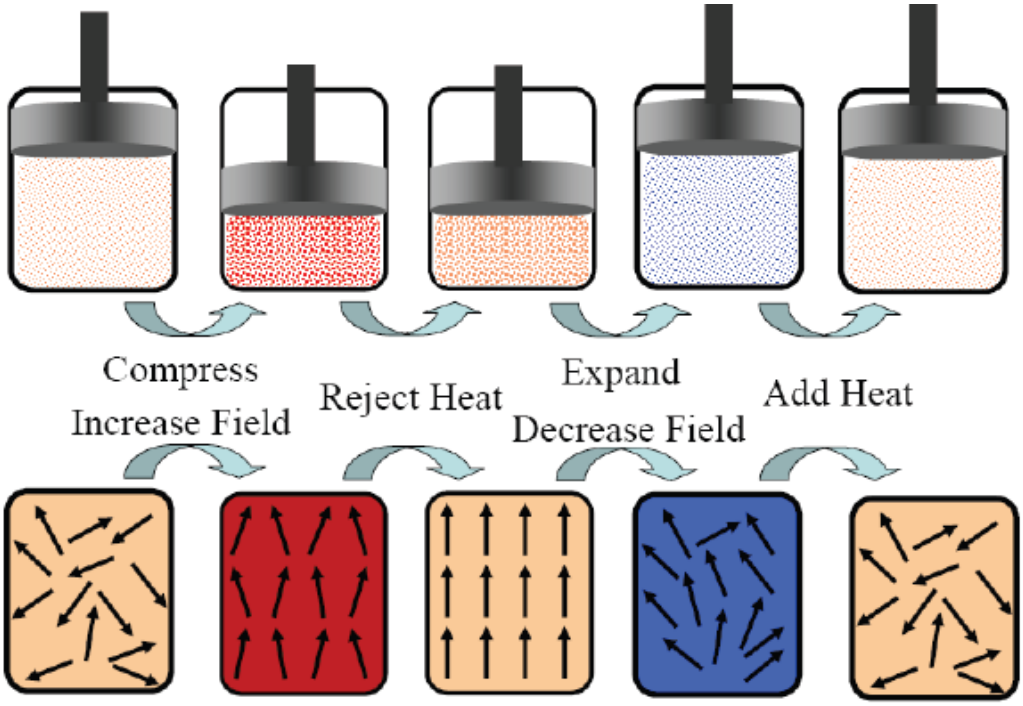

Figure 2.6: Analogy between MR and vapor-compression systems [1].

2.3.1 Carnot Cycle

Carnot cycle consists of two isothermal and two isentropic processes. Fig.2.7 shows a schema of the cycle [13].

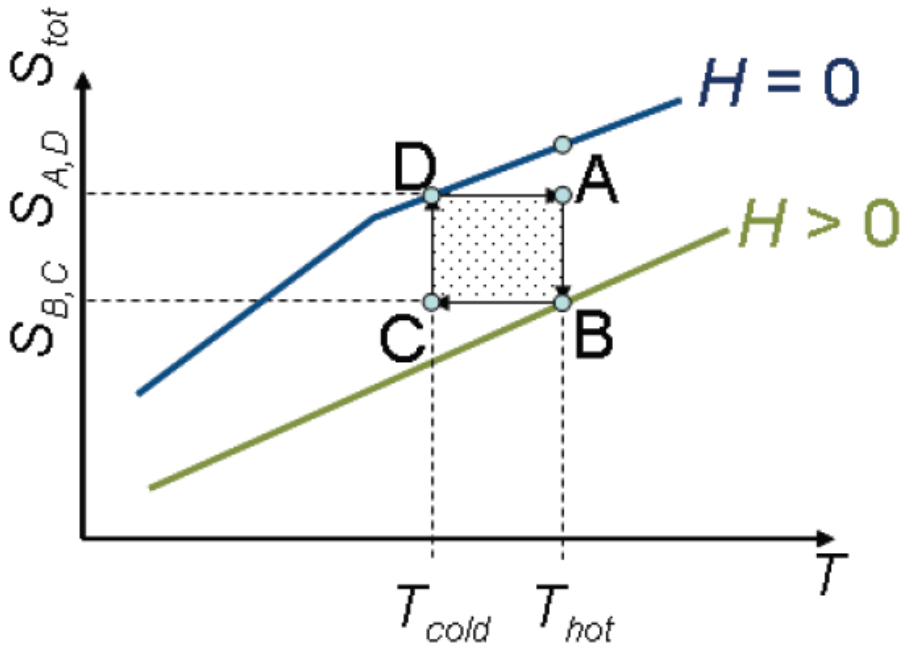

Figure 2.7: Thermomagnetic Carnot cycle [13].

From A to B an isothermal magnetization occurs while the refrigeration rejects heat as the magnetic field rises to the maximum magnetic field. From B to C the temperature of the refrigerant is decreased by partial adiabatic demagnetization. From C to D the magnetic field is removed under an isothermal demagnetization, meanwhile the refrigerant absorbs heat from the cold heat exchanger. From D to A the refrigerant undergoes partial adiabatic magnetization as the magnetic field enhances until the refrigerant returns to the initial state.

For convenient refrigeration, the range of temperature between the hot and cold reservoirs is confined by the high and low magnetic field strength. As a result, it is impossible o choose the hot and cold reservoir freely. On the other hand, varying magnetic field is required in this cycle, so each of the four points experiences a particular magnetic field. Therefore, an electromagnet or superconducting solenoid is

required where the field can be controlled [13]. Thus it is obvious that the Carnot cycle is not suitable for normal refrigeration.

2.3.2 Ericsson Cycle

Regeneration is needed in order to make the temperature range free from the cycle. The normal condition for MR is attained in this way.

Ericsson cycle includes two isothermal and two isofield processes as shown in Fig.2.8 [13]. During the isofield process, the magnetic field strength remains constant.

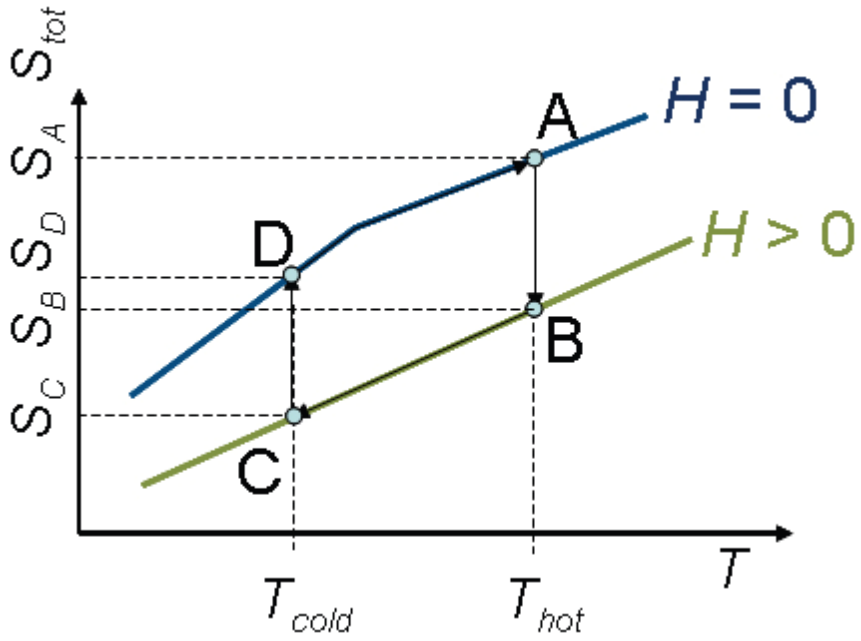

Figure 2.8: Thermomagnetic Ericsson cycle [13].

From A to B the refrigerant undergoes an isothermal magnetization, so heat is rejected. From B to C under an isofield process, the temperature of the refrigerant reduces and regeneration occurs. From C to D isothermal demagnetization happens while heat is absorbed by the refrigerant and from D to A isofield heating is achieved with regeneration.

2.3.3 Brayton Cycle

This cycle is very similar to the Ericsson cycle. In Brayton cycle isothermal magnetization and demagnetization are replaced with adiabatic magnetization and demagnetization. This cycle is shown in Fig.2.9 [13].

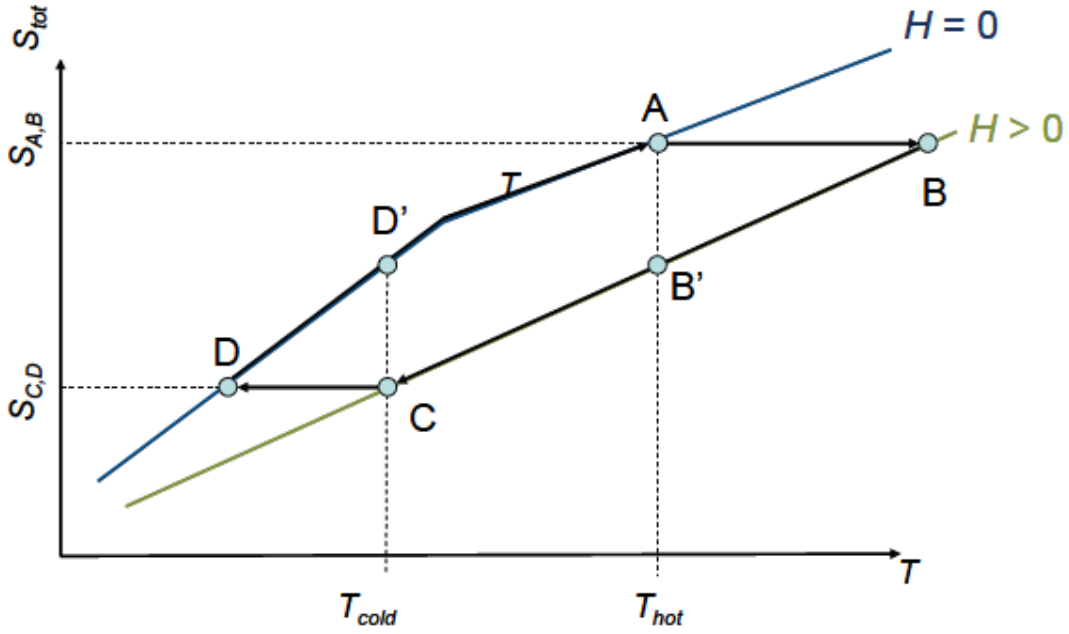

Figure 2.9: Thermomagnetic Brayton cycle [13].

From A to B an adiabatic magnetization leads to temperature increase, from B to C the heat is rejected to a hot reservoir under an isofield process and regeneration occurs by transferring the heat from the refrigerant to the heat transfer fluid, from C to D adiabatic demagnetization occurs while the temperature of the refrigerant decreases and from D to A the refrigerant absorbs heat from a cold reservoir with regeneration during which the heat is transferred from the refrigerant to the heat transfer fluid.

2.4 Principles of Magnetic Refrigeration

According to Eq.2.1 the total derivative of the total entropy is defined as it is shown in Eq.2.2 [14].

$$ds(T,H) = \left(\frac{\partial s}{\partial T}\right)_H dT + \left(\frac{\partial s}{\partial H}\right)_T dH \tag{2.2}$$

where T is temperature, s is specific entropy H is magnetic field strength.

One of Maxwell equations can be used in order to find the relationship between entropy and magnetic field, providing the magnetization and entropy are continuous functions of the temperature and magnetic field [15]. Eq.2.3 shows how entropy and mass magnetization are related [16].

$$\left(\frac{\partial s}{\partial \mu_0 H}\right)_T = \left(\frac{\partial M}{\partial T}\right)_H \tag{2.3}$$

where μ_0 is vacuum permeability and M accounts for mass magnetization.

On the other hand the relationship between specific heat and entropy is given by [14]:

$$\frac{c_H}{T} = \left(\frac{\partial s}{\partial T}\right)_H \tag{2.4}$$

where c_H is the specific heat in an isofield process.

By combining Eqs. 2.1 and 2.4, Eq.2.5 is obtained:

$$\begin{aligned} c_H &= T\left[\frac{\partial}{\partial T}\left(s_{mag} + s_{lat} + s_{el}\right)\right]_H = T\frac{\partial s_{mag}}{\partial T} + T\frac{\partial s_{lat}}{\partial T} + T\frac{\partial s_{el}}{\partial T} \\ &= c_{mag} + c_{lat} + c_{el} \end{aligned} \tag{2.5}$$

where c_{mag} , c_{lat} , and c_{el} are magnetic, lattice, and electronic entropies, respectively.

Substituting Eqs. 2.3 and 2.4 into 2.2, entropy as function of temperature and magnetic field strength is obtained:

$$ds = \frac{c_H}{T} dT + \left(\frac{\partial M}{\partial T}\right)_H d\mu_0 H \tag{2.6}$$

Setting dT equal to zero and integrating Eq.2.6 leads to isothermal magnetic entropy change.

$$ds = \left(\frac{\partial M}{\partial T}\right)_H d\mu_0 H \tag{2.7a}$$

$$\Delta s_{mag} = \mu_0 \int_{H_0}^{H_1} \left(\frac{\partial M}{\partial T}\right)_H dH \tag{2.7b}$$

In order to find ΔT_{ad}, ds in Eq.2.6 is set equal to zero and integrating gives:

$$dT = -\frac{T}{c_H}\left(\frac{\partial M}{\partial T}\right)_H d\mu_0 H \tag{2.8a}$$

$$\Delta T_{ad} = -\mu_0 \int_{H_0}^{H_1} \frac{T}{c_H}\left(\frac{\partial M}{\partial T}\right)_H dH \tag{2.8b}$$

Both Δs_{mag} and ΔT_{ad} are dependent on temperature and magnetic field strength and are regularly considered and stated as functions of temperature for a given ΔH, or as functions of magnetic field strength for a given temperature. The behavior of Δs_{mag} and ΔT_{ad} depends on the material, and is impossible to be predicted from the Eqs. 2.7b and 2.8b, and consequently, must be measured experimentally [15].

Eq.2.8 implies that high MCE is achieved by [2]:

1. Large magnetic filed
2. High $\left|\frac{\partial M}{\partial T}\right|$; which means that the magnetization must change rapidly with respect to temperature.
3. Small specific heat capacity.

2.5 Active Magnetic Regeneration Refrigeration (AMRR)

Permanent magnets do not need energy input to produce magnetic field, so they are used as the magnetic source. According to the literature, permanent magnets are restricted to about 2 Tesla, in which ΔT_{ad} normally is no greater than 8K [17]. This is considerably lower than the 30K to 50K temperature spans necessary for refrigeration. Consequently, the simple MR cycle shown cannot be used for realistic refrigeration and modern MR utilizes heat recovery in the form of regeneration to reach a broader range of temperature than that produced by the MCE. The AMR is

based on a porous magnetocaloric material as the refrigerant that allows a fluid to flow through. The fluid operates as a medium for heat transfer between the refrigerant and the cold reservoir and the hot reservoir. The regenerator may be constructed as parallel plates or packed beds and placed in an enclosed space with the fluid [2].

There are pistons or valves in both end of the enclosed space that shift the fluid into two heat exchangers situated in both ends. One heat exchanger is attached to the cold reservoir called cold heat exchanger (CHX) and the other heat exchanger is attached to the hot reservoir called hot heat exchanger (HHX).

Normally, the magnetic field is applied by bodily moving the regenerator into and out of a fixed magnetic field either linearly or rotationally. These two types are illustrated schematically in Fig.2.10 [5] [18].

Fig.2.11 depicts a very simple AMRR cycle [1]. Dashed lines in each step show the initial temperature of the regenerator. In Fig.2.11a, the initial temperature profile is for the regenerator in its demagnetized state. After applying magnetic field, the regenerator heats up because of the MCE of the refrigerants and the final magnetized regenerator temperature profile sets in. The amount the refrigerants warm is related to its initial temperature. Then, the cold fluid flows through the porous regenerator from the cold end to the hot end (Fig.2.11b). The regenerator is cooled by the fluid, dropping the temperature profile across the bed, and the fluid in turn is warmed by the regenerator, starting at a temperature around the temperature of the regenerator at the hot end. This temperature is higher than T_h, so heat is removed from the fluid at the hot reservoir as the fluid flows through the HHX. After the fluid becomes inert, the magnetic field is removed; causing the regenerator to cool down by the MCE (Fig.2.11c). The AMRR cycle is completed by pushing the

fluid to flow from the hot to the cold end of the regenerator (Fig.2.11d). The fluid is cooled by the regenerator, starting at a temperature below T_c and removes heat from the cold regenerator as the fluid passes through the CHX. The heat flow from cold to hot in this cycle is driven by the mechanical work input required to move the magnet with respect to the regenerator.

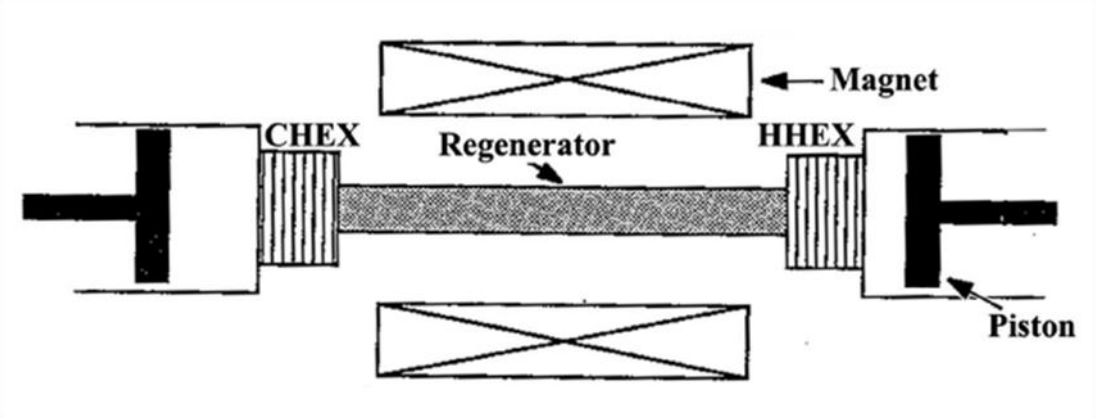

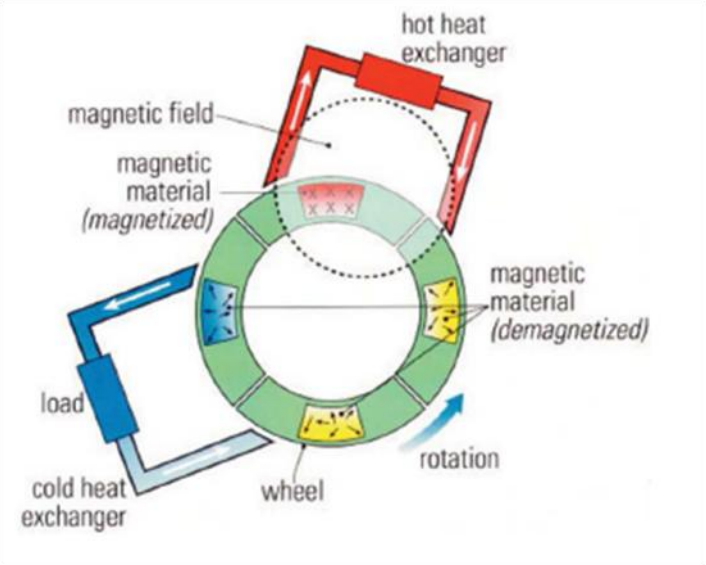

Figure 2.10: Reciprocating and rotating regenerators [11], [12].

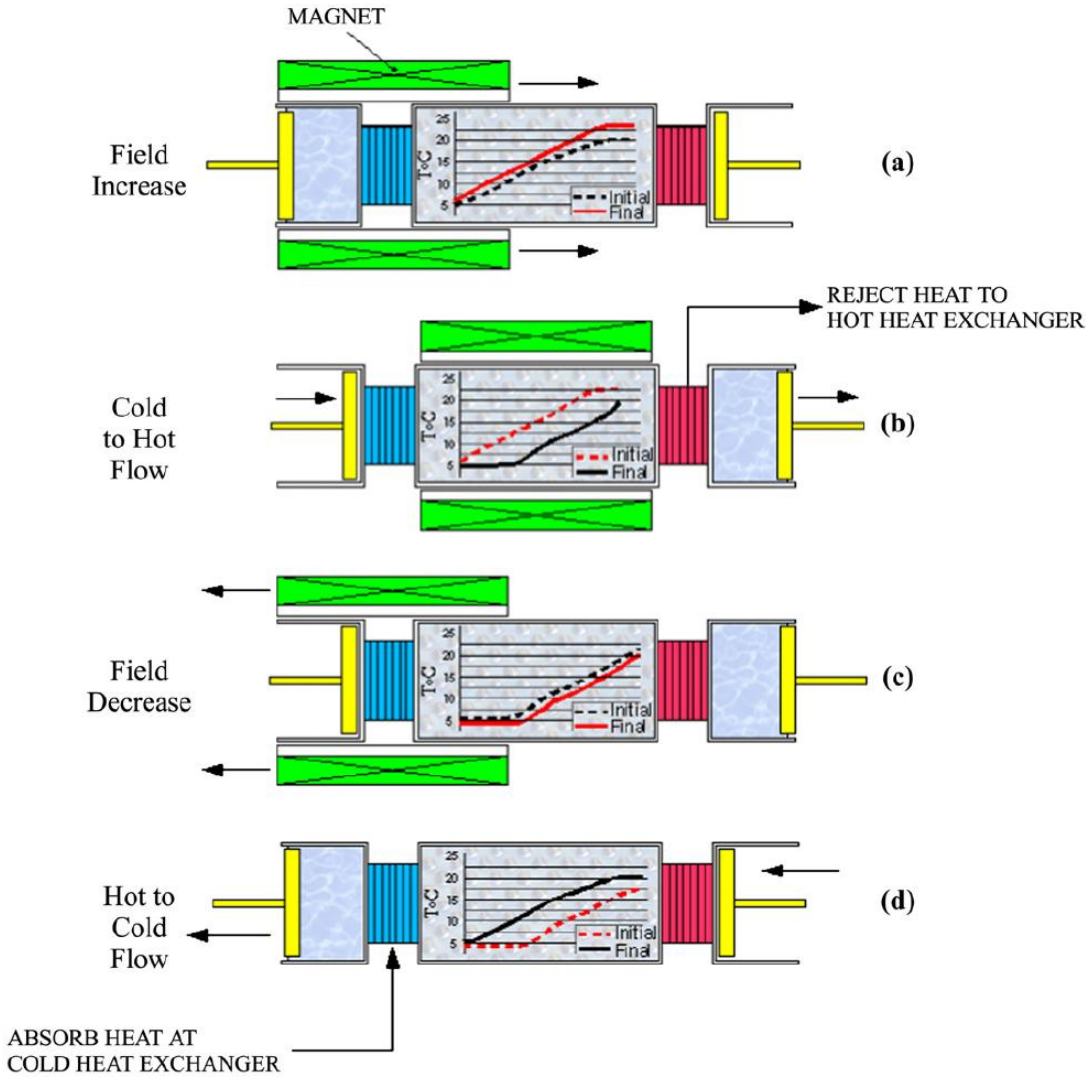

Figure 2.11: A simple AMRR cycle [1].

CHAPTER 3

BACKGROUND ON FeRh AND MR MODELING

3.1 An Introduction to FeRh

Ferrum-Rhodium (FeRh) alloys near an equiatomic composition show the first order phase transition antiferromagnetic-feromagnetic (AF-F) with rising temperature. Theoretically, if an alloy of FeRh undergoes an adiabatic magnetization of 7.5 Tesla, its temperature will change about 20 K providing the initial temperature is 333K [19].

In 1992, Annaorazov et al. [20] investigated the MCE, specific heat capacity and initial magnetic permeability of annealed and quenched FeRh alloys near the AF-F first-order phase transition. Figs.3.1 and 3.2 show the specific heat capacity and MCE of annealed and quenched samples, respectively.

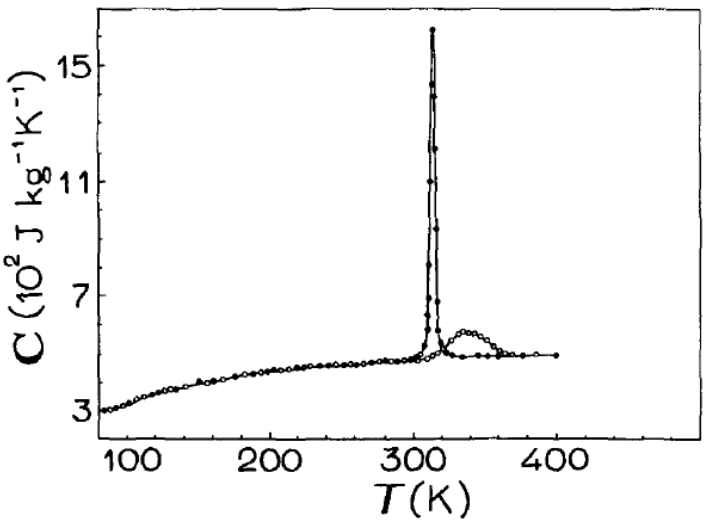

Figure 3.1: Specific heat capacity of annealed and quenched FeRh alloy [20].

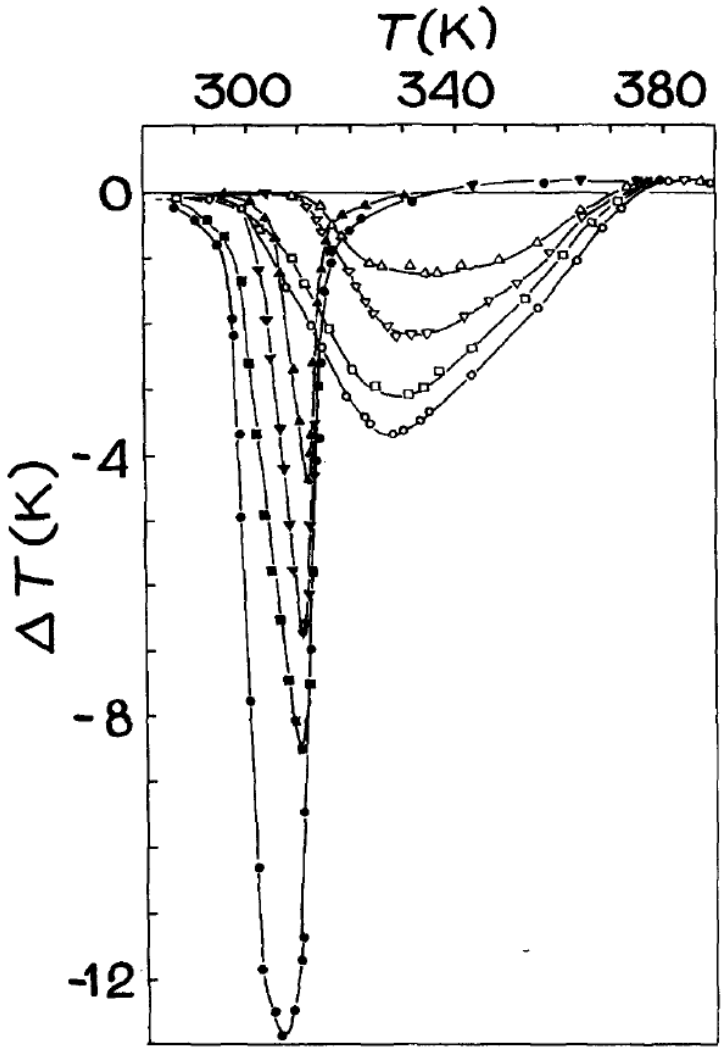

Figure 3.2: MCE on annealed and quenched FeRh samples [20].

A magnetic field of 2 Tesla applied on a quenched sample at 308.2 K led to reduction in temperature of 12.9 K in an adiabatic process and the value of the refrigerant capacity of a quenched sample at 1.95Tesla was reported as 135 J kg^{-1} K^{-1} which is considerably higher than in famous magnetocaloric materials [20]: 2.5 times larger than that of the Gd in 6.0 Tesla field [21].

The values of the entropy changes in the alloy in the transition process and the latent heat of the transition gained by various scientists are disposed between 5.5 J kg^{-1} K^{-1} and 19.26 J kg^{-1} K^{-1}, and between 3.43×10^3 J kg^{-1} and 6.74×10^3 J kg^{-1}, correspondingly. It is possible to compare the last data with a ~4.0×10^3 J kg^{-1}

thermal effect in Gd as a standard reference material under an isothermally applied field of 7.0 Tesla close to the Curie point (293 K) [21].

One of the advantages of the FeRh system is that it has the main characteristics of metals: its hardness is between 24 HRA and 42 HRA depending on thermal and mechanical treatment, the Young's modulus varies from 2.4×10^{11} Pa to 2.7×10^{11} Pa in the transition region; rupture strength is about 6.0×10^{8} Pa. The alloy yields to forging and rolling well, has an excellent corrosion resistance and large melting point of ~1880K [21].

A cooling cycle is proposed to transmit the heat to the surroundings at a temperature above the one of a low heat reservoir. The FeRh alloy can discharge the latent heat of transition along the thermal hysteresis loop branch corresponding to cooling the alloy only. The maximum temperature of such a branch is that corresponding to cooling the alloy in zero magnetic field. Consequently, this transition can be used to build up the cooling cycles only in the temperature region below the temperature corresponding to beginning of the reverse transition in zero field.

In Ref. [20] it was shown that the change in temperature of the FeRh alloy of ~13 K can be reached when the AF-F transition is induced in it by applying ~2-Tesla magnetic field, which is about 3 times greater than magnetocaloric effect of Gadolinium, as conventional magnetic refrigerant (ΔT = 14 K in B = 7 Tesla).

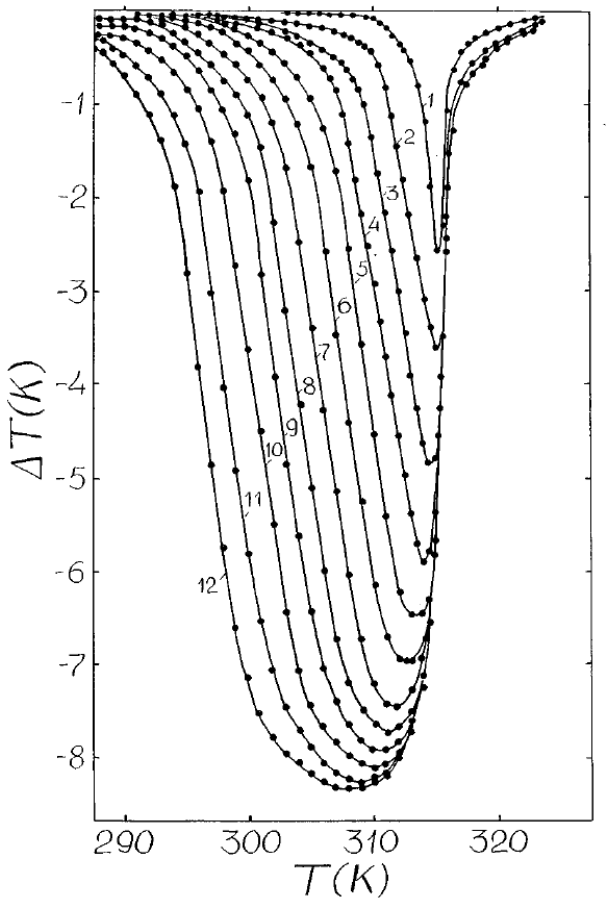

Figure 3.3: Temperature change in a FeRh alloy in various magnetic field. Numbers on the curves denote the magnetic filed in Tesla [21].

COP of cooling cycles around the AF-F transition in FeRh was calculated based on experimental data by Annaorazov et al. [21].

The value of the COP of the cycles gained from the entropy-temperature diagram drawn on the base of experimental data on specific heat capacity (Fig.3.1) and magnetocaloric effect (Fig.3.3), in the assumption that the heat exchange between magnetic refrigerant and the surroundings and between magnetic refrigerant and cold reservoir is absolutely perfect, was found to be 37 to 55 in a 2.5-Tesla field, which is the same as computed by the model entropy–temperature diagram of the sample drawn up under the assumption that the transition is perfectly isothermal [21].

The relation between COP and temperature under fixed magnetic fields is shown in Fig.3.4a, and Fig.3.4b depicts the relations between COP and magnetic field under constant temperatures [21].

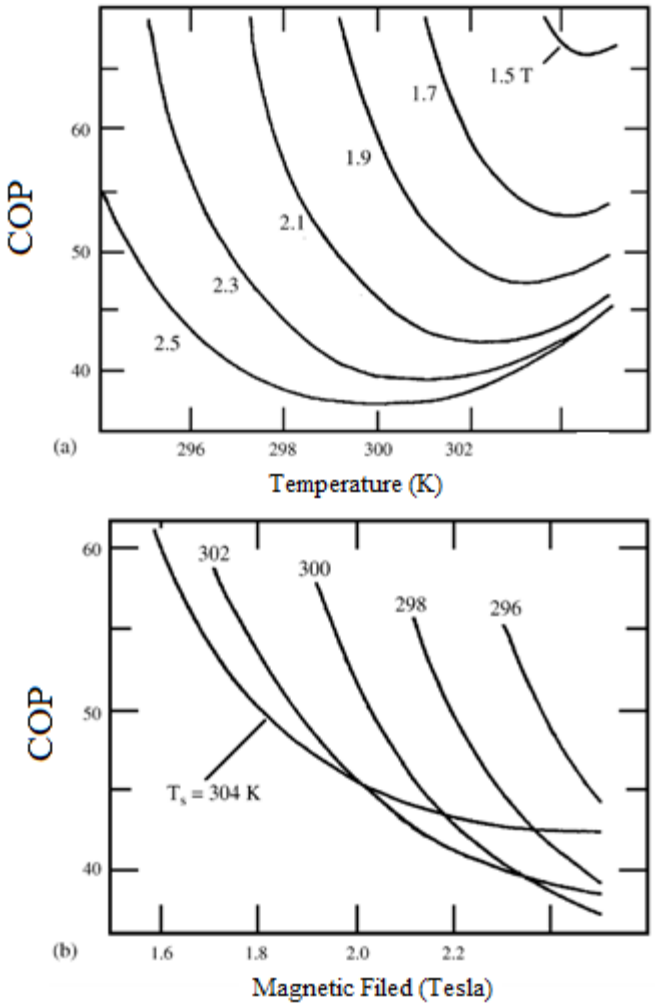

Figure 3.4: (a) COP vs. T under fixed magnetic fields, (b) COP vs. H for constant temperatures [20].

Unfortunately the price of Rhodium ($20,000 per kilogram) makes this material unsuitable for commercial device [8]. However there are some areas where the FeRh alloys system is irreplaceable, such as highly chemical aggressive environment.

3.2 Earlier Mathematical Models of AMRR

The first mathematical model was introduced by Schroeder et al. [22] in 1990 based on the AMRR shown in Fig.3.5.

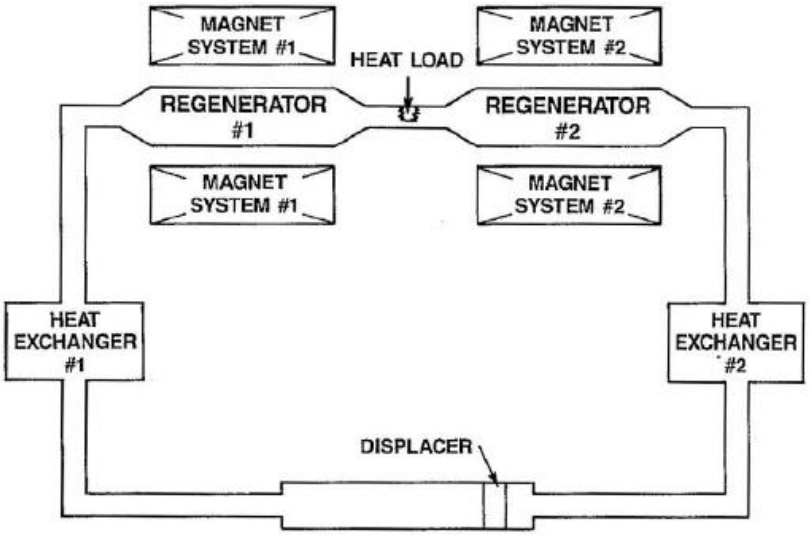

Figure 3.5: The schema of the AMR modeled by Schroeder [22].

In his model he used a porous bed of Gd as regenerator and compressed nitrogen as the heat transfer fluid and applied a magnetic field of 7 Tesla. He developed Eqs. 3.1a and 3.1b as energy equation for regenerator and fluid, respectively [2].

$$\rho_r c_r \frac{\partial T_r}{\partial t} = k_r \frac{\partial^2 T_r}{\partial x^2} + \frac{a_s h}{V_r}\left(T_f - T_r\right) \tag{3.1a}$$

$$\rho_f c_f \frac{\partial T_f}{\partial t} = k_f \frac{\partial^2 T_f}{\partial x^2} - \rho_f c_f u \frac{\partial T_f}{\partial t} + \frac{a_s h}{V_f}\left(T_r - T_f\right) + \frac{A_w h}{V_f}\left(T_w - T_f\right) + \dot{Q} \tag{3.1b}$$

where ρ, c, k, T, and V are densities, heat capacities, thermal conductivity, temperature, and volume, respectively while f and r as subscripts represent fluid and regenerator correspondingly. h is the heat transfer coefficient for the heat transfer

between the fluid and regenerator. a_s, A_w are the surface areas between the regenerator and fluid and the fluid and AMR enclosure walls, respectively. u is the fluid velocity and $\dot{Q}$ is heat generation.

Schroeder does not express how the MCE influences the model unambiguously; however he assumed adiabatic magnetization in the AMR. Besides, throughout the magnetization and demagnetization periods, the temperature of the fluid is assumed to be identical to that of regenerator. This assumption is acceptable, because the superconducting magnet needs several seconds to affect or eliminate the magnetic field, which seems to be sufficient time for heat transfer between fluid and regenerator; therefore, the temperature distinctions between the solid and the fluid are insignificant [2].

The result of his model and the real AMR is compared in Fig.3.6 [22]. According to the figure the difference between real and calculated models is about 5K which seems to be accurate enough for the first mathematical model.

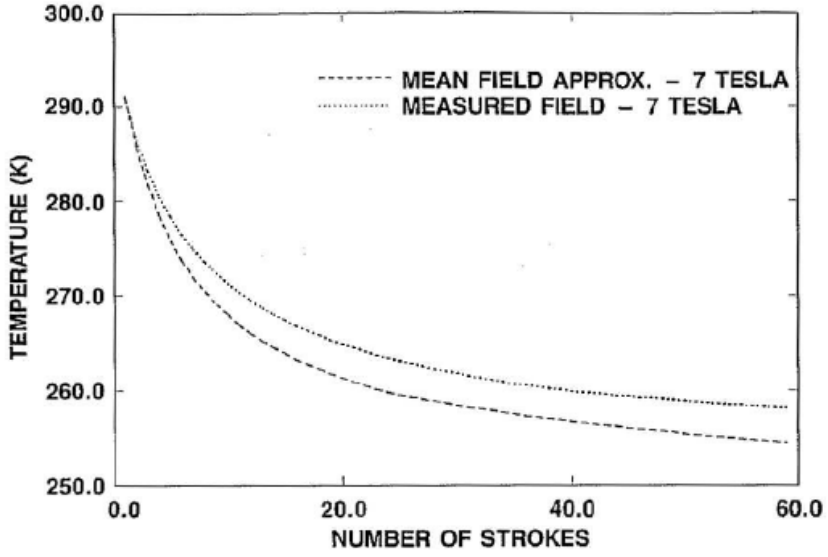

Figure 3.6: Comparison between real and mathematical model by Schroeder [22].

In 1998 Smaili et al. [23] developed a model based on two simple equations introduced by Matsumoto in 1990 [23]. Eqs.3.2a and 3.2b are regenerator and fluid energy equations, correspondingly [23].

$$m_r c_r \frac{\partial T_r}{\partial t} = a_s h L \left(T_f - T_r\right) \tag{3.2a}$$

$$\dot{m}_f c_f \frac{\partial T_f}{\partial t} = a_s h \left(T_r - T_f\right) \tag{3.2b}$$

where m_r and L are mass and length of regenerator, respectively and $\dot{m}_f$ stands for the mass flow rate of the fluid. Smaili et al. [23] has presented two dimensionless parameters in order to simplify the above equations. These two parameters are number of transferred units, NTU, and utilization, Φ, which are expressed in Eqs, 3.3 and 3.4

$$NTU = \frac{a_s h L}{\dot{m}_f c_f} \tag{3.3}$$

$$\Phi = \frac{\dot{m}_f c_f \tau}{m_r c_r} \tag{3.4}$$

where τ is time period in cold and hot blows.

The large thermal diffusivity of a gas when compared to that of the regenerator material validates the simplifications, i.e. the gas responds quickly to temperature changes in the surroundings. But if a liquid is used instead of a gas, the assumptions fail, due to the small diffusivity of the liquids in comparison with gases. Fig.3.7 shows the COP of AMR modeled by Smaili et al. versus utilization [23].

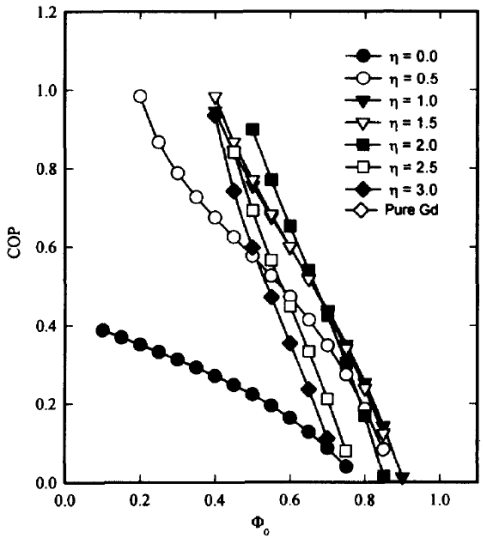

Figure 3.7: COP vs. Φ by Smaili et al. [23].

In 2005 Shir et al. [24] published a paper in which they had modeled an AMR consisting of Gd particles as regenerator and non-specific gas as the heat transfer fluid. The magnetic field of 2T was applied. The AMR is illustrated in Fig.3.8 [24].

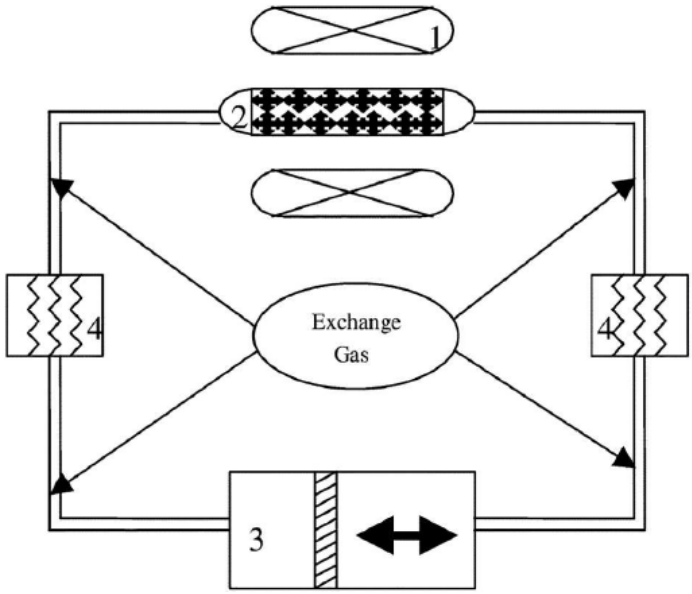

Figure 3.8: The representation of AMR modeled by Shir et al. [24].

The energy balance equation was simplified such that they did not consider axial conduction in the regenerator and fluid and ignored losses to the walls of the AMR and heat generation. Eqs. 3.5a and 3.5b give the energy equations for regenerator and fluid, respectively, as:

$$\frac{\partial T_r}{\partial t} = \frac{a_s h}{\rho_r c_r (1-\varepsilon)}\left(T_f - T_r\right) \tag{3.5a}$$

$$\frac{\partial T_f}{\partial t} + u\frac{\partial T_f}{\partial x} = \frac{a_s h}{\rho_f c_f \varepsilon}\left(T_r - T_f\right) \tag{3.5b}$$

where ε stands for porosity.

Typically, the convection in a fluid is larger than conduction. On the other hand, thermal conductivity in gas is negligible compared to solids. That is why the assumptions in Eqs. 3.5a and 3.5b are reasonable.

Fig.3.9 depicts the results of the mathematical modeling and experimental results, showing temperature profile at both ends of magnetic regenerative refrigeration test bed [24].

Room temperature AMRs usually utilize liquids as the heat transfer fluid in which the amount of the thermal conductivity is larger than that of gasses which invalidate the assumptions. Therefore, the efficiency of the AMR may be misvalued due to the simplifications and ignoring the losses to the walls [2].

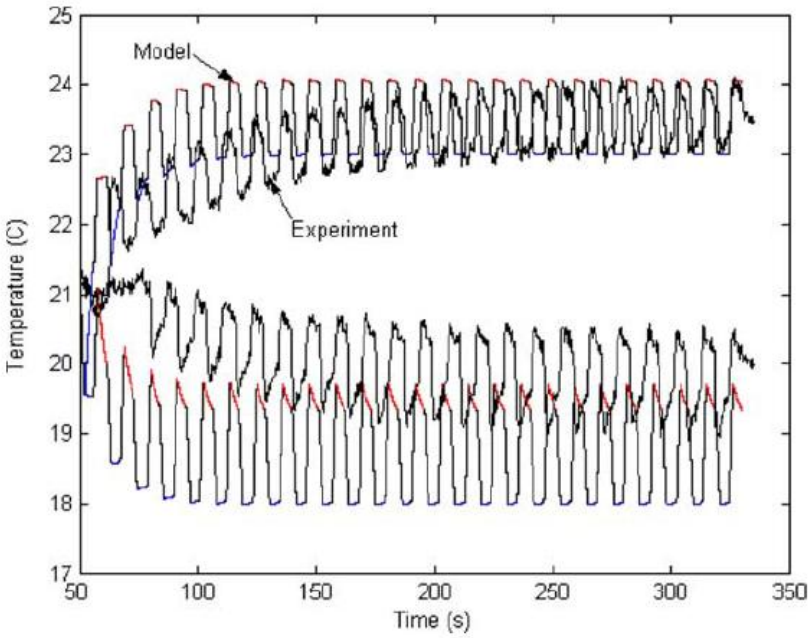

Figure 3.9: Comparison between the model and experimental results by Shir et al. [24].

One of the most complete models has been devised by Siddikov in 2005 [25]. In order to do the modeling, he used the unabridged energy equations presented in Eqs. 3.6a and 3.6b.

$$\frac{\partial T_f}{\partial t} = -\frac{\dot{V}}{A_c \varepsilon \rho_f c_f}\frac{\partial}{\partial x}\left(\rho_f c_f T_f\right) + \frac{h a_s}{\rho_f c_f \varepsilon}\left(T_r - T_f\right) + \frac{1}{\rho_f c_f \varepsilon}\frac{\partial}{\partial x}\left[\left(\varepsilon . k_f + d\right)\frac{\partial T_f}{\partial x}\right] + \frac{(1-\varepsilon)\dot{V}^3 f_f}{\varepsilon^4 {A_c}^3 D_p} \tag{3.6a}$$

$$\frac{\partial T_r}{\partial t} = \frac{h a_s}{\rho_r c_r (1-\varepsilon)}\left(T_f - T_r\right) + \frac{\partial T_r}{\partial H}\frac{dH}{dt} + \frac{1}{\rho_r c_r}\frac{\partial}{\partial x}\left[k_r . \frac{\partial T_r}{\partial x}\right] \tag{3.6b}$$

In Eq.3.6a $\dot{V}$ is volume flow rate and A_c accounts for cross-sectional area of the regenerator. The effective thermal conductivity is $\left(\varepsilon . k_f + d\right)$ where d is dispersion and a function of Reynolds number. $\frac{(1-\varepsilon)\dot{V}^3 f_f}{\varepsilon^4 {A_c}^3 D_p}$ is heat generation due to viscous dissipation. D_p and f_f are particles diameter and friction factor, respectively.

In Eq.3.6b the second term in right hand side of the equation represents the magnetic work done on the regenerator during magnetization and demagnetization. H stands for magnetic field strength.

Siddikov has divided the whole cycle into two main processes.

1. Active regenerator model in which the magnetization and demagnetization occur, so the flow rate and dispersion factor are zero in Eq.3.6a.
2. Passive regenerator model where the hot and cold blows take place, so the magnetization work term in Eq.3.6b is zero and the regenerator works as a thermal sponge.

He has modeled an AMR with Gd particles as regenerator and water as heat transfer fluid under a magnetic field of 5T.

Fig.3.10 states the temperature profile over the last complete AMR cycle which has been obtained by Siddikov [25].

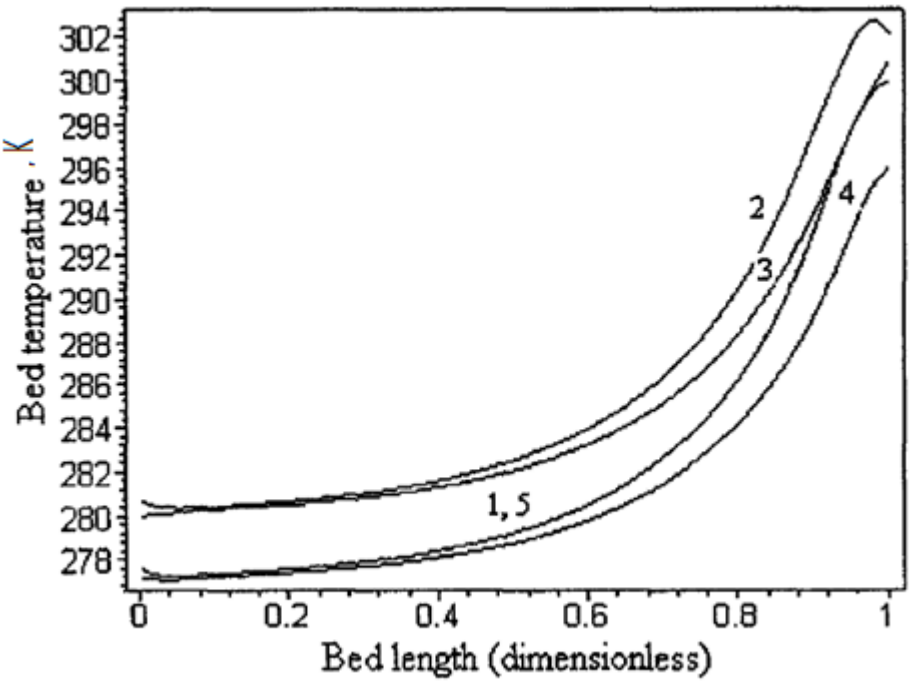

Figure 3.10: Temperature profile over the last complete cycle of AMR by Siddikov [25].

CHAPTER 4

PROPERTIES OF FeRh ALLOY SYSTEM

The properties which are considered for magnet material are entropy, density, and thermal conductivity. Special attention should be paid to the properties of the magnetic material, since these properties play a significant role in the performance and the efficiency of the system.

4.1 Density and Thermal Conductivity

In this study, the density is assumed to be constant and taken as 10164 kg/m^3 [26].

Thermal conductivity is related to electrical resistivity by Wiedemann-Franz equation [27]:

$$k_r = \frac{\pi^2}{3}\left(\frac{k_B}{e}\right)^2 \frac{T}{\rho_{el}} \tag{4.1}$$

where k_B and e are Boltzmann constant and elementary charge, respectively, T denotes temperature and ρ_{el} is electrical resistivity.

According to Eq.4.1, thermal conductivity is a function of electric resistivity and temperature. Researchers have shown that the electric resistivity is related to temperature and magnetic field. Fig.4.1 depicts how electrical resistivity is linked to temperature and magnetic field [28].

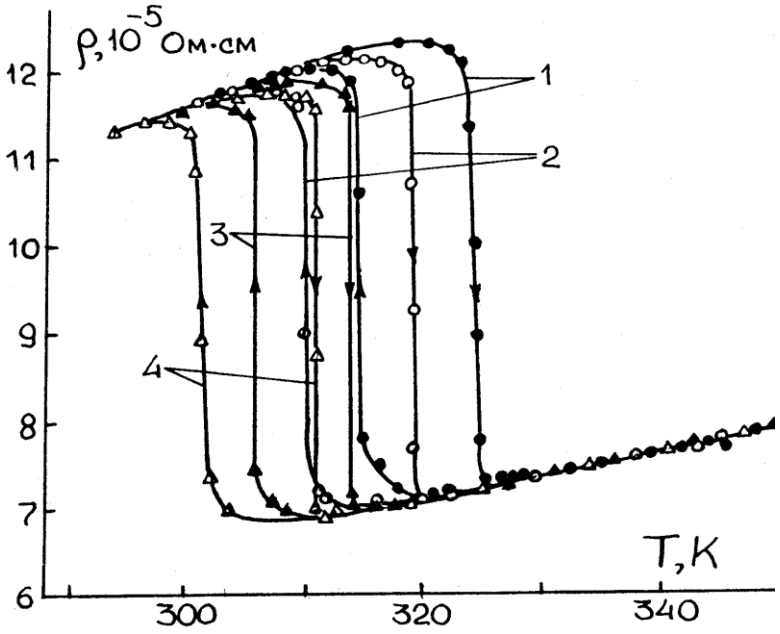

Figure 4.1: Electrical resistivity based on temperature and magnetic field. The numbers different magnetic fields: (1) 0T, (2) 0.72T, (3) 1.3T, (4) 1.74 Tesla [28].

4.2 Specific Heat and Entropy

In this study, the entropy of the FeRh system have been calculated through an indirect way based on specific heat and MCE data which had been already obtained by Annaorazov et al. [20].

The entropy of the material is gained according to the fact that entropy and specific heat are related by the following equation.

$$ds = \frac{c_p}{T} dT \tag{4.2}$$

The first step is to draw a diagram of specific heat versus temperature. Fig.4.2 shows c_p-T.

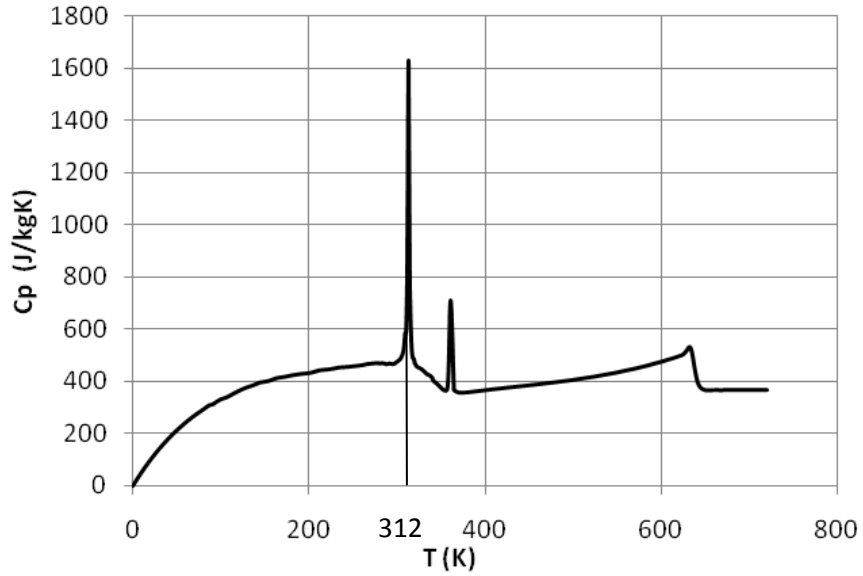

Figure 4.2: Specific heat vs. temperature.

In the second step, c_p/T versus temperature should be calculated and drawn. Fig.4.3 depicts the relation between c_p/T and T.

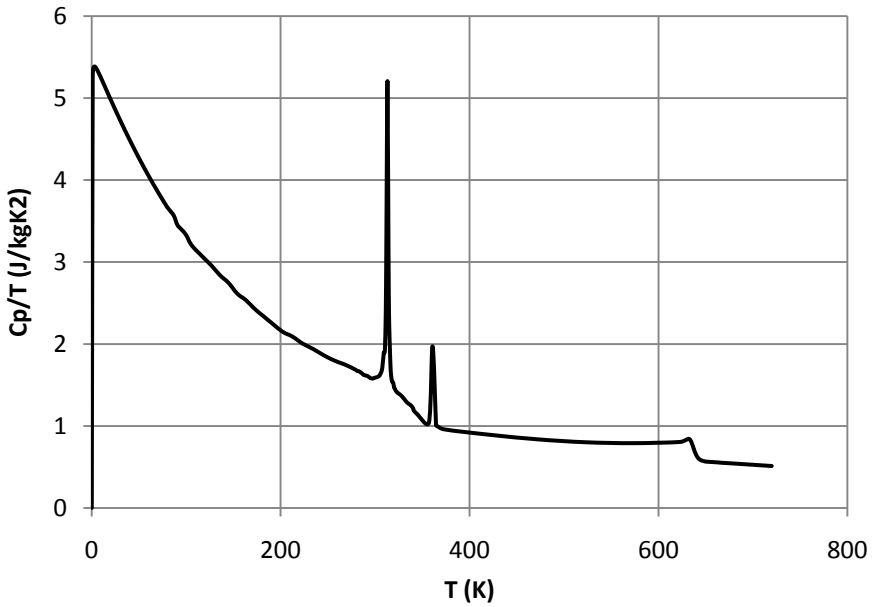

Figure 4.3: c_p/T vs. T.

In accordance with Eq.4.2, in order to find the entropy of the material, one should compute the integration of the c_p/T with respect to temperature. As it is seen in Fig.4.3, it is impossible to find the suitable function for c_p/T; thus we are unable to

integrate c_p/T analytically, so it should be done numerically by finding area under the diagram. The result is shown in Fig.4.4.

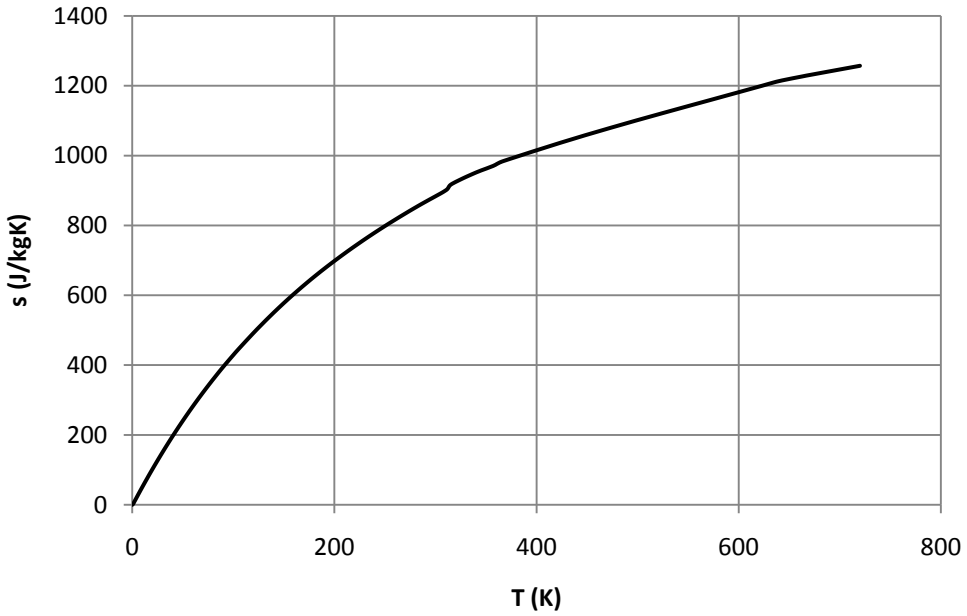

Figure 4.4: Entropy vs. temperature.

Fig.4.4 illustrates a vast range of temperature, but the important range for this study is between 280K and 320K which is shown in Fig.4.5.

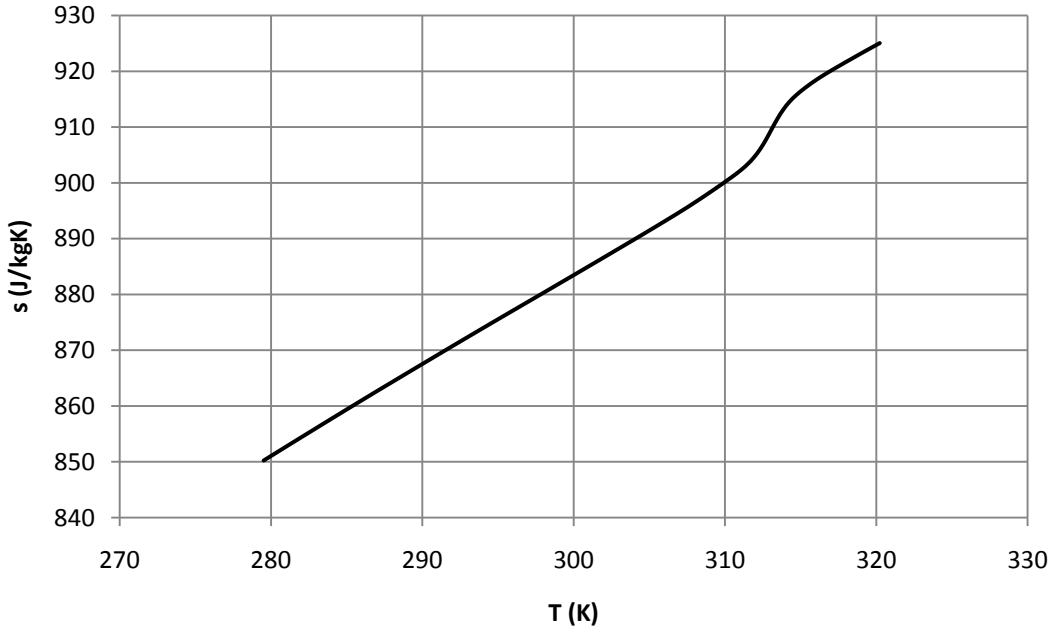

Figure 4.5: Entropy versus temperature between 280 and 320K.

What is shown in Fig.4.5 is entropy changes with respect to temperature at zero field, but in magnetic refrigeration, it necessary to find the entropy in different magnetic fields. In order to do so, we need to implement the MCE on zero-filed entropy diagram. Temperature dependences of the magnetocaloric effect in FeRh is shown in Fig.4.6 [21].

To find the entropy for a given magnetic field, one should find the temperature change related to that specific magnetic field at different temperature from Fig.4.6, and then draw the associated points based on entropy diagram shown in Fig.4.5. Two and three dimensional illustration of the results is depicted in Figs.4.7 and 4.8 respectively.

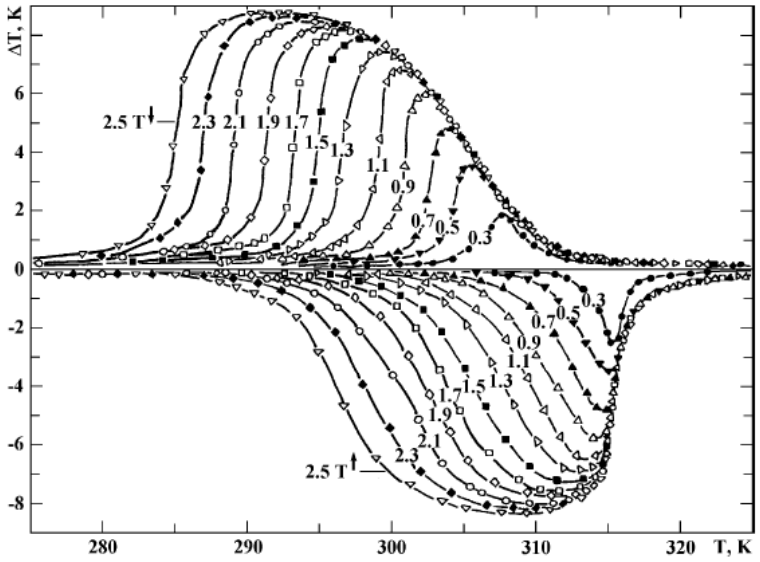

Figure 4.6: Temperature dependences of the magnetocaloric effect in FeRh. The numbers denote the magnetic field in Tesla [21].

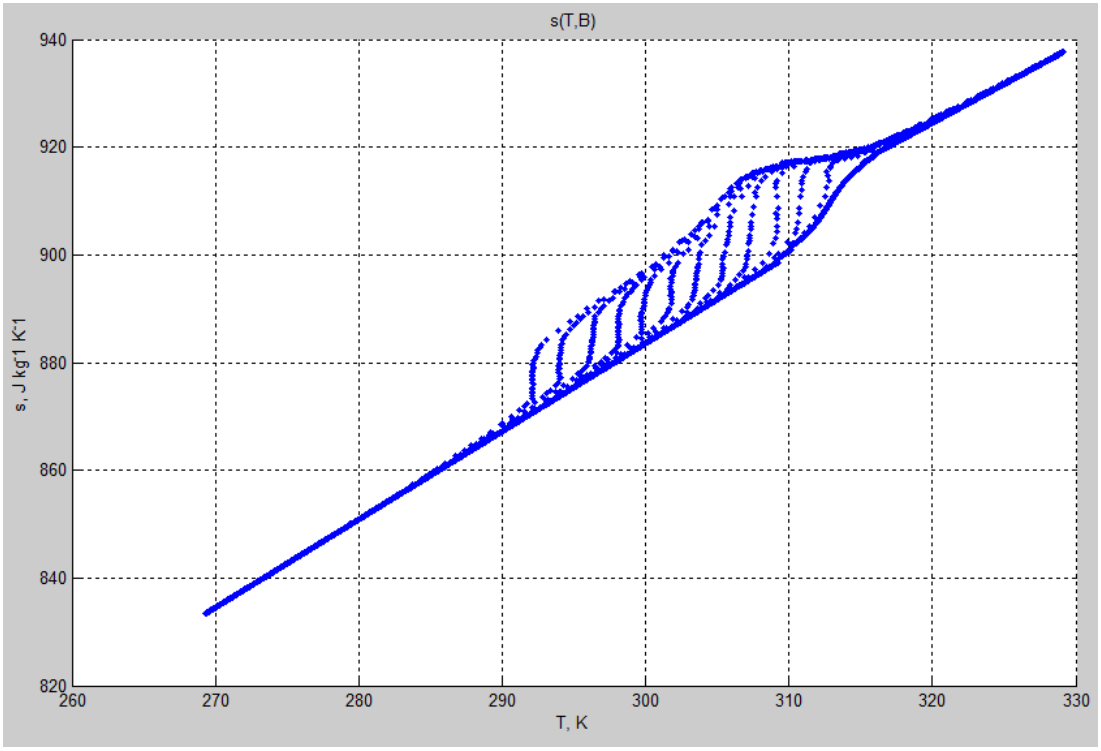

Figure 4.7: Two dimensional illustration of FeRh entropy diagram at different magnetic fields from 0 to 2.5T.

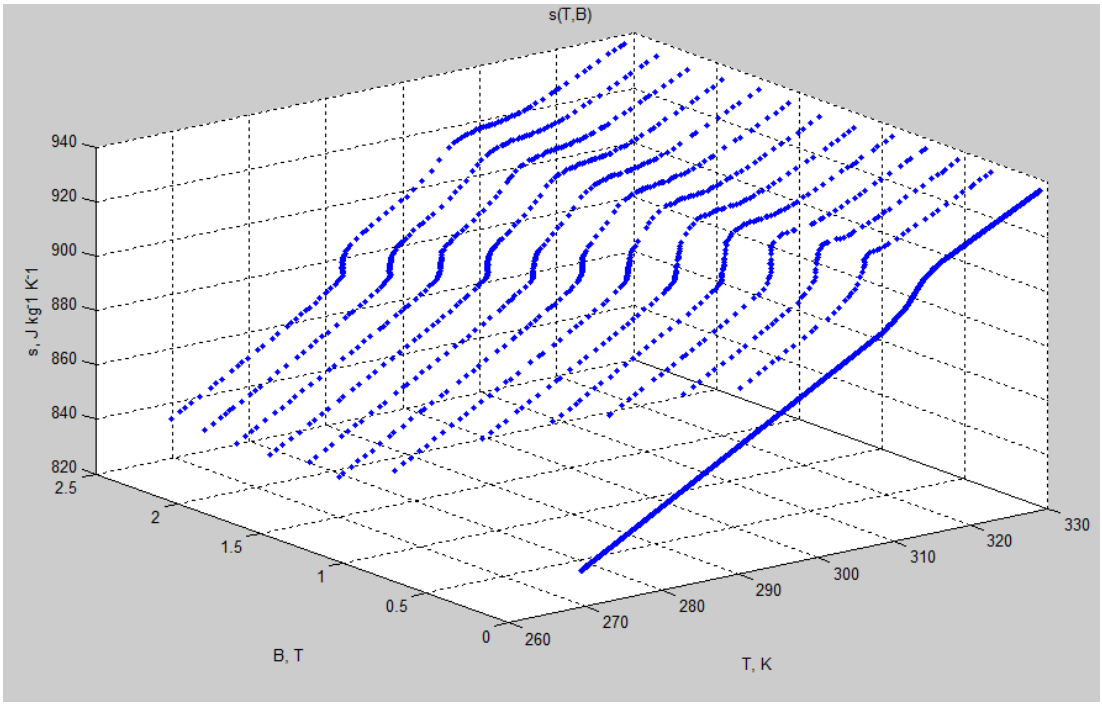

Figure 4.8: Three dimensional illustration of FeRh entropy at different magnetic fields from 0 to 2.5T.

4.3 Coding the Entropy Diagram

One of the obstacles of this study was to code the properties of the magnet material and the fluid for various magnetic fields and temperatures. The usual way is to functionalize the properties. If there is just one independent variable, the functionalizing process will be very easy, but in the case of more than one independent variable, the procedure becomes very laborious and needs a high mathematical intuition.

Our first purpose was to find a suitable function of temperature and magnetic field for entropy. About 20 functions were tested; some of which were mathematically appropriate[1], but none of them was physically acceptable; because the function should not only fit the data in Fig.4.8 but also be consistent with the specific heat diagram illustrated in Fig.4.2.

After being unsuccessful to find the fitting function we decided to find a fitting surface for Fig.4.8. It was done by doing curve fitting for each set of data related to a specific magnetic field and combining the curves. Fig.4.9 shows the result of the surface fitting.

The data shown in Fig.4.9 and additional interpolation was used in codes as entropy input for various temperatures and magnetic fields.

Table 4.1 summarizes the concise entropy data which were used as the input before interpolation.

[1] In some cases the R value reached 98% which shows a very high accuracy.

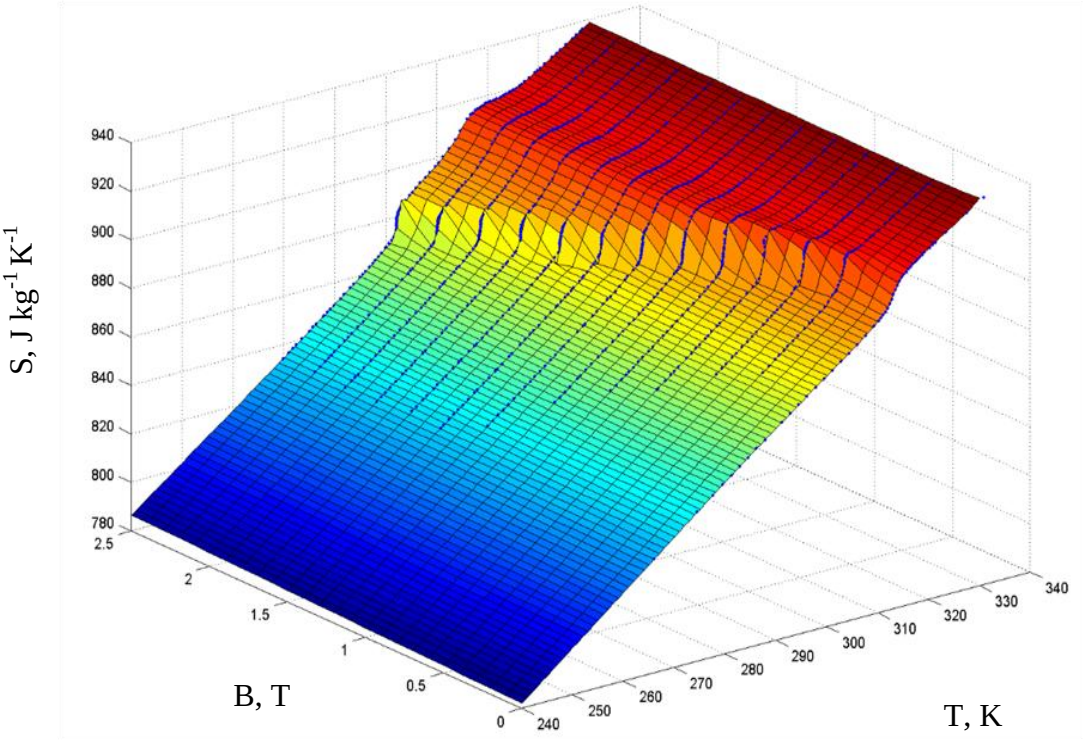

Figure 4.9: Surface fitted for entropy.

Table 4.1: Abridged table of entropy.

	B (Tesla) = $\mu_0 H$				
T (K)	**0**	**0.5**	**1.1**	**1.7**	**2.5**
270	833.9369	835.109	834.504	834.5156	834.5874
275	842.5657	843.1425	842.6697	842.736	842.767
280	851.047	851.176	850.8659	850.9336	850.9851
285	859.38	859.2095	859.0774	859.1356	859.4607
290	867.5301	867.2444	867.2907	867.3904	868.6844
295	875.5441	875.4085	875.5024	876.0701	888.2339
300	883.4573	883.6796	884.0555	892.6697	897.0675
305	891.4584	892.012	894.2512	908.5322	909.6028
310	900.1651	902.6831	916.8382	917.1424	917.2099
315	916.3913	919.0174	919.3083	919.5279	919.5521
320	924.7061	924.9667	925.152	925.1828	925.2364
325	931.8458	931.818	931.9116	931.9372	931.9415
330	938.6899	938.8853	938.9662	938.9113	938.9647

CHAPTER 5

SYSTEM MODELING AND BENCHMARKING

5.1 System Description

The system which is modeled in this thesis shows up as probably the best description of actual performance [25]. In order to develop the mathematical model, the following characteristics were considered.

There are particles of 200-μm diameter in the bed as the refrigerant. The temperature of the cold and hot ends is 280K and 300K, respectively. The hot and cold blow periods are 3s, while the magnetization and demagnetization periods are 1s. The cross-sectional area of the bed and its length are 0.08 m^2 and 0.1 m, correspondingly.

Fig.5.1 shows a schematic illustration of the modeled system, where (1) is the suitable device to produce magnetic field, which can be a superconducting solenoid, electromagnet, or permanent magnet, (2) is the porous regenerator which includes metallic refrigerant particles located in a bed, (3) is the cold heat exchanger which is in contact with the desired space, (4) is a displacer which is used to push the fluid in the network, and (5) is the hot heat exchanger which is in contact with the environment.

It should be noted that in the conventional AMRR, Gd is used as the refrigerant and a superconducting solenoid is used to produce magnetic field.

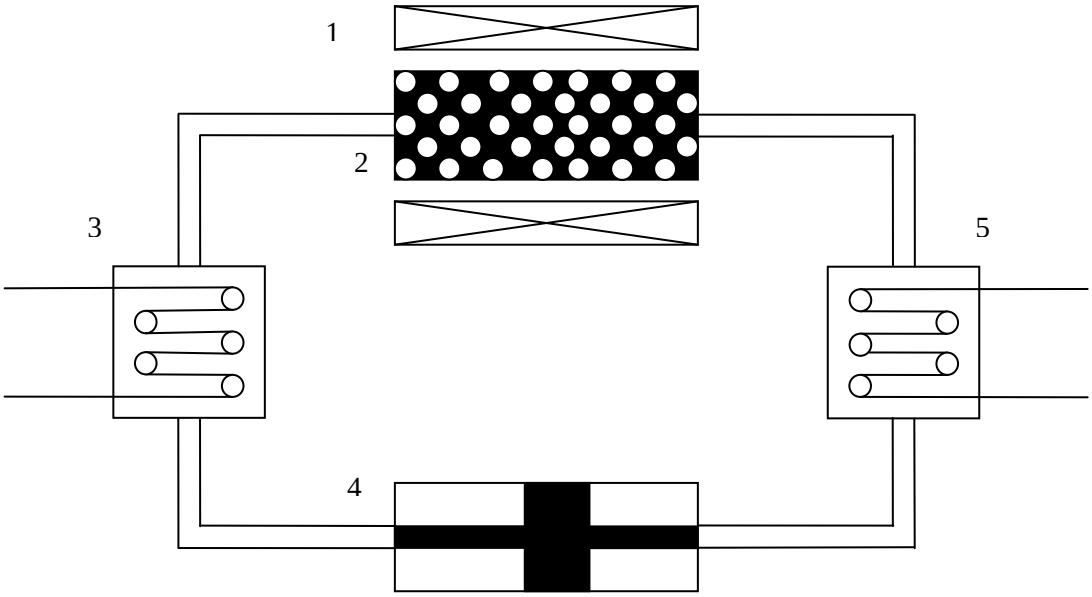

Figure 5.1: Schematic illustration of the modeled system.

5.2 Energy Equations for the System

In order to reach a suitable mathematical model it is necessary to find the analytical equation first. A one-dimensional analytical energy equation is obtained in this study.

The model consists of two energy equations for regenerator and the fluid each of which includes partial differential terms of time and space. Solving theses equation leads to temperature profile in regenerator and fluid. The auxiliary devices such as heat exchangers are not modeled. However their impact on the fluid and regenerator is executed. The following assumptions are considered in order to find the analytical model

- Uniform and unidirectional mass flow rate.
- Temperature of regenerator and fluid change in the flow direction.
- Incompressible flow, i.e. the fluid density is constant.
- Reversible process, i.e. negligible magnetic hysteresis.
- Uniform geometry for the regenerator, i.e. the same porosity and identical particle diameter.

- Energy losses to the surrounding are insignificant.

The modeling is done based on Fig.5.2 which shows the arrangement of particles in bed, hot and cold heat exchangers, effect of magnetic field strength, direction of positive flow as well as the infinitesimal elements of fluid and regenerator.

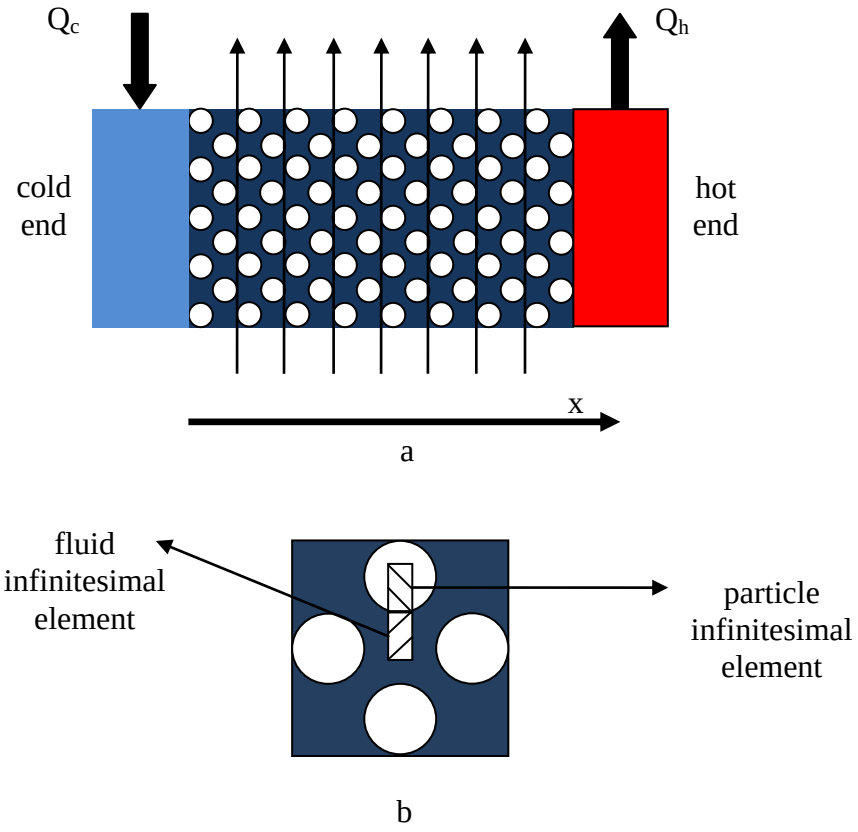

Figure 5.2: Schematic illustration of particles and infinitesimal elements of fluid and regenerator.

5.2.1 Energy Equation for Regenerator

Fig.5.3 depicts an infinitesimal element of regenerator and its energy exchange with fluid as well as the effect of magnetic field as magnetization work.

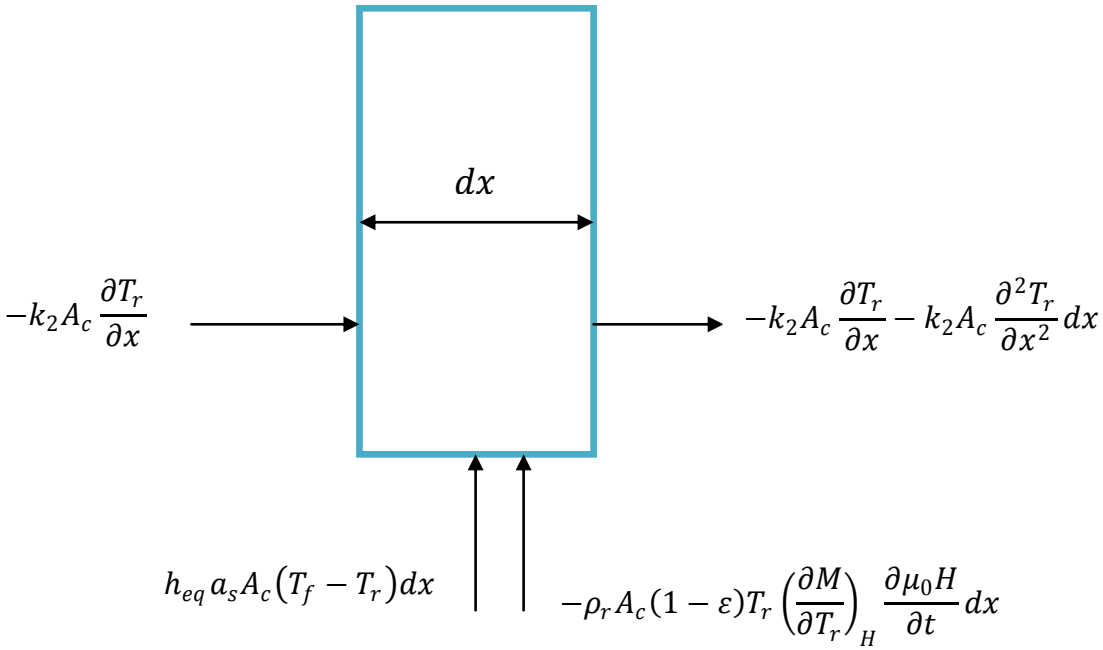

Figure 5.3: Infinitesimal element of regenerator.

The energy equation of the regenerator is obtained by using first law of thermodynamics.

$$\rho_r A_c (1-\varepsilon) c_r \frac{\partial T_r}{\partial t} dx = -k_2 A_c \frac{\partial T_r}{\partial x} + k_2 A_c \frac{\partial T_r}{\partial x} + k_2 A_c \frac{\partial^2 T_r}{\partial x^2} dx - h_{eq} a_s A_c (T_f - T_r) dx - \rho_r A_c (1-\varepsilon) T_r \left(\frac{\partial M}{\partial T_r}\right)_H \frac{\partial \mu_0 H}{\partial t} dx \quad (5.1)$$

After simplifications:

$$\frac{\partial T_r}{\partial t} = \frac{k_2}{\rho_r (1-\varepsilon) c_r} \frac{\partial^2 T_r}{\partial x^2} + \frac{h_{eq} a_s}{\rho_r (1-\varepsilon) c_r} (T_f - T_r) - \frac{T_r}{c_r} \left(\frac{\partial M}{\partial T_r}\right)_H \frac{\partial \mu_0 H}{\partial t} \quad (5.2)$$

Eq.5.2 includes effective thermal conductivity of regenerator (k_2), density of regenerator (ρ_r), porosity (ε), specific heat capacity of regenerator (c_r), equivalent heat transfer coefficient (h_{eq}), specific area (a_s), magnetic field ($\mu_0 H$), and magnetization (M). The terms in Eq.5.2 are interpreted as follows:

$\frac{\partial T_r}{\partial t}$: Energy storage in material (per heat capacity)

$\frac{k_2}{\rho_r(1-\varepsilon)c_r}\frac{\partial^2 T_r}{\partial x^2}$: Energy transferred by conduction (per heat capacity)

$\frac{h_{eq}\,a_s}{\rho_r(1-\varepsilon)c_r}\left(T_f - T_r\right)$: Energy transfer between fluid and material (per heat capacity)

$\frac{T_r}{c_r}\left(\frac{\partial M}{\partial T_r}\right)_H \frac{\partial \mu_0 H}{\partial t}$: Magnetic work (per heat capacity)

It is possible to replace $\left(\frac{\partial M}{\partial T_r}\right)_H$ in Eq.5.2 with Eqs. 2.3 and 2.8b for isothermal and isentropic processes, respectively. Eqs. 5.3a and 5.3b are related to isothermal and isentropic processes, correspondingly.

$$\frac{\partial T_r}{\partial t} = \frac{k_2}{\rho_r(1-\varepsilon)c_r}\frac{\partial^2 T_r}{\partial x^2} + \frac{h_{eq}\,a_s}{\rho_r(1-\varepsilon)c_r}\left(T_f - T_r\right) - \frac{T_r}{c_r}\left(\frac{\partial s_r}{\partial \mu_0 H}\right)_T \frac{\partial \mu_0 H}{\partial t} \qquad (5.3a)$$

$$\frac{\partial T_r}{\partial t} = \frac{k_2}{\rho_r(1-\varepsilon)c_r}\frac{\partial^2 T_r}{\partial x^2} + \frac{h_{eq}\,a_s}{\rho_r(1-\varepsilon)c_r}\left(T_f - T_r\right) + \left(\frac{\partial T_r}{\partial \mu_0 H}\right)_s \frac{\partial \mu_0 H}{\partial t} \qquad (5.3b)$$

In this research, the isothermal process is studied, so the discretization procedure is based on Eq.5.3a.

5.2.2 Energy Equation for Fluid

Fig.5.4 depicts an infinitesimal element of fluid and its energy exchange with regenerator as well as the effect of magnetic field as magnetization work.

The energy equation of the fluid is obtained by using first law of thermodynamics.

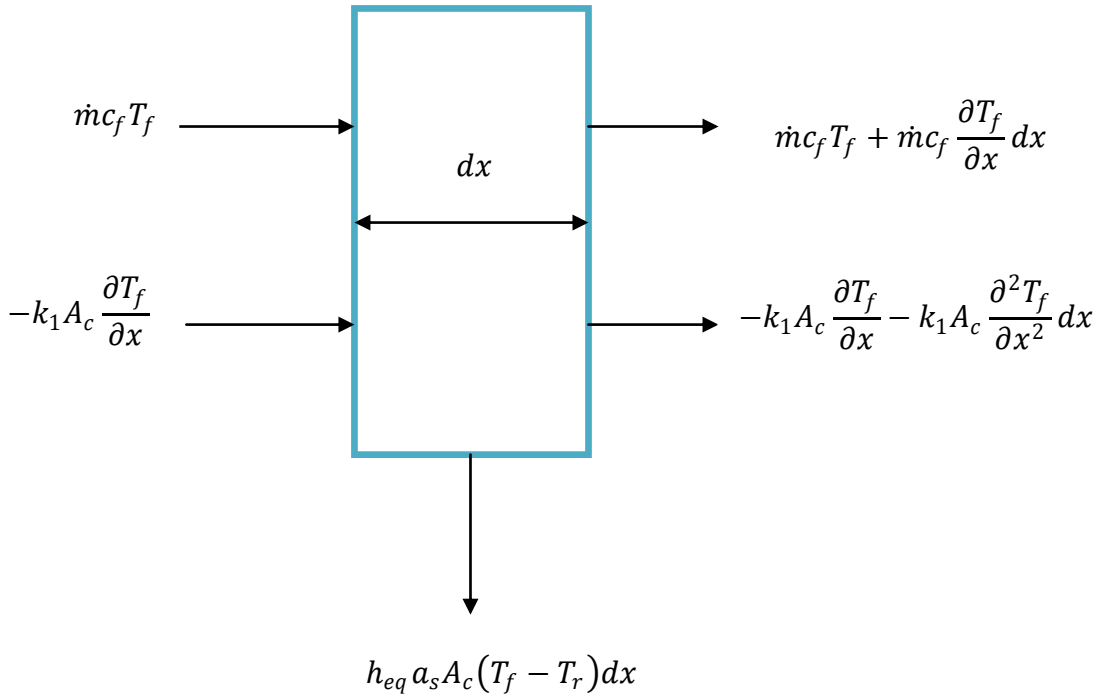

Figure 5.4: Infinitesimal element of fluid.

$$\rho_f A_c \varepsilon c_f \frac{\partial T_f}{\partial t} dx = \dot{m}c_f T_f - \dot{m}c_f T_f - \dot{m}c_f \frac{\partial T_f}{\partial x} dx - k_1 A_c \frac{\partial T_f}{\partial x} + k_1 A_c \frac{\partial T_f}{\partial x} + k_1 A_c \frac{\partial^2 T_f}{\partial x^2} dx - h_{eq} a_s A_c (T_f - T_r) dx + \Phi A_c dx \quad (5.4)$$

After simplifications:

$$\frac{\partial T_f}{\partial t} = -\frac{\dot{m}}{\rho_f A_c \varepsilon} \frac{\partial T_f}{\partial x} + \frac{k_1}{\rho_f \varepsilon c_f} \frac{\partial^2 T_f}{\partial x^2} - \frac{h_{eq} a_s}{\rho_f \varepsilon c_f} (T_f - T_r) + \frac{\Phi}{\rho_f \varepsilon c_f} \quad (5.5)$$

Eq.4.9 consists of mass flow rate ($\dot{m}$), density of fluid (ρ_f), cross-sectional area of bed (A_c), porosity (ε), specific heat capacity of fluid (c_f), equivalent heat transfer coefficient (h_{eq}), specific area (a_s), pressure drop according to viscous dissipation (Φ). The terms in Eq.5.5 are interpreted as follows:

$\frac{\partial T_f}{\partial t}$: Energy storage in fluid (per heat capacity)

$\frac{\dot{m}}{\rho_f A_c \varepsilon} \frac{\partial T_f}{\partial x}$: Energy transfer by convection (per heat capacity)

$\frac{k_1}{\rho_f \varepsilon c_f}\frac{\partial^2 T_f}{\partial x^2}$: Energy transfer by conduction (per heat capacity)

$\frac{h_{eq} a_s}{\rho_f \varepsilon c_f}\left(T_f - T_r\right)$: Energy transfer between fluid and material (per heat capacity)

$\frac{\Phi}{\rho_f \varepsilon c_f}$: Energy generation according to viscous dissipation (per heat capacity)

So the energy balance for the fluid can be expressed as:

$$\frac{\partial T_f}{\partial t} = -\frac{\dot{m}}{\rho_f A_c \varepsilon}\frac{\partial T_f}{\partial x} + \frac{k_1}{\rho_f \varepsilon c_f}\frac{\partial^2 T_f}{\partial x^2} - \frac{h_{eq} a_s}{\rho_f \varepsilon c_f}\left(T_f - T_r\right) + \frac{\Phi}{\rho_f \varepsilon c_f} \tag{5.6}$$

5.3 AMR Cycle for FeRh

As mentioned before, a complete cycle of AMR consists of four steps. Special attention must be paid to this cycle when the FeRh is used as the refrigerant, since it is different from other magnetic materials. As a common magnetic material is subjected to the magnetic field, its temperature rises in an adiabatic process, but FeRh behavior is in contrast with other materials, such that its temperature decreases when magnetic field is applied; thus, the cycle will be as described below:

1. Magnetization: in the first step the fluid is stationary and the magnetic field increases with time, so mass flow rate and dispersion[1] must set equal to zero ($\dot{m} = 0$, $d = 0$, and $\frac{\partial \mu_0 H}{\partial t} > 0$).
2. Hot to cold flow (cold blow): in the second step the magnetic field remains constant, the fluid moves from the hot end to the cold. In this case according to Fig 4.1 the mass flow rate is negative ($\dot{m} < 0$, $d \neq 0$, and $\frac{\partial \mu_0 H}{\partial t} = 0$).

[1] Dispersion factor is included in fluid effective conductivity which is discussed later.

3. Demagnetization: in the third step the magnetic field decreases with time. The fluid is stationary, so the dispersion factor and mass flow rate are set equal to zero again ($\dot{m} = 0$, $d = 0$, and $\frac{\partial \mu_0 H}{\partial t} < 0$).
4. Cold to hot flow (hot blow): in the forth step the fluid is pushed from the cold end to the hot end. In this case the mass flow rate is positive referred to Fig 4.1 ($\dot{m} > 0$, $d \neq 0$, and $\frac{\partial \mu_0 H}{\partial t} = 0$).

The steps are summarized in Fig.5.5

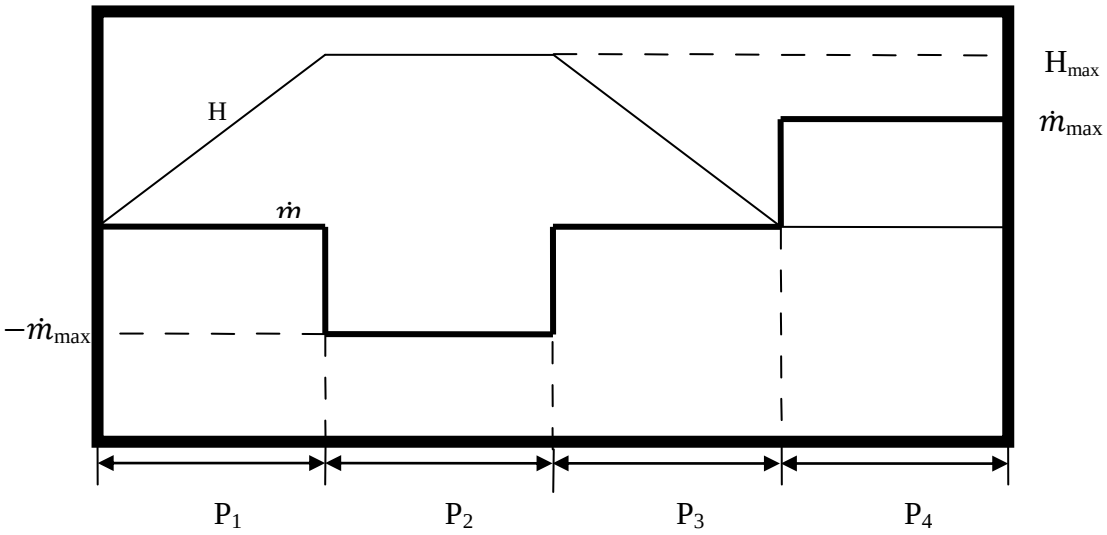

Figure 5.5: Changes of mass flow rate and magnetic field strength during the four step of AMRR.

5.4 Discretization Energy Equations

After finding the energy equations for fluid and regenerator, it is possible to obtain numerical equations for fluid and regenerator based on Eqs. 5.3a and 5.6 and section 5.2.

The increments for space and time are $\Delta x = \frac{L}{N}$ and $\Delta t = \frac{P}{M}$ in which N and M are number of cells for space and time, correspondingly.

where L and P are the length of the bed and required time in each step, respectively. so

$$\begin{gathered} x_i = (i-1)\Delta x \\ t_j = (j-1)\Delta t \\ i = 1, 2, \dots, N+1 \\ j = 1,2, \dots, M+1 \end{gathered} \tag{5.7}$$

Finite difference method is used to discretize the analytical equations.

For fluid:

Explicit forward difference for time: $\frac{\partial T_f}{\partial t} = \frac{T_f(i,j+1) - T_f(i,j)}{\Delta t}$

Backward difference for convection ($\dot{m} > 0$): $\frac{\partial T_f}{\partial x} = \frac{T_f(i,j) - T_f(i-1,j)}{\Delta x}$

Forward difference for convection ($\dot{m} < 0$): $\frac{\partial T_f}{\partial x} = \frac{T_f(i+1,j) - T_f(i,j)}{\Delta x}$

Central difference for conduction: $\frac{\partial^2 T_f}{\partial x^2} = \frac{T_f(i+1,j) - 2T_f(i,j) + T_f(i-1,j)}{\Delta x^2}$

For regenerator:

Explicit forward difference for time: $\frac{\partial T_r}{\partial t} = \frac{T_r(i,j+1) - T_r(i,j)}{\Delta t}$

Central difference for conduction: $\frac{\partial^2 T_r}{\partial x^2} = \frac{T_r(i+1,j) - 2T_r(i,j) + T_r(i-1,j)}{\Delta x^2}$

5.4.1 Discretized Energy Equation for Regenerator

According to the discretization rules and Eq.5.3a the numerical model of the regenerator is:

$$\begin{aligned} &\frac{T_r(i,j+1) - T_r(i,j)}{\Delta t} \\ &\qquad = -\frac{T_r(i,j)}{c_r}\frac{\partial s_r}{\partial \mu_0 H_T}\frac{\partial \mu_0 H}{\partial t} \\ &\qquad + \frac{k_2}{\rho_r c_r (1-\varepsilon)}\frac{T_r(i+1,j) - 2T_r(i,j) + T_r(i-1,j)}{\Delta x^2} \\ &\qquad + \frac{h_{eq} a_s}{\rho_r c_r (1-\varepsilon)}\Big(T_f(i,j) - T_r(i,j)\Big) \end{aligned} \tag{5.8}$$

After simplification:

$$T_r(i,j+1) = B_{r1}T_r(i,j) + B_{r2}[T_r(i-1,j) + T_r(i+1,j)] + B_{r3}T_f(i,j)$$
$$i = 2,3,\dots,N \tag{5.9}$$
$$j = 1,2,\dots,M$$

where,

$$B_{r1} = 1 - \left[\frac{1}{c_r}\frac{\partial s_r}{\partial \mu_0 H_T}\frac{\partial \mu_0 H}{\partial t} + \frac{h_{eq}\,a_s}{\rho_r c_r(1-\varepsilon)}\right]\Delta t - \frac{2k_2}{\rho_r c_r(1-\varepsilon)}\frac{\Delta t}{\Delta x^2}$$

$$B_{r2} = \frac{k_2}{\rho_r c_r(1-\varepsilon)}\frac{\Delta t}{\Delta x^2}$$

$$B_{r3} = \frac{h_{eq}\,a_s}{\rho_r c_r(1-\varepsilon)}\Delta t$$

5.4.2 Discretized Energy Equation for Fluid

Numerical energy equation for fluid is derived based on Eq.5.6.

For $\dot{m} > 0$:

$$\begin{aligned}\frac{T_f(i,j+1) - T_f(i,j)}{\Delta t} &= -\frac{\dot{m}}{\rho_f A_c \varepsilon}\frac{T_f(i,j) - T_f(i-1,j)}{\Delta x} \\ &+ \frac{k_1}{\rho_f \varepsilon c_f}\frac{T_f(i+1,j) - 2T_f(i,j) + T_f(i-1,j)}{\Delta x^2} \\ &- \frac{h_{eq}\,a_s}{\rho_f \varepsilon c_f}\big(T_f(i,j) - T_r(i,j)\big) + \frac{\Phi}{\rho_f \varepsilon c_f}\end{aligned} \tag{5.10}$$

After simplification:

$$\begin{aligned}T_f(i,j+1) &= B_{f1}T_f(i,j) + B_{f2}T_f(i-1,j) + B_{f3}T_f(i+1,j) \\ &+ B_{f4}T_r(i,j) + F \\ &i = 2,3,\dots,N \\ &j = 1,2,\dots,M\end{aligned} \tag{5.11}$$

where,

$$B_{f1} = 1 - \frac{h_{eq}\,a_s}{\rho_f \varepsilon c_f}\Delta t - \frac{\dot{m}}{\rho_f A_c \varepsilon}\frac{\Delta t}{\Delta x} - \frac{2\,k_1}{\rho_f \varepsilon c_f}\frac{\Delta t}{\Delta x^2}$$

$$B_{f2} = \frac{\dot{m}}{\rho_f A_c \varepsilon}\frac{\Delta t}{\Delta x} + \frac{k_1}{\rho_f \varepsilon c_f}\frac{\Delta t}{\Delta x^2}$$

$$B_{f3} = \frac{k_1}{\rho_f \varepsilon c_f} \frac{\Delta t}{\Delta x^2}$$

$$B_{f4} = \frac{h_{eq} a_s}{\rho_f \varepsilon c_f} \Delta t$$

$$F = \frac{\Phi}{\rho_f \varepsilon c_f}$$

For $\dot{m} < 0$:

$$\begin{aligned} \frac{T_f(i,j+1) - T_f(i,j)}{\Delta t} &= -\frac{\dot{m}}{\rho_f A_c \varepsilon} \frac{T_f(i+1,j) - T_f(i,j)}{\Delta x} \\ &+ \frac{k_1}{\rho_f \varepsilon c_f} \frac{T_f(i+1,j) - 2T_f(i,j) + T_f(i-1,j)}{\Delta x^2} \\ &- \frac{h_{eq} a_s}{\rho_f \varepsilon c_f} \big(T_f(i,j) - T_r(i,j)\big) + \frac{\Phi}{\rho_f \varepsilon c_f} \end{aligned} \tag{5.12}$$

After simplification:

$$\begin{aligned} T_f(i,j+1) = B_{f5} T_f(i,j) + B_{f6} T_f(i-1,j) + B_{f7} T_f(i+1,j) \\ + B_{f4} T_r(i,j) + F \\ i = 2,3,\dots,N \\ j = 1,2,\dots,M \end{aligned} \tag{5.13}$$

where,

$$B_{f5} = 1 - \frac{h_{eq} a_s}{\rho_f \varepsilon c_f} \Delta t + \frac{\dot{m}}{\rho_f A_c \varepsilon} \frac{\Delta t}{\Delta x} - \frac{2\, k_1}{\rho_f \varepsilon c_f} \frac{\Delta t}{\Delta x^2}$$

$$B_{f6} = \frac{k_1}{\rho_f \varepsilon c_f} \frac{\Delta t}{\Delta x^2}$$

$$B_{f7} = -\frac{\dot{m}}{\rho_f A_c \varepsilon} \frac{\Delta t}{\Delta x} + \frac{k_1}{\rho_f \varepsilon c_f} \frac{\Delta t}{\Delta x^2}$$

5.5 Initial and Boundary Conditions

The initial condition for fluid and regenerator is

$$\begin{aligned} T_{r,f}(x,1) = T_C + (T_H - T_C)x \\ 0 \le x \le L \end{aligned} \tag{5.14}$$

Eq.5.14 is applied at the beginning of the process. During the procedure, initial condition for each step is equal to the last temperature profile of the previous step.

5.5.1 Boundary Conditions for Regenerator

Both end of the regenerator bed is isolated, so the boundary conditions of the regenerator are:

$$\left(\frac{\partial T_r}{\partial x}\right)_{x=0,L} = 0 \tag{5.15}$$

Eq.5.15 is discretized by central difference:

$$\begin{gathered} T_r(i+1,j) - 2T_r(i,j) + T_r(i-1,j) = 0 \\ i = 1, N+1 \\ j = 1,2,\dots,M \end{gathered} \tag{5.16}$$

By setting i equal to 1 and *N+1* into Eqs. 5.9 and 5.16, and substituting $T_r(0,j)$ and $T_r(N+2,j)$ from Eq.5.16 into Eq.5.9, boundary conditions are obtained:

$$T_r(1,j+1) = (B_{r1} + 2B_{r2})T_r(1,j) + B_{r3}T_f(1,j) \tag{5.17a}$$

$$\begin{gathered} T_r(N+1,j+1) = (B_{r1} + 2B_{r2})T_r(N+1,j) + B_{r3}T_f(N+1,j) \\ j = 1,2,\dots,M \end{gathered} \tag{5.17b}$$

5.5.2 Boundary Conditions for Fluid

The boundary condition for fluid is divided into two categories: positive mass flow rate and negative mass flow rate. In each case, one of the boundary conditions is equal to the entrance temperature and the other boundary condition is gained by fully developed conditions [29] and the procedure is the same as that of regenerator, so:

For $\dot{m} > 0$:

$$T_f(1,j+1) = T_C \tag{5.18a}$$

$$T_f(N+1,j+1) = \left(B_{f1}+2B_{f3}\right)T_f(N+1,j) + \left(B_{f2}-B_{f3}\right)T_f(N,j) + B_{f4}T_r(N+1,j) + F \qquad j = 1,2,\dots,M \tag{5.19b}$$

For $\dot{m} < 0$:

$$T_f(N+1,j+1) = T_H \tag{5.20a}$$

$$T_f(1,j+1) = \left(B_{f5}+2B_{f6}\right)T_f(1,j) + \left(B_{f7}-B_{f6}\right)T_f(2,j) + B_{f4}T_r(1,j) + F \qquad j = 1,2,\dots,M \tag{5.20b}$$

5.6 Properties and Correlations

In order to calculate the terms and coefficients in Eqs. 5.9 and 5.11, it is necessary to find the properties of the fluid and regenerator as well as their correlations.

5.6.1 Fluid Properties

Two fluids were used in this study: water and water/ethylene glycol mixture. In this study, the thermal conductivity (k), dynamic viscosity (μ), and specific heat (c_p), are used as a function of temperature, but density (ρ) is assumed to be constant, since the fluid is incompressible.

The following functions were used for water properties [25]:

$$c_p\left(T_f\right) = \exp\left(10.2192 + 0.00133455.T_f - 0.40046.Ln\left(T_f\right) + \frac{0.090449}{T_f - 264}\right) \tag{5.21a}$$

$$k_f\left(T_f\right) = -0.71942 + 0.0072455.T_f - 0.00000937.{T_f}^2 \tag{5.21b}$$

$$\mu_f\left(T_f\right) = \exp\left(9.2252 - 0.085639.T_f + 0.0001047.{T_f}^2\right) \tag{5.21c}$$

Eqs. 5.22a to 5.22c show the properties of water/ethylene glycol mixture [12]:

$$c_p(T_f) = 1874.60 + 3.78990120.T_f + 0.00123010.{T_f}^2 \quad (5.22a)$$

$$k_f(T_f) = 0.226624 + 0.00042756.T_f + 1.58181053 \times 10^{-7}.{T_f}^2 \quad (5.22b)$$

$$\begin{aligned}\mu_f(T_f) = {} & 667.5282 - 11.84019356.T_f + 0.08753776.{T_f}^2 \\ & - 0.00034520.{T_f}^3 + 7.65655422 \times 10^{-7}.{T_f}^4 \\ & - 9.05460854 \times 10^{-10}.{T_f}^5 + 4.45978126 \\ & \times 10^{-13}.{T_f}^6\end{aligned} \quad (5.22c)$$

The density of water and water/ethylene glycol mixture was taken as 998.2 and 1055.7 kg/m^3, respectively.

Figs.5.6 to 5.8 compare specific heat, heat conductivity, and dynamic viscosity between water and water/ethylene glycol water mixture.

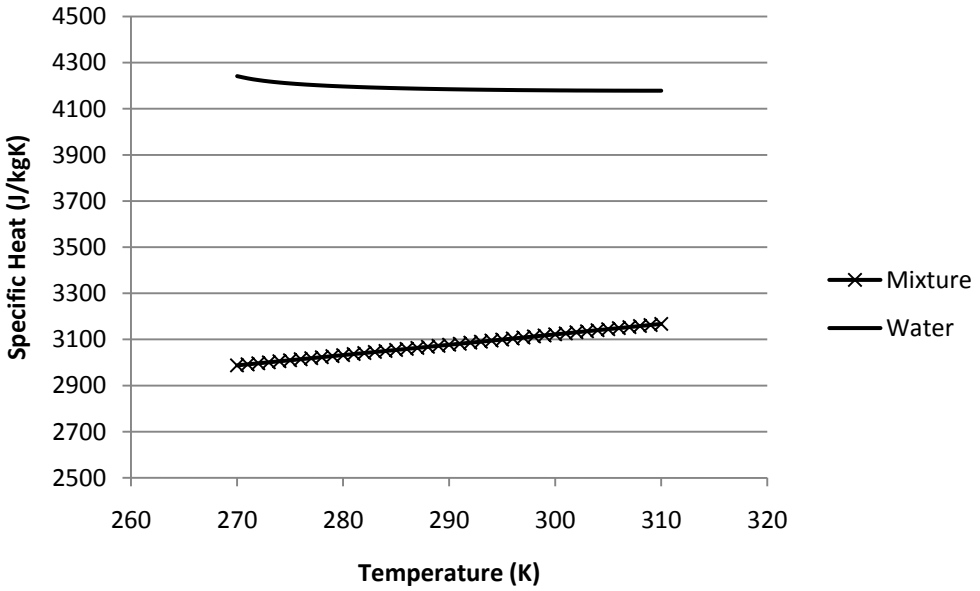

Figure 5.6: Specific heat of water and water/ethylene glycol mixture.

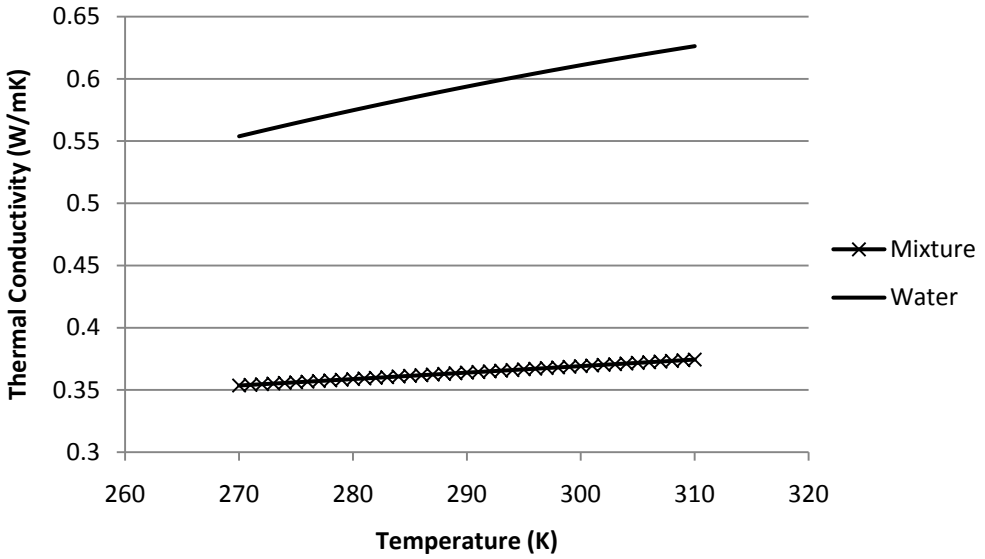

Figure 5.7: Thermal conductivity of water and water/ethylene glycol mixture.

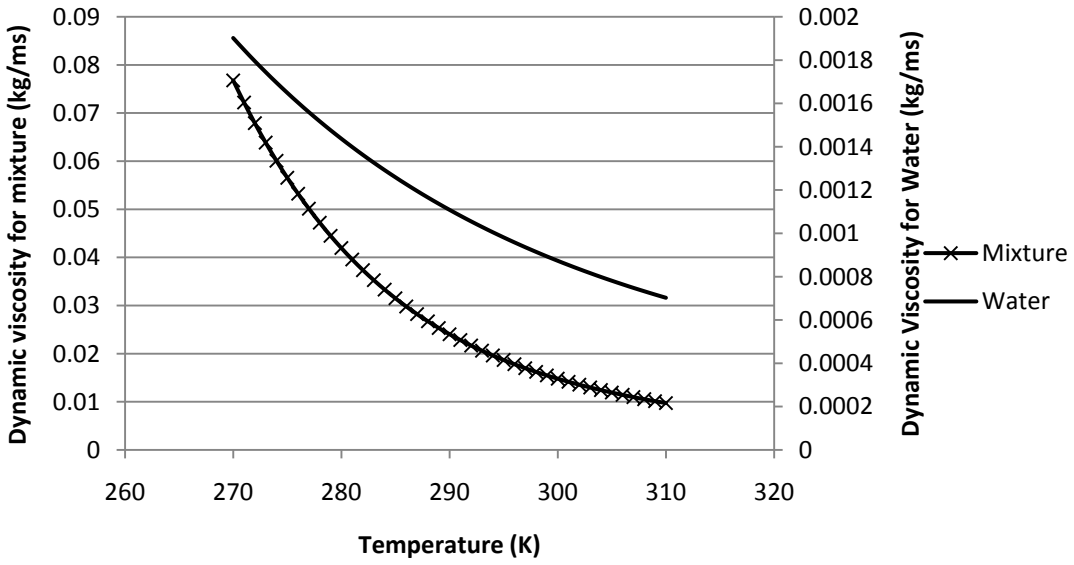

Figure 5.8: Dynamic viscosity of water and water/ethylene glycol mixture.

5.6.2 Correlations

To be able to solve Eqs.5.3a and 5.6, suitable correlations should be used for fluid and regenerator effective thermal conductivity (k_1 and k_2), equivalent heat transfer coefficient (h_{eq}), and dissipation (Φ).

Eqs.5.24 and 5.25 show effective thermal conductivity for fluid and regenerator, correspondingly [30].

$$k_1 = \varepsilon k_f + 0.5 k_f RePr \tag{5.24}$$

$$k_2 = (1 - \varepsilon) k_r \tag{5.25}$$

in which Reynolds (Re) and Prandtl (Pr) numbers are defined in Eqs.5.26 and 5.27, respectively.

$$Re = \frac{\dot{m} d_h}{\mu_f A_c} \tag{5.26}$$

$$Pr = \frac{c_f \mu_f}{k_f} \tag{5.27}$$

In the problems that involve both surface convection and conduction, special attention must be paid to the temperature gradient within the material [31]. In order to realize whether the temperature gradient within the material is negligible or not, Biot number is defined in Eq.5.28.

$$Bi = \frac{h d_h}{2 k_r} \tag{5.28}$$

Bi less than 0.1 means that the heat conduction within the material is much faster than its surface. In this study it is assumed that the Bi is not less than 0.1, so it is necessary to approximate the heat transfer coefficient. In order to approximate the heat transfer coefficient, equivalent heat transfer is introduced in Eq.5.29.

$$h_{eq} = \frac{h}{1 + \frac{Bi}{5}} \tag{5.29}$$

In Eq.5.29, *h* is heat transfer coefficient which is defined as $\frac{Nu k_f}{d_h}$, where *Nu* is Nusselt number and correlated based on the following equation [32]:

$$Nu = 2 + 1.1 Re^{0.6} Pr^{1/3} \tag{5.30}$$

The above correlation for *Nu* covers *Re* up to 8500 [33].

Dissipation is related to viscosity of the fluid which leads to pressure drop and heat generation. Based on Darcy's law it is defined as [34]:

$$\Phi = \frac{\mu_f}{K} u^2 \tag{5.31}$$

In Eq.5.31, u is velocity and K is permeability which is not dependant on nature of the fluid but the geometry of the medium and for a bed of particles is defined by Eq.5.32 [35].

$$K = \frac{\varepsilon^3 {d_h}^2}{150(1-\varepsilon)^2} \tag{5.32}$$

It is possible to make dissipation independent of permeability. The velocity is related to pressure drop and mass flow rate by the following equations.

$$u = -\frac{K}{\mu_f}\frac{dP}{dx} \tag{5.33a}$$

$$u = \frac{\dot{m}}{\rho_f A_c} \tag{5.33b}$$

By replacing u in Eq.5.31 by 5.33a and 5.33b, dissipation will be:

$$\Phi = -\frac{dP}{dx}\frac{\dot{m}}{\rho_f A_c} \tag{5.34}$$

There are different correlations for pressure gradient. The well-known correlation was introduced by Irmay [35]:

$$\frac{dp}{dx} = \frac{\beta \mu_f (1-\varepsilon)^2 u}{\varepsilon^3 {d_p}^2} + \frac{\alpha \rho_f (1-\varepsilon) u^2}{d_p \varepsilon^3} \tag{5.35}$$

With α=1.75 and β=150, Eq.5.35 is known as Ergun's equation [35]. In some references pressure drop is linked to friction factor by Eq.5.36 [36]:

$$f_f = \frac{dp/dx}{\rho_f u^2/2} d_h \tag{5.36}$$

Combining Eqs. 5.35 and 5.36, with α=1.75 and β=150, leads to Eq.5.37.

$$f_f = 300\frac{(1-\varepsilon)^2}{\varepsilon^3 Re} + 3.5\frac{1-\varepsilon}{\varepsilon^3} \tag{5.37}$$

Specific area is defined as the total heat transfer area divided by total volume of the bed.

$$a_s = \frac{\pi {d_h}^2}{\pi {d_h}^3} 6(1-\varepsilon) = \frac{6(1-\varepsilon)}{d_h} \tag{5.38}$$

5.7 Solution Procedure

Before running the steps described in 5.3, the program reads the initial parameters and set the boundary and initial conditions. Each stage consists of nested loops. The inner loop accounts for space and runs until the program reaches the end of the bed. The outer loop is responsible for time. It stops once the suitable period for the given stage finishes.

The initial and boundary conditions for the each stage are set based on the results obtained from the last chronological step of the previous stage.

The stages are repeated until the AMR reaches a steady state.

The steady state condition is fulfilled with the following criteria:

$$\begin{gathered} \left|\{T_r(x,1)\}_{pc} - \{T_r(x,1)\}_{pc-1}\right| < \delta \\ 0 \le x \le L \end{gathered} \tag{5.39}$$

pc is the present cycle and δ is convergence criteria which is empirically equals 10^{-6} K [25].

Finally the program calculates refrigeration capacity, power consumption, coefficient of performance, and the efficiency of the cycle.

The COP of the system is calculated by using Eq.5.40:

$$COP = \frac{\dot{Q}_c}{\dot{W}_{tot}} \tag{5.40}$$

where $\dot{Q}_c$ is refrigeration capacity and $\dot{W}_{tot}$ is total input work which consists of pumping and magnetization work. Eqs. 5.41, 5.44, and 5.45 show the refrigeration capacity, pumping work and magnetization work, respectively.

$$\dot{Q}_c = \dot{m}\bar{c}_f(T_c - \bar{T}_c) \tag{5.41}$$

Where $\bar{T}_c$ is average value of the temperature of the exiting fluid at the cold end and $\bar{c}_f$ is the average specific heat of the flow between T_c and $\bar{T}_c$.

$$\bar{T}_c = \frac{1}{P}\int_0^P T_f(0,t)dt \tag{5.42}$$

$$\bar{c}_f = \frac{1}{T_c - \bar{T}_c}\int_{\bar{T}_c}^{T_c} c_f(T_f)dT_f \tag{5.43}$$

$$\dot{W}_{pump} = \frac{\dot{m}}{\rho_f}\Delta P \tag{5.44}$$

$$\dot{W}_{mag} = \left(\rho_r A_c(1-\varepsilon)\int_0^L\int_0^P T_r \frac{ds_r}{d\mu_0 H}\frac{d\mu_0 H}{dt}dt\,dx\right)/dt \tag{5.45}$$

$$\dot{W}_{tot} = \dot{W}_{pump} + \dot{W}_{mag} \tag{5.46}$$

Eq. 5.47 shows how to compute the second law efficiency.

$$\eta = \frac{COP}{COP_{carnot}} \tag{5.47}$$

Where COP_{carnot} is calculated by Eq. 5.48.

$$COP_{carnot} = \frac{T_c}{T_H - T_c} \tag{5.48}$$

Fig. 5.9 shows the flowchart of the solution procedure.

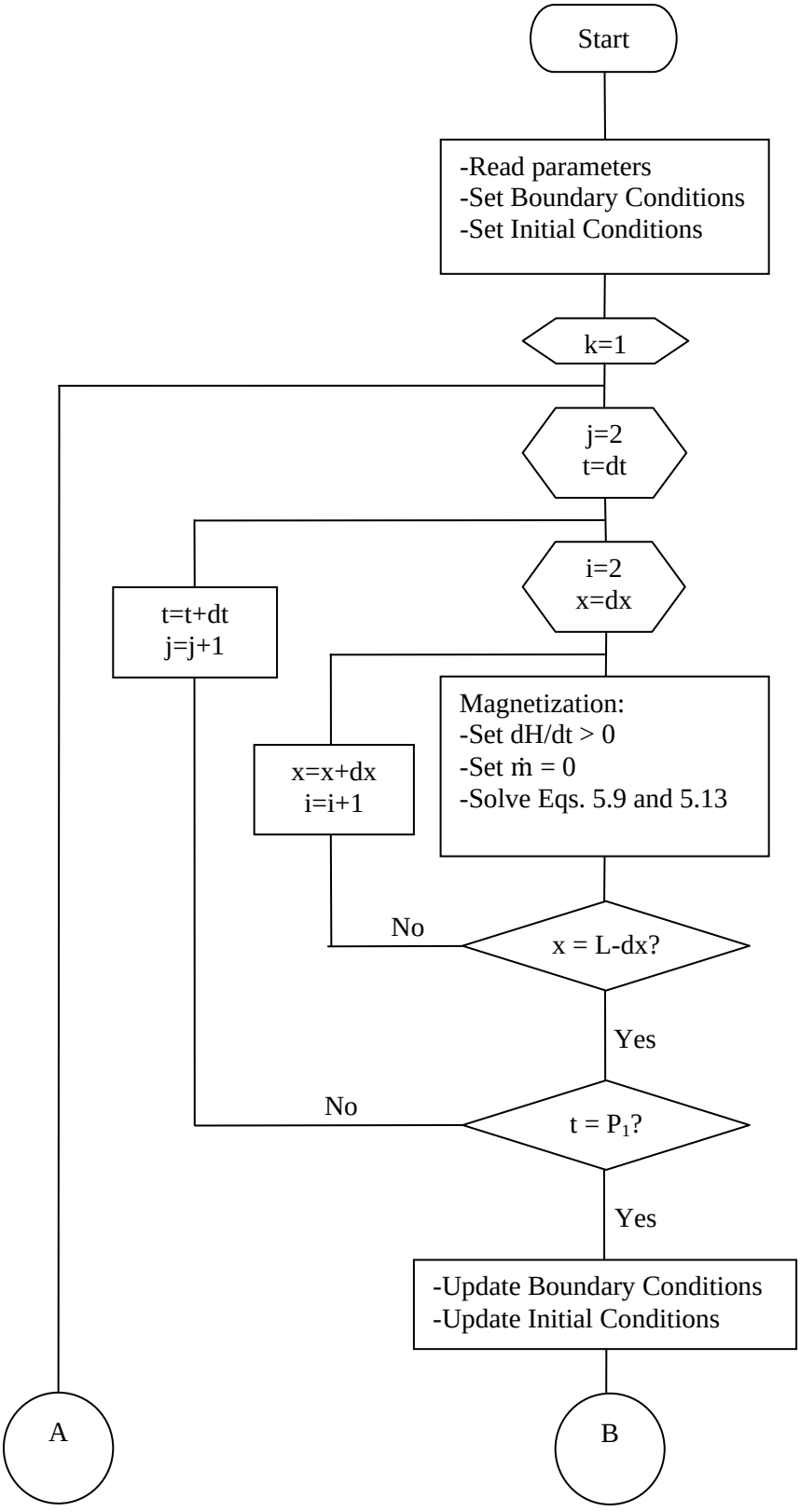

Figure 5.9: Flowchart of the solution procedure.

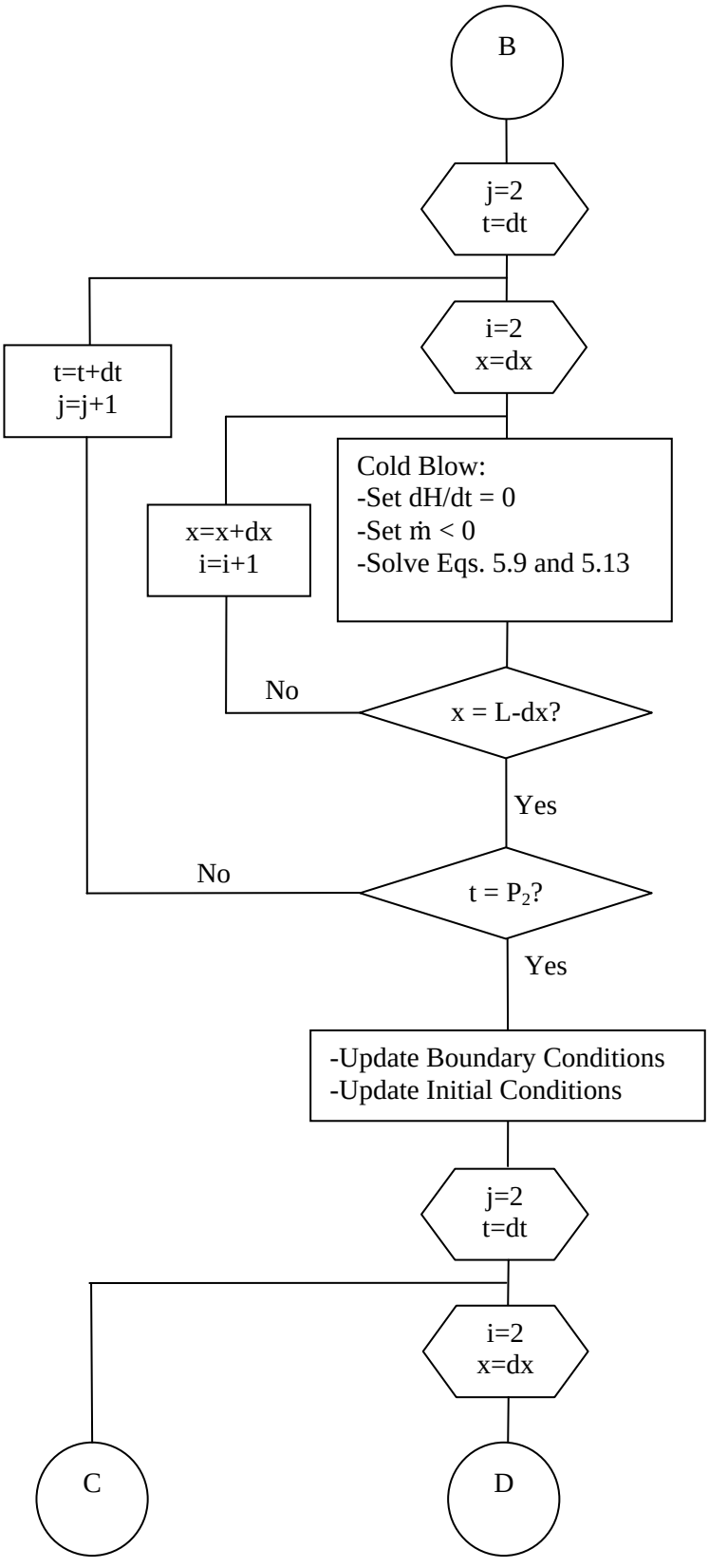

Figure 5.9: Flowchart of the solution procedure (Contd.).

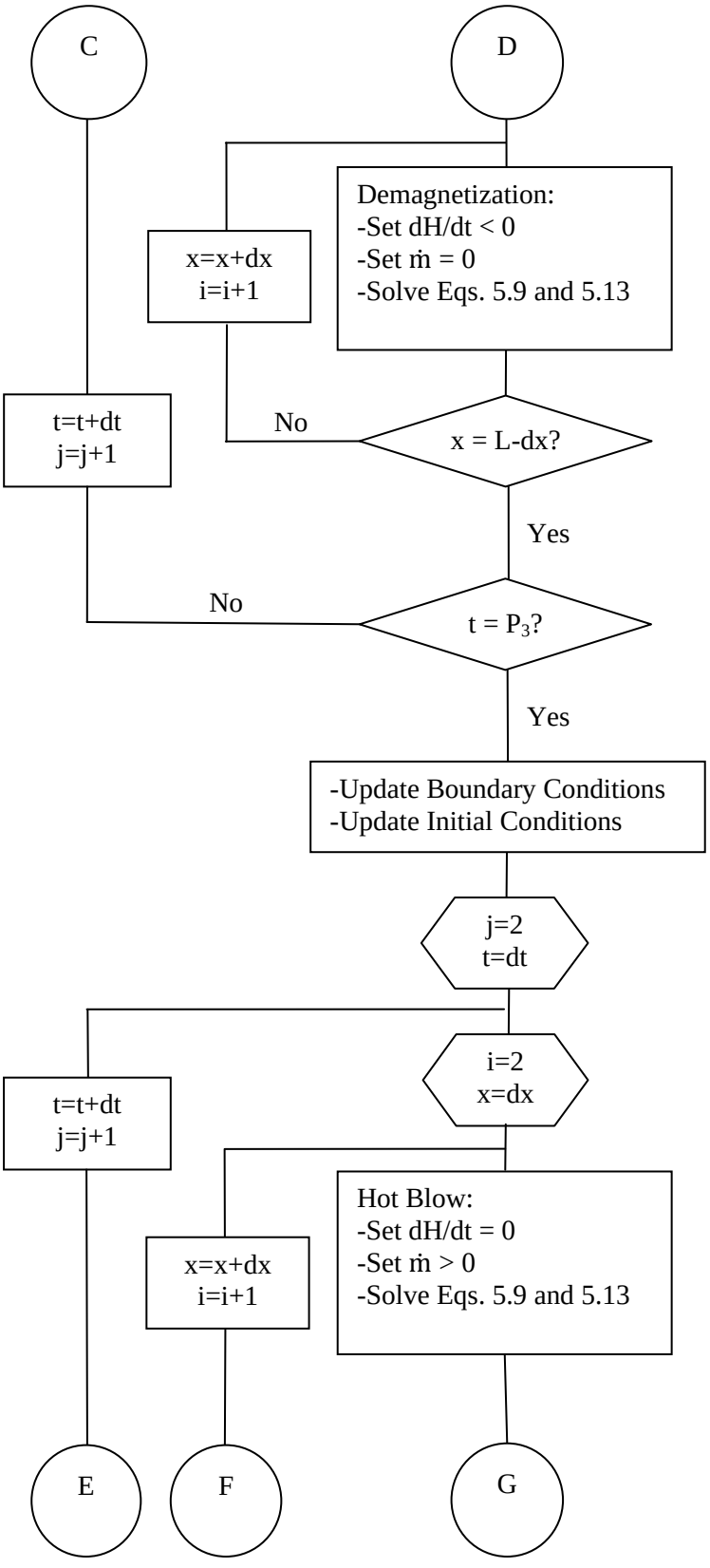

Figure 5.9: Flowchart of the solution procedure (Contd.).

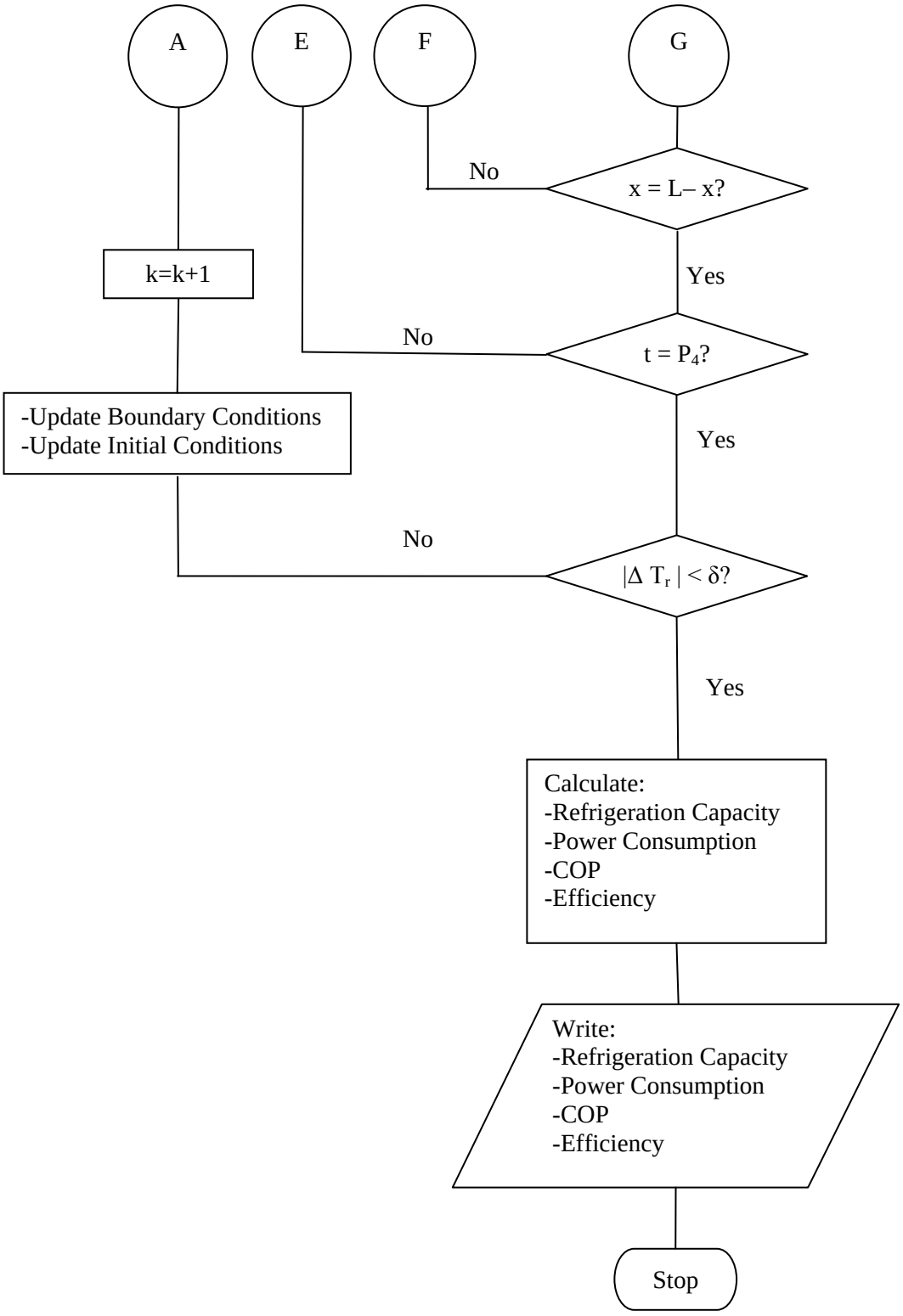

Figure 5.9: Flowchart of the solution procedure (Contd.).

5.8 Verification of the Model

Verification of the model presented in this chapter was validated by making the following changes and comparing the results with the results obtained by Siddikov et al. [25].

1. Using Gd instead of FeRh as the refrigerant which led to changes in the properties of the regenerator, such as thermal conductivity (11 W/mK), density (7901 kg/m^3), specific heat, MCE.
2. Applying isentropic process as an alternative to isothermal process by using Eq.5.3b.

Figs. 5.10 to 5.13 compare the published and calculated results. The following reasons rationalize the inaccuracy shown in the figures:

1. The boundary conditions in this study are different from boundary conditions in the published paper.
2. Siddikov et al. [25] has used a finer grid which means their result is more accurate.
3. Dissipation factor in fluid energy equation is different in two studies.

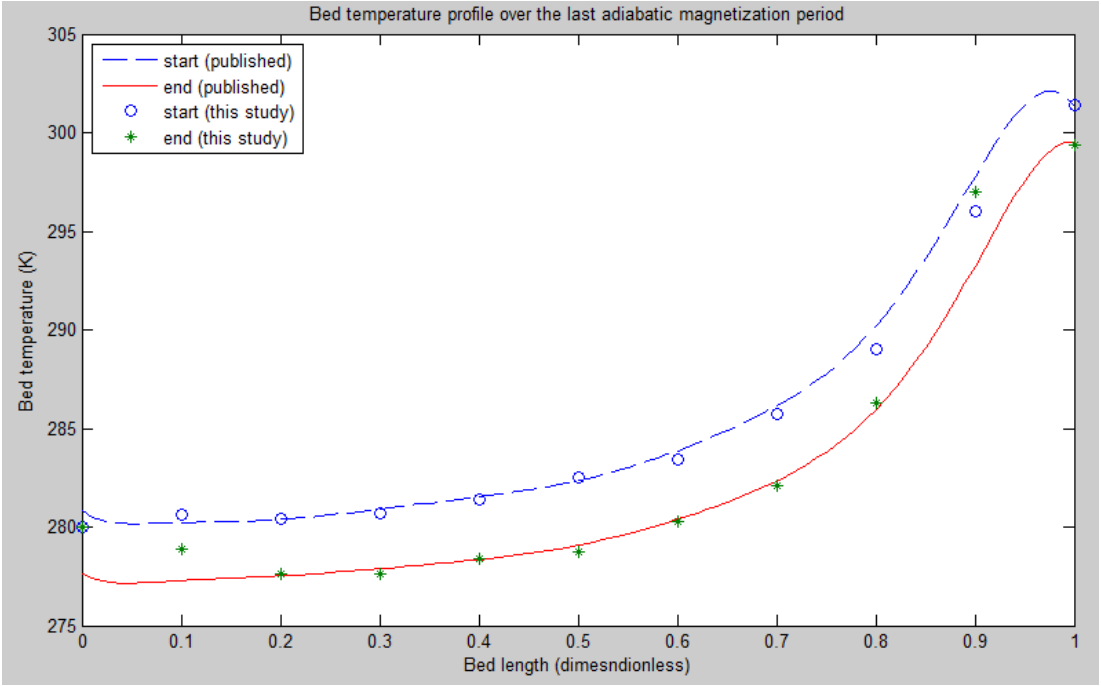

Figure 5.10: Bed temperature profile over the last adiabatic magnetization period (published results are obtained from [25]).

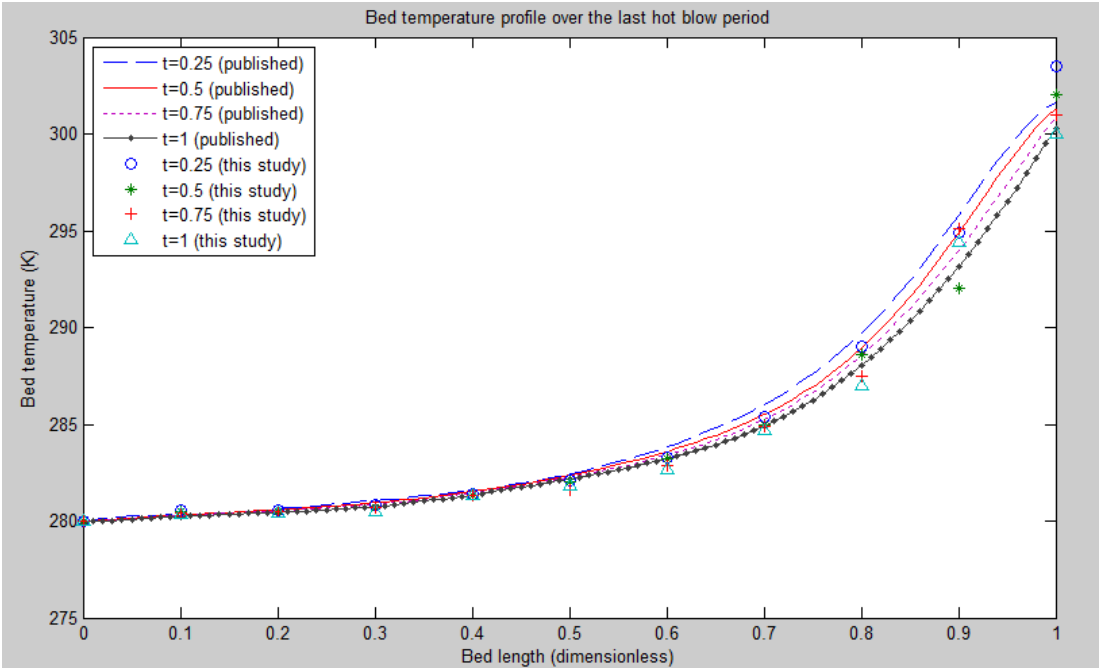

Figure 5.11: Bed temperature profile over the last hot blow period (published results are obtained from [25]).

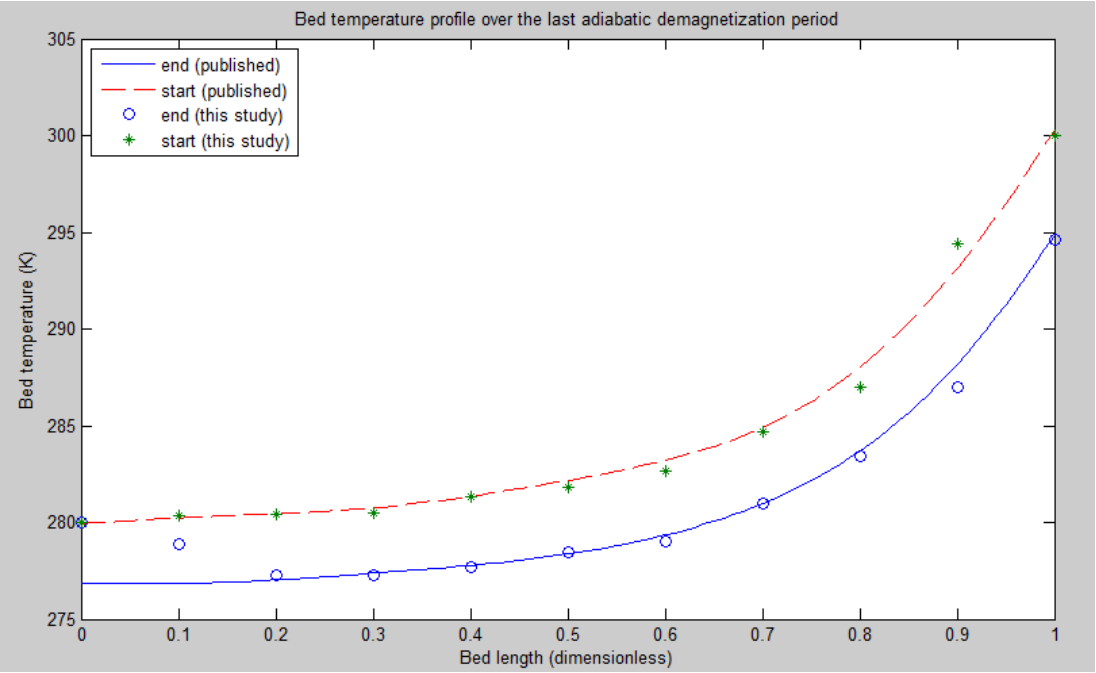

Figure 5.12: Bed temperature profile over the last demagnetization period (published results are obtained from [25]).

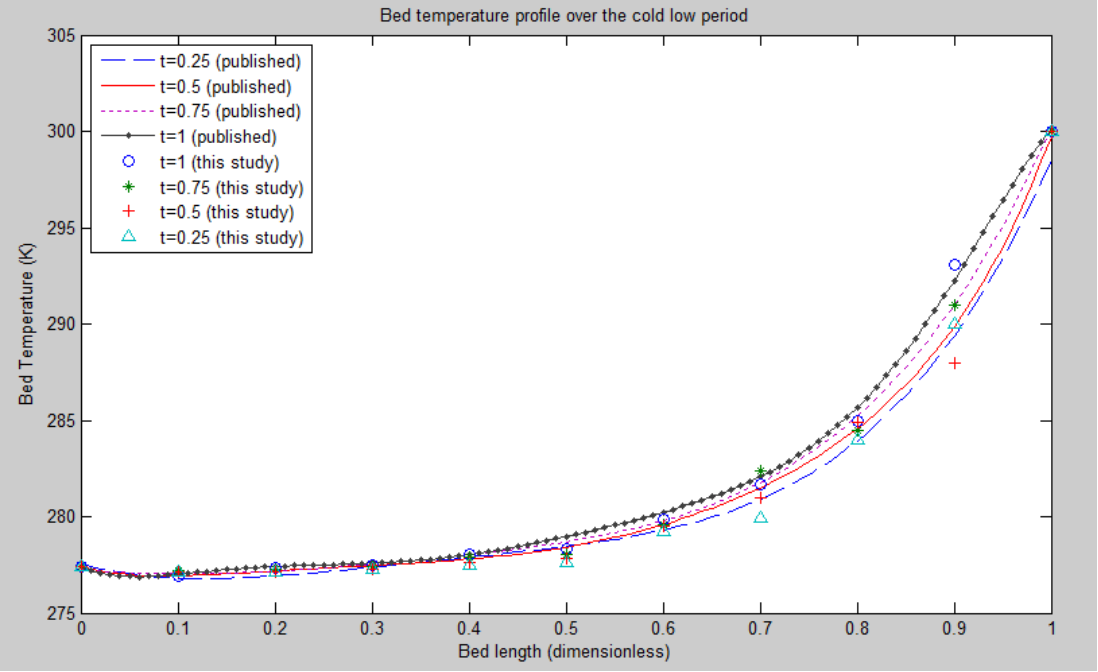

Figure 5.13: Bed temperature profile over the cold blow period (published results are obtained from [25]).

CHAPTER 6

SIMULATION AND RESULTS

The COP of an AMRR is dependent on various factors; for instance, the heat transfer fluids, the refrigerant, the duration of each cycle, porosity, mass flow rate, temperature of hot and cold ends, and the volume of the bed. In order to investigate the effect of these factors, they should be subjected to parametric studies. This chapter offers the results of parameter studies of porosity and mass flow rate, as well as heat transfer fluid of an AMRR applying one dimensional, time-varying mathematical model. In this way we are able to study the concepts of MR easily. On the other hand, we can evaluate the effect of each parameter on the performance of the AMRR.

The optimization process for mass flow rate was performed while the porosity kept constant at 0.35. The porosity optimization procedure was done based on the optimized mass flow rate.

The results in this chapter are separated into two major groups: optimization based on mass flow rate, and optimization based on porosity. Each group is also divided into two subgroups: the results for water and the results for water/ethylene glycol mixture.

6.1 Optimization of Mass Flow Rate

The aim of this section is to analyze the effect of the mass flow rate on refrigeration capacity, power consumption, and COP of the AMRR. Theoretically,

refrigeration capacity changes linearly with mass flow rate. However, the mean exit temperature of the cold blow may cause some nonlinearity in the results.

The pumping work seems to be related to mass flow rate linearly, but the pressure drop is also dependent upon mass flow rate. On the other hand, the magnetization work is independent of mass flow rate; thus it is expected that the mass flow rate affects the total work nonlinearly.

In order to find the optimized mass flow rate, various mass flow rates were applied ranging from 0.05 to 0.3 kg/m^3.

6.1.1 Results and Discussion

Figs.6.1 to 6.4 show the mass flow rate optimization results for pure water.

Fig.6.1 shows how mass flow rate influences the refrigeration capacity. According to the figure, the maximum refrigeration capacity obtained is 513W at 0.25kg/s and the trend shows after 0.25kg/s the refrigeration capacity decreases.

Power consumption is depicted in Fig.6.2. It is obvious that the power consumption increases with mass flow rate because pumping work is related to mass flow rate directly.

Figs.6.3 and 6.4 show COP and efficiency, respectively. As it is shown the COP and efficiency follow the same trend. The maximum for both of them occurs at 0.15kg/s at which the COP is 7.31 and the efficiency is 54.99%.

The large difference between COP presented in Ref [20] and this thesis is explained by that in Ref. [20] the heat exchange conditions are assumed absolutely perfect in contrast to this thesis.

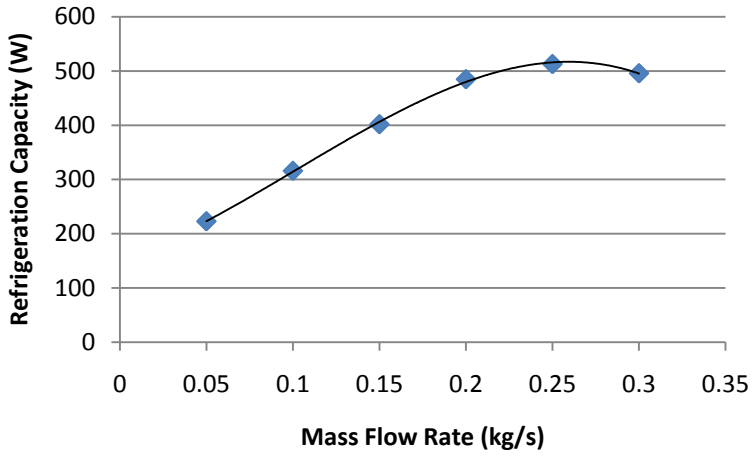

Figure 6.1: Refrigeration capacity vs. mass flow rate (water).

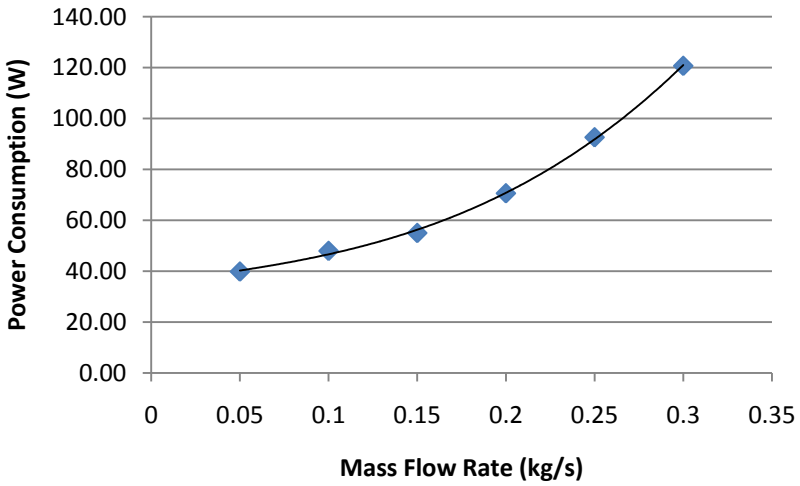

Figure 6.2: Power consumption vs. mass flow rate (water).

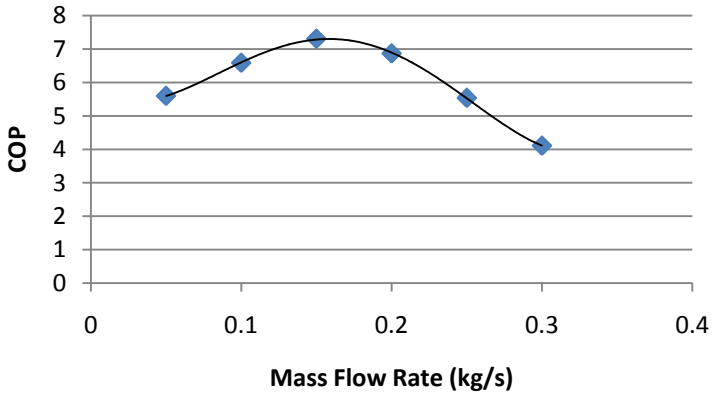

Figure 6.3: COP vs. mass flow rate (water).

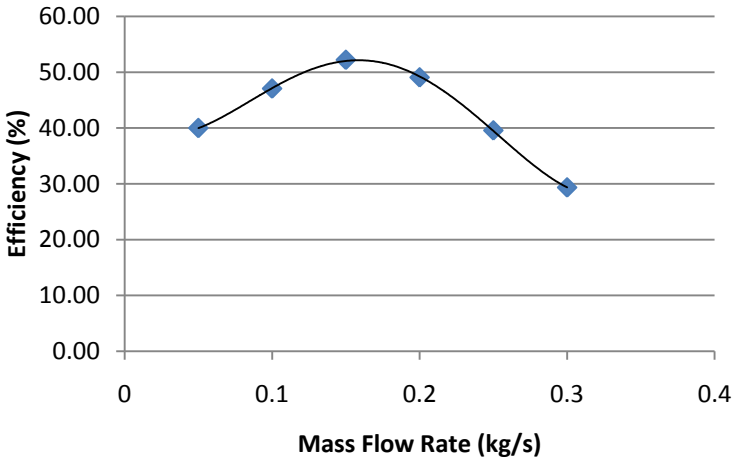

Figure 6.4: Efficiency vs. mass flow rate (water).

Figs.6.5 to 6.8 illustrate the results for optimum mass flow rate for the mixture of water and ethylene glycol.

As it is depicted in Fig.6.5, the maximum refrigeration capacity is 340W and reached at 0.15Kg/s. this value is not as large as the maximum refrigeration capacity for water. The low thermal conductivity and specific heat of the mixture compared to the pure water is the reason (see Figs.5.6 and 5.7)

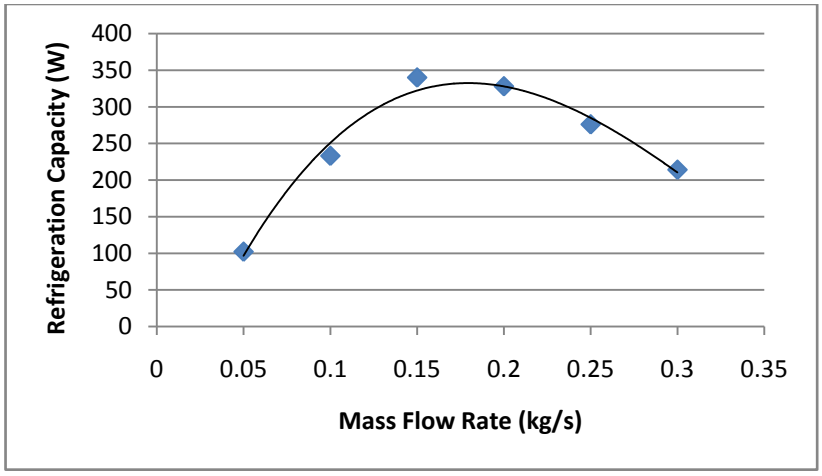

Figure 6.5: Refrigeration capacity vs. mass flow rate (water/glycol ethylene).

Fig.6.6 shows that the power consumption is increasing with mass flow rate, but the values are much more than that for pure water. This is because the dynamic

viscosity of the mixture is larger than that of water (see Fig.5.8) and the magnetization work is the same for both cases.

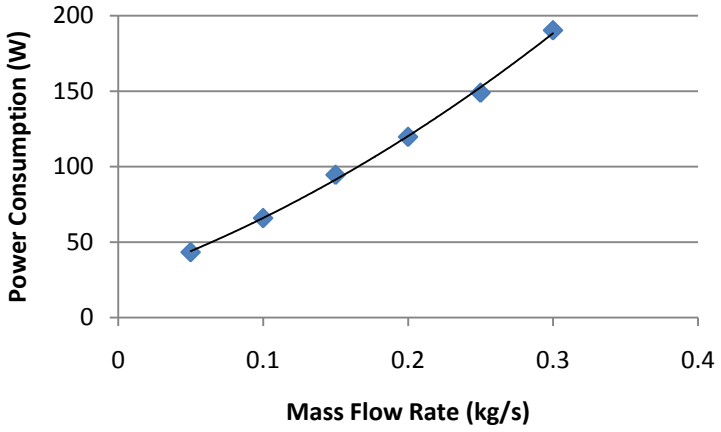

Figure 6.6: Power consumption vs. mass flow rate (water/glycol ethylene).

Figs.6.7 and 6.8 depict the COP and efficiency for the mixture. Based on them, the COP and efficiency are 3.6 and 25.6%, respectively which is two time smaller than COP and efficiency for the water.

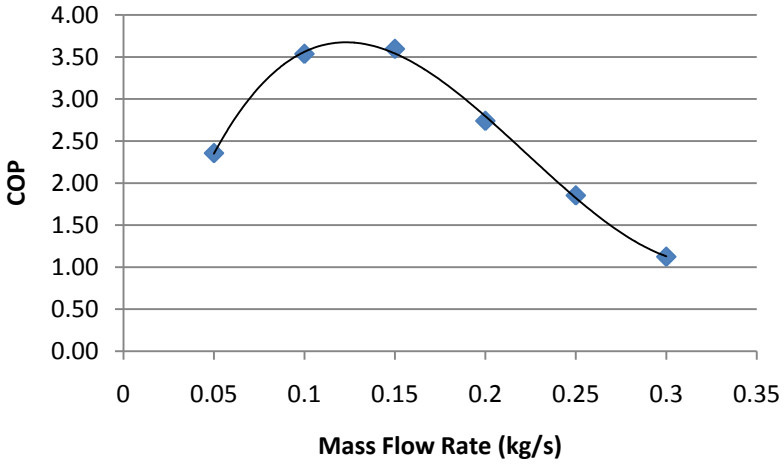

Figure 6.7: COP vs. mass flow rate (water/glycol ethylene).

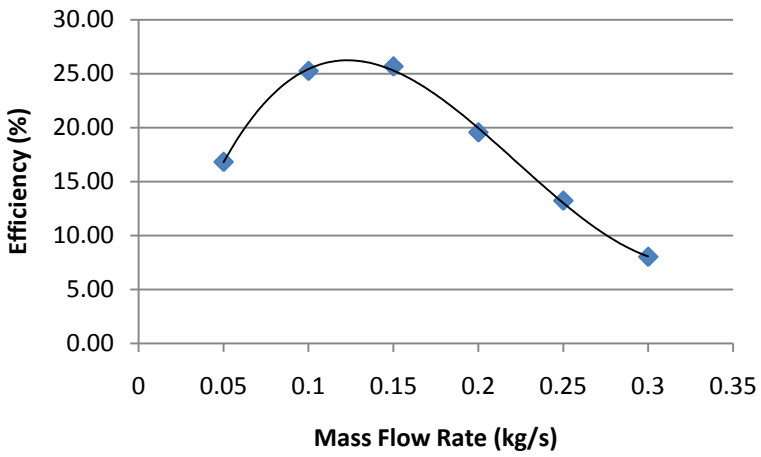

Figure 6.8: Efficiency vs. mass flow rate (water/glycol ethylene).

Although the transition temperature of the FeRh alloy is not in the working interval of the AMRR and the magnetic field is limited to 1.5T, the COP of the system is much more than that of conventional vapor compression systems, provided water is used as the heat transfer fluid.

6.2 Optimization of Porosity

The goal of this section is to study how the porosity influences refrigeration capacity, power consumption, and COP of the AMRR.

Clearly, the pumping work decreases with porosity, because the movement of the fluid is facilitated. The magnetization work also reduces, because the magnetization work is related to the mass of the magnetic material, so the total work decreases with porosity.

It is predicted that the refrigeration capacity lessens too, since the refrigeration capacity is related to the interaction between the magnetic materials and the fluid. The higher porosity, the lesser interactions.

The process of porosity optimization was done for the optimum mass flow rate obtained in the previous section which was 0.15kg/s for both cases.

6.2.1 Results and Discussion

Figs.6.9 to 6.12 illustrate the results of the porosity optimization for pure water.

Fig.6.9 shows that the refrigeration capacity decreases with the increase of porosity. It was expected, since the refrigeration capacity is implicitly depends on the mass of the regenerator. The rise in the porosity leads to the reduction in mass of the regenerator, so the trend seems to be logical.

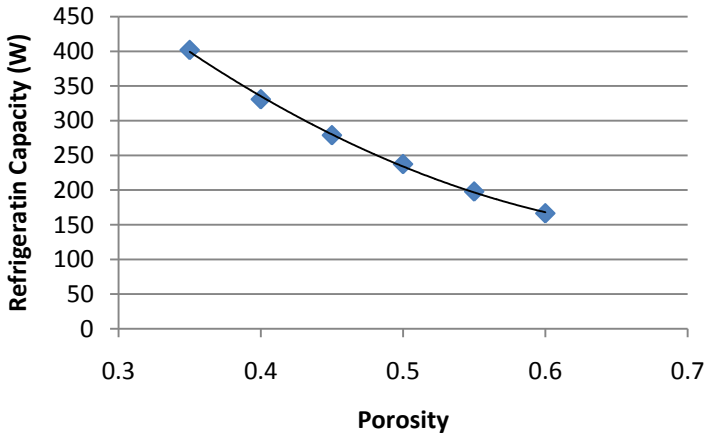

Figure 6.9: Refrigeration capacity vs. porosity (water).

Power consumption versus porosity is shown in Fig.6.10. Power consumption is also decreasing, because as the porosity increases, the work needed to pump the fluid decreases. On the other hand, the magnetization work is related to the mass of the regenerator explicitly.

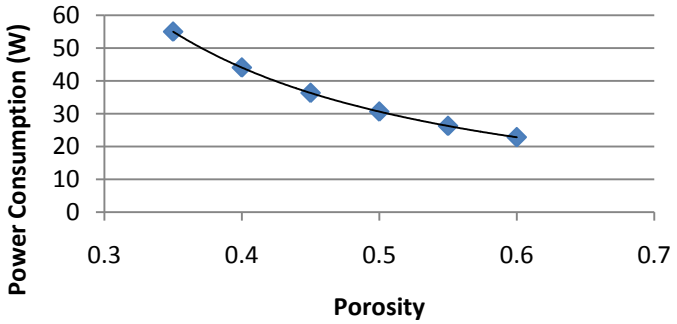

Figure 6.10: Power consumption vs. porosity (water).

COP and efficiency of the system versus porosity are shown in Figs.6.11 and 6.12. Although both the refrigeration capacity and power consumption reduces with the rise of porosity, there is peak in COP and efficiency diagrams. This is because the slop of the lines in Figs. 6.9 and 6.10.

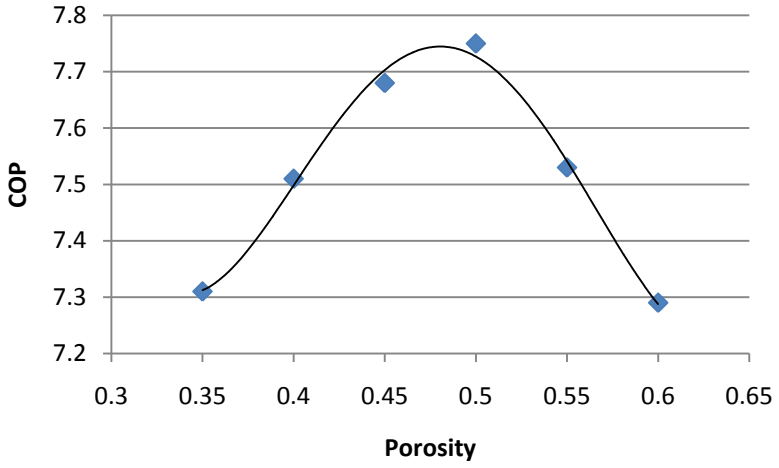

Figure 6.11: COP vs. porosity (water).

As it is seen the porosity does not affect the COP and efficiency so much. By the way, the optimum COP and efficiency are 7.75 and 55.35% in which the porosity is 0.5.

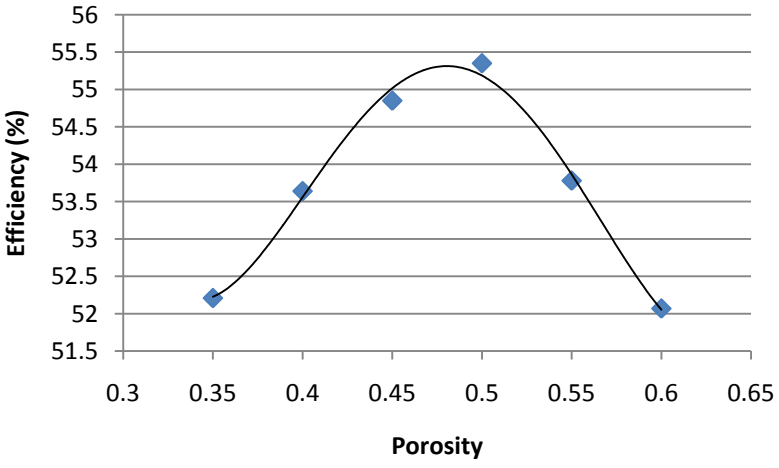

Figure 6.12: Efficiency vs. porosity (water).

The optimization results for water/ ethylene glycol mixture, based on porosity is expressed in Figs.6.13 to 6.16. The similar shapes for refrigeration capacity and power consumption as that for water are obtained.

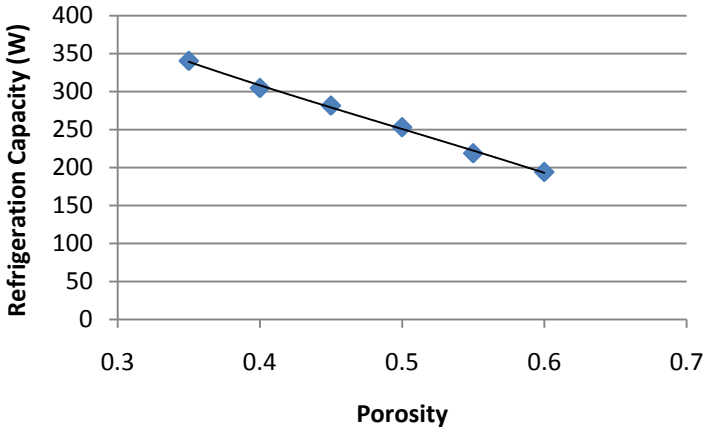

Figure 6.13: Refrigeration capacity vs. porosity (water/ethylene glycol).

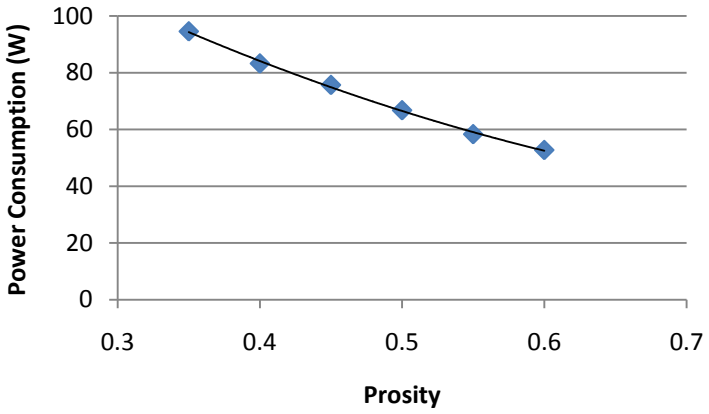

Figure 6.14: Power consumption vs. porosity (water/ethylene glycol)

The optimized porosity for the maximum COP and efficiency is 0.5 where the COP and efficiency are 3.79 and 27.07%, respectively.

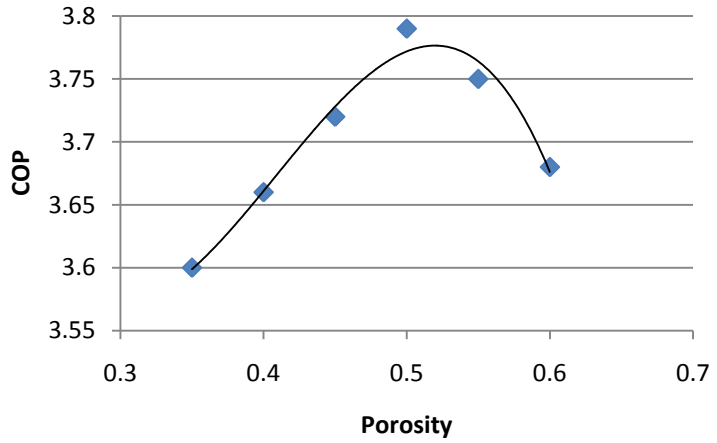

Figure 6.15: COP vs. porosity (water/ethylene glycol).

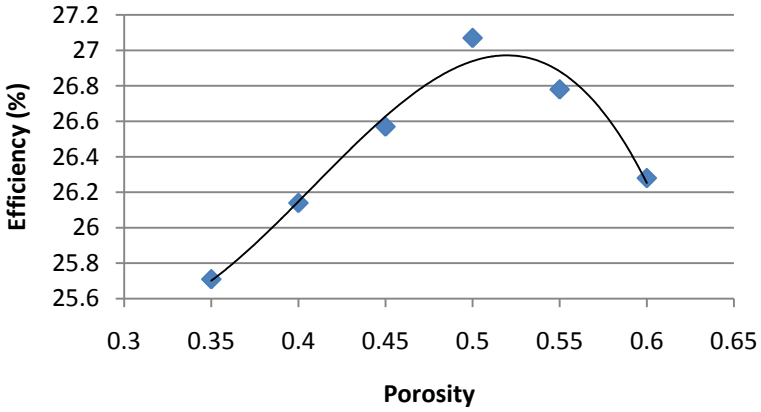

Figure 6.16: Efficiency vs. porosity (water/ethylene glycol).

Overally, the effect of porosity on the performance of the AMR is negligible (6.13% for water and 5.01% for the mixture).

6.3 Heat Transfer Fluid

In most AMRRs, water is used as the heat transfer fluid. But in some cases the cold end of the system gets to the temperatures below 273 (0^{o}C). In such cases, other fluids like ethylene glycol can be added to the water as an antifreezing agent. That is why we investigated the influence of water/ethylene glycol mixture on the performance of the AMRR.

As the results shown in previous section the performance of the AMRR decreases sharply when the water/ethylene glycol mixture was applied. The reasons

of low performance are mainly due to high viscosity and low specific heat of the mixture. The former increases the pumping work while the latter leads to refrigeration capacity reduction; therefore, the use of antifreezing is not recommended unless it is necessary.

CHAPTER 7

CONCLUSION

The main purpose of this study was to introduce a mathematical model to predict the performance of an active magnetic regenerative refrigerator. Although the obtained results are based on a particular AMRR, the method described here has the ability to be used for all other AMRRs with minor changes. The second aim was to optimize an AMRR based on mass flow rate of the heat transfer fluid and porosity of the bed. The properties of the magnetic material play an important role in the modeling process, particularly the entropy. In this study, FeRh is used as the refrigerant. The third purpose of this work was to obtain and code the entropy of the FeRh alloy.

The investigated AMRR is a reciprocating AMRR consisting of FeRh alloy as the refrigerant and water or water/ethylene glycol mixture as the heat transfer fluid. The one-dimensional, time-dependant model solves the energy equation for the fluid and regenerator explicitly.

The model was verified with published results. The accuracy of the model is acceptable to some extents. However there are some reasons which rationalize the inaccuracies.

After defining the suitable mathematical model, the AMRR was optimized based on the mass flow rate of the fluid and the porosity of the bed. According to the

results, it is concluded that it is possible to obtain a significant COP in an AMR with a packed bed regenerator and containing water at 1.5T magnetic field.

Unfortunately, the transition temperature of the FeRh alloy sample which was used in the study was 312K; on the other hand, the magnetic field was limited to 1.5T, thus, based on the temperature of the hot and cold ends, the magnetic refrigerant did not experience magnetocaloric effect at the transition temperature, which made us unable to utilize the complete cooling potential of the alloy.

In principle, it is possible to have FeRh samples whose transition temperatures are within the required intervals, but in practice it needs more investigations.

Design studies presented here, have proved that the active magnetic regenerative refrigeration system executed with magnetic materials that are practical in the close future, have the potential to reach efficiencies that are comparable to vapor compression system provided optimized factors are applied; therefore, magnetic refrigeration has the prospective to become a realistic choice instead of present vapor compression refrigeration systems. The magnetic refrigerant has basically zero vapor pressure and consequently causes zero ozone depleting gases.

In order to expand the model, one can add the mathematical model of the heat exchangers to the main model. It is also possible to optimize the system based on the length and the cross-sectional area of the bed, hot and cold periods, magnetization and demagnetization period, the temperatures of the hot and cold ends.

REFERENCES

[1] S. L. Russek, C. B. Zimm, Potenrial for Cost Effective Magnetocaloric Air Conditioning System, International Journal of Refrigeration, Volume 29, 2006 Pages 1336-1373.

[2] T. F. Petersen, Numerical modelling and analysis of a room temperature magnetic refrigeration system. Fuel Cells and Solid State Chemistry Department, Technical University of Denmark. Roskilde , 2007.

[3] B.F. Yu, Q. Gao, B. Zhang, X. Z. Meng, Z. Chen, Review on Research of Room Temperature Magnetic Refrigeration, Internationa Journal of Refrigeration, Volume 26, 2003.

[4] V. K. Pecharsky, K. A. Gschneidner Jr, Magnetocaloric effect and magnetic refrigeration, Journal of Magnetism and Magnetic Materials, Volume 200, 1999, Pages 44-56.

[5] K. Engelbrecht, A Numerical Model of an Active Magnetic Regenerator Refrigeration System. University of Wisconsin-Madison, 2004.

[6] T. F. Petersen, N. Pryds, A. Smith, S. Linderoth, and S. Jeppesen, H. H. Knudsen, Magnetic Refrigeration and the Magnetocaloric Effect, Danske Koledage Conference, 2006.

[7] A. Kitanovski, P. W. Egolf, Thermodynamics of magnetic refrigeration, International Journal of Refrigeration, Volume 29, 2008, Pages 3-21.

[8] K. A. Gschneidner Jr. and V. K. Pecharsky, Magnetocaloric Materials, Annual Reviews, Volume 30, 2000, Pages 387–429.

[9] Morrish, A. The Physical Principles of Magnetism, John Wiley & Sons, Inc., 1965.

[10] K. A. Gschneidner, V. K. Pecharsky, Advanced magnetocaloric materials: What does the future hold?, International Journal of Refrigeration, Volume 29, 2006, Pages 1239-1249.

[11] K.A. Gschneidner Jr., V.K. Pecharsky, Prospects, Thirty years of near room temperature magnetic cooling: Where we are today and future, Internationa Journal of Refrigeration, Volume 31, 2008, Pages 945-961.

[12] A. DeGregoria, Modeling the active magnetic regenerator, Advances in Cryogenic, Volume 37, 1991, Pages 867-873.

[13] A. M. Tishin, Magnetocaloric effect: Current situation and future trends, Journal of Magnetism and Magnetic Materials, Volume 316, 2007.

[14] J. A. Barclay, W. A. Steyert, W.A. Active magnetic regenerator, 1982.

[15] L. D. Kirol, M. W. Dacus, Magnetic heat pump design 1987. Twenty Second Intersociety Energy Conversion Engineering Conference. Volume 22, 1987, Pages 1133-1137.

[16] K. A. Gschneidner Jr, V. K. Pecharsky, A. O. Tsokol. Recent developments in magnetocaloric materials, Institute of Physics Publishing, 2005.

[17] C. B. Zimm, A. Sternberg, A. G. Jastrab, A. M. Boeder, L. M. Lawton, J. J. Chell, Rotating bed magnetic refrigeration apparatus, 2003.

[18] C. Zimm, J. Auringer, A. Boeder, J. Chells, S. Russek, A. Sternberg, Design and initial performance of a magnetic refrigerator with a rotating permanent magnet,. Proceedings of the Second International Conference on Magnetic Refrigeration at Room Temperature, 2007, Pages 341–347.

[19] S. A. Nikitin, G. Myalikgulyev, A. M. Tishin, M. P. Annaorazov, K. A. Asatryan, A. L. Tyurin, The magnetocaloric effect in $Fe_{49}Rh_{51}$ compound , Physics Letter, Volume 148, 1990, Pages 363-366.

[20] M. P. Annaorazov, K. A. Asatryan, G. Myalikgulyev, S. A. Nikitin, A. M. Tishin, A. L. Tyurin, Alloys of the Fe-Rh system as a new class of working material for magnetic refrigerators, Cryogenics, Volume 32, 1992, Pages 867-872.

[21] M. P. Annaorazov, H. M. Guven, K. Barner, COP of cooling cycles around the AF–F transition in FeRh based on experimental data, Journal of Alloys and Compounds, Volume 397, 2005, Pages 26-30.

[22] E. Schroeder, G. Green, J. Chafe, Performance predictions of a magnetocaloric refrigerator using a finite element model, Advances in Cryogenic Engineering, Volume 35, 1990, Pages 1149-1155.

[23] A. Smaili, R. Chahine, Thermodynamic investigations of optimum active magnetic refgenerators, Cryogenics, Volume 38, 1998, Pages 247-252.

[24] F. Shir, C, Mavriplis, L. H. Bennett, E. D. Torre, Analysis of room temperature magnetic regenerative refrigeration, International Journal of Refrigeration, Volume 28, 2005, Pages 616-627.

[25] B. M. Siddikov, B. A. Wade, D. H. Schultz, Numerical Simulation of the Active Magnetic Regenerator, Computers and Mathematics with Applications, Volume 49, 2005, Pages 1525-1538.

[26] E. Hren, G. Paroczi, P. Szabo, α'-FeRh otvozetek rontgenes neutrondiffrakcios vizsgalata, KFKI, Volume 12, 1964, Pages 17-23.

[27] W. Benenson, J.W. Harris, H. Lutz, Handbook of Physics, AIP, 2006.

[28] G. Myalikgulyeu, M. P. Annaorazov, A. L. Tyurin, The temperature dependencies of electrical resistivity, thermal electromotive force, magnetization curves of iron-rhodium alloys, Izv. Acad. Nauk Turkmen SSR, 1988, Pages 77-81.

[29] H. K. Versteeg, W. Malalasekera, An Introduction to Computational Fluid Dynamics, The Finite Volume Method, Prentice Hall, 1995.

[30] N. Wakao, S. Kaguei, Heat and mass transfer in packed, Gordon and Breach Science Publishers, 1982.

[31] F. P. Incropera, D. P. Dewitt, Fundamentals of Heat and Mass Transfer, 4th. John Wiley and Sons Inc., 1996.

[32] M. Kaviany, Principles of Heat Transfer Porous Media. 2nd edition, Springer, 1995.

[33] A. Amiri, K. Vafai, Transient analysis of incompressible flow through a packed, International Journal of Heat and Mass Transfer, Volume 41, 1998, Pages 3148-3168.

[34] K. Vafai, Handook of Porous Media, 2nd edition, Taylor's and Francis, 2005.

[35] D. A. Nield, A. Beajn, Convection in Porous Media. 3rd edition, Springer, 2006

[36] K. Vafai, Handook of Porous Media. 1st edition, Marcel Dekker Inc, 2000.

[37] K. Engelbrecht, G. Nellis, S. Klein. Comparing modelling predictions to experimental data for active magnetic regeneration refrigeration systems, Second IIF-IIR International Conference on Magnetic Refrigeration at Room Temperature, 2007

[38] C. P. Jeffreson, Prediction of Breakthrough Curves in Packed Beds, AIChE Journal, Volume 18, 1972.

[39] J. H. Mathews, K. D. Fink, Numerical Methods Using Matlab, 4th edition, Pearson Prentice Hall, 2004.

[40] M. N. Özişik, Finite Difference Methods in Heat Transfer, 1st edition, CRC Press Inc., 1994.

APPENDIX

Developed Code

```
%Preallocation
Tf = zeros(N+1,M+1);
Tr = zeros(N+1,M+1);

%Told and error initialization
Toldf = zeros(N+1,1);
Toldr = zeros(N+1,1);
ferror = zeros(N+1,1);
rerror = zeros(N+1,1);

%Stating intitial conditions
for i=1:N+1, Tf(i,1) = Tc + (Th - Tc)*(i-1)*Dx; end
for i=1:N+1, Tr(i,1) = Tc + (Th - Tc)*(i-1)*Dx; end

wpc=0;
wph=0;
wp=0;
qmag=0;
qdemag=0;
wmag=0;

for k=1:s
   k
    for j = 1:M
        mdot = 0;
        Hr = Hmax*(j-1)*Dt;
        DHDt = Hmax;

        [cf, kf, Muf, Rhof,fac] = FProp(Tf,j,fac);

        [kr, heq, Re, Pr] = kr_heq (Tr, Hr, mdot, dh, Ac, Muf, cf,
kf, j);

        [Bf1, Bf2, Bf3, Bf4, F] = FCoefficients (eps, kf, mdot, dh,
...
            Ac, cf, As, Dt, Rhof, Dx, heq, Re, Pr);

        [Br1, Br2, Br3,s1] = RCoefficients(Hr, Tr, eps, DHDt, Dx,
Dt, kr, ...
            heq, As, RhoR, j);

        Tf(1,j+1) = Tc;
        Tf(N+1,j+1) = (Bf1(N+1) + 2*Bf3(N+1))*Tf(N+1,j) + ...
            (Bf2(N+1) - Bf3(N+1))*Tf(N,j) + Bf4(N+1)*Tr(N+1,j) +
F(N+1);

        Tr(1,j+1) = (Br1(1) + 2*Br2(1))*Tr(1,j) + Br3(1)*Tf(1,j);
        Tr(N+1,j+1) = (Br1(N+1)+2*Br2(N+1))*Tr(N+1,j) +
Br3(N+1)*Tf(N+1,j);

        for i = 2:N

            Tf(i,j+1) = Bf1(i)*Tf(i,j) + Bf2(i)*Tf(i-1,j) + ...
                Bf3(i)*Tf(i+1,j) + Bf4(i)*Tr(i,j) + F(i);

            Tr(i,j+1) = Br1(i)*Tr(i,j) + Br2(i)*(Tr(i-1,j) + ...
```

```
                Tr(i+1,j)) + Br3(i)*Tf(i,j);
        end
        qmag=qmag+RhoR*Ac*(1-eps)*trapz(s1,Tr(:,j));
    end


        for i=1:N+1, Tf(i,1) = Tf(i,M+1); end
    for i=1:N+1, Tr(i,1) = Tr(i,M+1); end

    for j = 1:M
                mdot = -Mdot;
        Hr = Hmax;
        DHDt = 0;

        [cf, kf, Muf, Rhof,fac] = FProp(Tf,j,fac);

        [kr, heq, Re, Pr] = kr_heq (Tr, Hr, mdot, dh, Ac, Muf, cf,
kf, j);

        [Bf1, Bf2, Bf3, Bf4, F] = FCoefficients (eps, kf, mdot, dh,
...
            Ac, cf, As, Dt, Rhof, Dx, heq, Re, Pr);

        [Br1, Br2, Br3,s1] = RCoefficients(Hr, Tr, eps, DHDt, Dx,
Dt, kr, ...
            heq, As, RhoR, j);


        Tf(N+1,j+1) = Th;
        Tf(1,j+1) = (Bf1(1) + 2*Bf2(1))*Tf(1,j) + ...
            (Bf3(1) - Bf2(1))*Tf(N,j) + Bf4(1)*Tr(1,j) + F(1);

        Tr(1,j+1) = (Br1(1) + 2*Br2(1))*Tr(1,j) + Br3(1)*Tf(1,j);
        Tr(N+1,j+1) = (Br1(N+1)+2*Br2(N+1))*Tr(N+1,j) +
Br3(N+1)*Tf(N+1,j);

        for i = 2:N

            Tf(i,j+1) = Bf1(i)*Tf(i,j) + Bf2(i)*Tf(i-1,j) + ...
                Bf3(i)*Tf(i+1,j) + Bf4(i)*Tr(i,j) + F(i);

            Tr(i,j+1) = Br1(i)*Tr(i,j) + Br2(i)*(Tr(i-1,j) + ...
                Tr(i+1,j)) + Br3(i)*Tf(i,j);
        end
        dp=(150*Muf*(1-eps^2)*Mdot/(dh^2*eps^3) - ...
            1.75*(1-eps)*Mdot^2/(Rhof*dh*eps^3))*Dx;
        dwp=Mdot*dp/Rhof;
        wpc=wpc+sum(dwp);
    end
   Tfc=Tf;


    for i=1:N+1, Tf(i,1) = Tf(i,M+1); end
    for i=1:N+1, Tr(i,1) = Tr(i,M+1); end

    for j = 1:M
        mdot = 0;
        Hr = Hmax*(1-(j-1)*Dt);
```

```
        DHDt = -Hmax;

        [cf, kf, Muf, Rhof,fac] = FProp(Tf,j,fac);

        [kr, heq, Re, Pr] = kr_heq (Tr, Hr, mdot, dh, Ac, Muf, cf,
kf, j);

        [Bf1, Bf2, Bf3, Bf4, F] = FCoefficients (eps, kf, mdot, dh,
...
            Ac, cf, As, Dt, Rhof, Dx, heq, Re, Pr);

        [Br1, Br2, Br3,s1] = RCoefficients(Hr, Tr, eps, DHDt, Dx,
Dt, kr, ...
            heq, As, RhoR, j);


        Tf(1,j+1) = Tc;
        Tf(N+1,j+1) = (Bf1(N+1) + 2*Bf3(N+1))*Tf(N+1,j) + ...
            (Bf2(N+1) - Bf3(N+1))*Tf(N,j) + Bf4(N+1)*Tr(N+1,j) +
F(N+1);

        Tr(1,j+1) = (Br1(1) + 2*Br2(1))*Tr(1,j) + Br3(1)*Tf(1,j);
        Tr(N+1,j+1) = (Br1(N+1)+2*Br2(N+1))*Tr(N+1,j) +
Br3(N+1)*Tf(N+1,j);

        for i = 2:N

            Tf(i,j+1) = Bf1(i)*Tf(i,j) + Bf2(i)*Tf(i-1,j) + ...
                Bf3(i)*Tf(i+1,j) + Bf4(i)*Tr(i,j) + F(i);

            Tr(i,j+1) = Br1(i)*Tr(i,j) + Br2(i)*(Tr(i-1,j) + ...
                Tr(i+1,j)) + Br3(i)*Tf(i,j);
        end
        qdemag=qdemag+RhoR*Ac*(1-eps)*trapz(s1,Tr(:,j));
    end



    for i=1:N+1, Tf(i,1) = Tf(i,M+1); end
    for i=1:N+1, Tr(i,1) = Tr(i,M+1); end

    for j = 1:M
        mdot = Mdot;
        Hr = 0;
        DHDt = 0;

        [cf, kf, Muf, Rhof,fac] = FProp(Tf,j,fac);

        [kr, heq, Re, Pr] = kr_heq (Tr, Hr, mdot, dh, Ac, Muf, cf,
kf, j);

        [Bf1, Bf2, Bf3, Bf4, F] = FCoefficients (eps, kf, mdot, dh,
...
            Ac, cf, As, Dt, Rhof, Dx, heq, Re, Pr);

        [Br1, Br2, Br3,s1] = RCoefficients(Hr, Tr, eps, DHDt, Dx,
Dt, kr, ...
            heq, As, RhoR, j);
```

```
        Tf(1,j+1) = Tc;
        Tf(N+1,j+1) = (Bf1(N+1) + 2*Bf3(N+1))*Tf(N+1,j) + ...
            (Bf2(N+1) - Bf3(N+1))*Tf(N,j) + Bf4(N+1)*Tr(N+1,j) +
F(N+1);

      Tr(1,j+1) = (Br1(1) + 2*Br2(1))*Tr(1,j) + Br3(1)*Tf(1,j);
        Tr(N+1,j+1) = (Br1(N+1)+2*Br2(N+1))*Tr(N+1,j) +
Br3(N+1)*Tf(N+1,j);

        for i = 2:N

            Tf(i,j+1) = Bf1(i)*Tf(i,j) + Bf2(i)*Tf(i-1,j) + ...
                Bf3(i)*Tf(i+1,j) + Bf4(i)*Tr(i,j) + F(i);

            Tr(i,j+1) = Br1(i)*Tr(i,j) + Br2(i)*(Tr(i-1,j) + ...
                Tr(i+1,j)) + Br3(i)*Tf(i,j);
        end
        dp=(150*Muf*(1-eps^2)*Mdot/(dh^2*eps^3) - ...
            1.75*(1-eps)*Mdot^2/(Rhof*dh*eps^3))*Dx;
        dwp=Mdot*dp/Rhof;
        wph=wph+sum(dwp);
    end

    for i=1:N+1, ferror(i) = abs(Toldf(i) - Tf(i,M+1)); end
    for i=1:N+1, rerror(i) = abs(Toldr(i) - Tr(i,M+1)); end

    if all(rerror<error)
        break
    else
        for i=1:N+1, Toldf(i) = Tf(i,M+1); end
        for i=1:N+1, Toldr(i) = Tr(i,M+1); end
        for i=1:N+1, Tf(i,1) = Tf(i,M+1); end
        for i=1:N+1, Tr(i,1) = Tr(i,M+1); end
    end

end

 wp=wp+wpc+wph;
 wmag=wmag+(qmag+qdemag)/N;

[COP, etha, Qc, W] = results(M, Tfc, Tc, Th, Mdot, wp, wmag, eps,
fac);
```